Electromagnetics and emerging technologies for pervasive applications: Internet of Things, Health and Safety

Radiative and Non-radiative Wireless Power Transfer: Theory and Applications

<u>Giuseppina Monti</u>[1], L. Tarricone[1], L. Corchia[1], M. V. De Paolis[1], M. Mongiardo[2], A. Costanzo[3], F. Mastri[3]

[1]*EML^2, Dept. of Engineering for Innovation, Univ. of Salento, Lecce, Italy*

[2]*Dept. of Engineering, University of Perugia, Perugia, Italy*

[3]*Dept. of Electrical, Electronic and Information Engineering "Guglielmo Marconi", Univ. of Bologna, Bologna, Italy*

Outline

- Introduction:
  - Motivations
  - Classification
- Two-port network representation of a WPT link
  - Figures of merit
  - Closed form analytical formulas for the optimal load
- Applications:
  - WPT for wearable devices
  - WPT for medical implants

WPT: Motivations

Enabling Technology for

Energy Autonomous System

"An electronic system that has been designed to operate and/or communicate as long as possible in known/unknown environments providing, elaborating and storing information without being connected to a power grid"

M. Belleville et al, "Energy Autonomous Systems: Future Trends in Devices, Technology, and Systems" Report, CATRENE Working Group on Energy Autonomous Systems, 2008.

EAS: Applications

Structural Monitoring

Wireless Sensor Networks

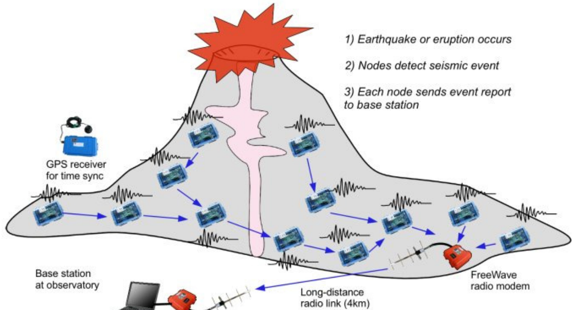

Body Area Network

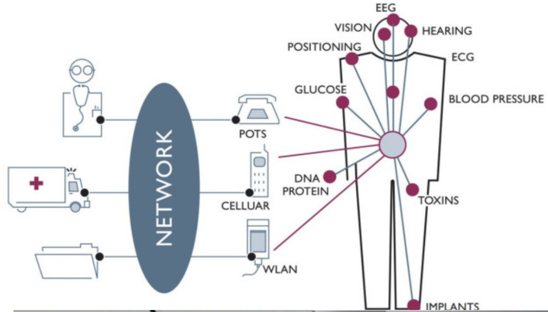

Security

Building Automation

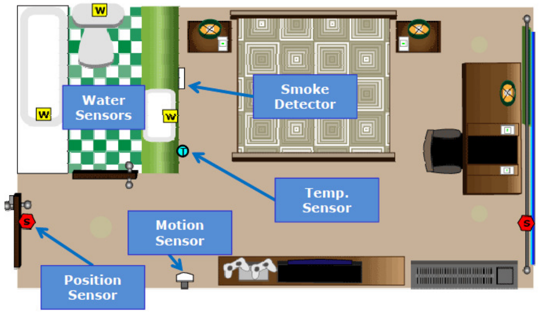

Medical and Military Devices

EAS Architecture

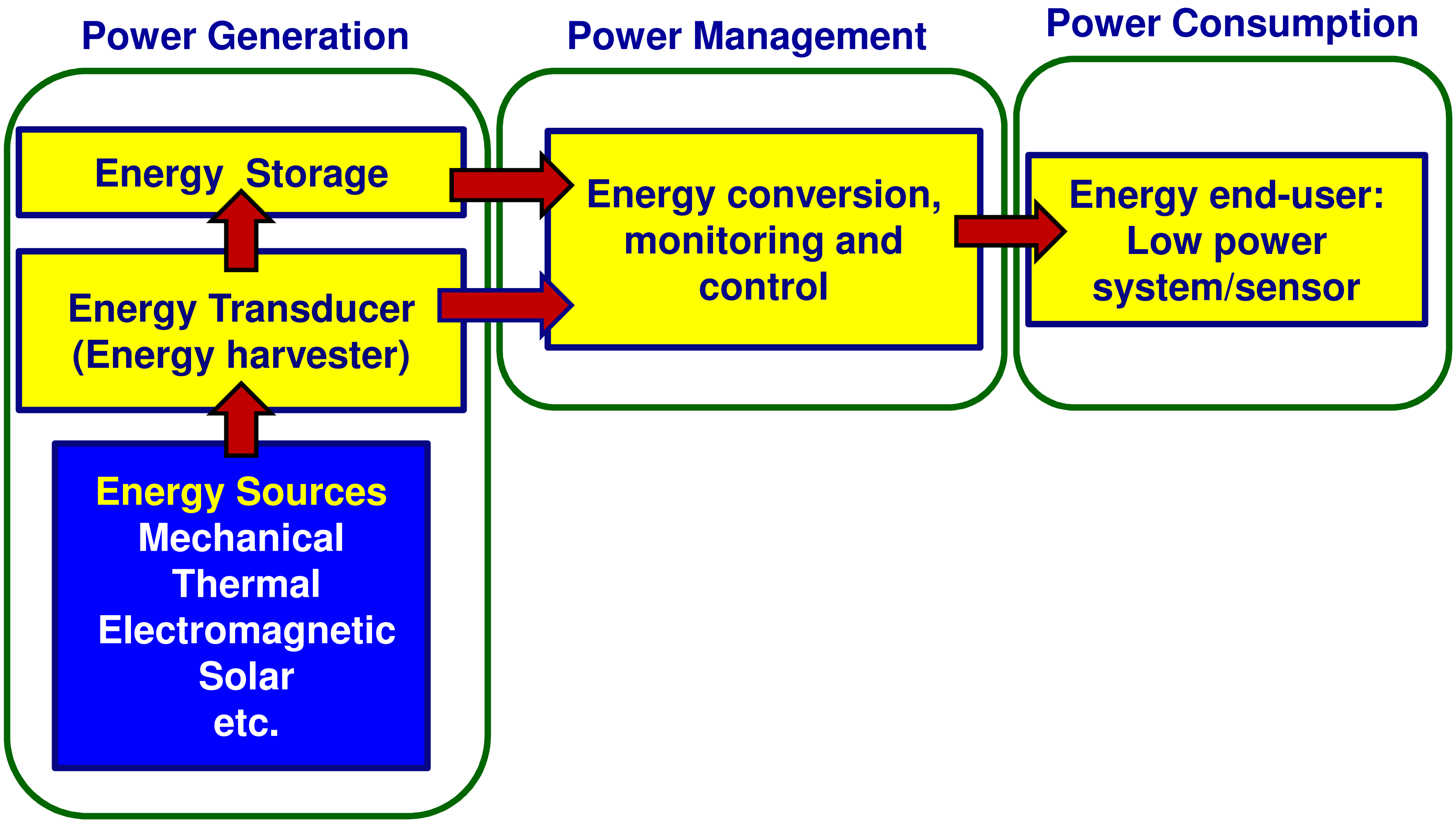

EAS- Key Aspects

- Conversion Efficiency

the ability of converting the power delivered by the source into electrical power and this last one in the form of storable energy

-Energy storage capabilities

The ability of storing the exceeding incoming energy in a reliable way, with the lowest internal dissipation

-The end-user power consumption

The WPT/harvesting system should guarantee the power required by the end-user in the worst energy case.

EAS based on EM Energy: Classifications

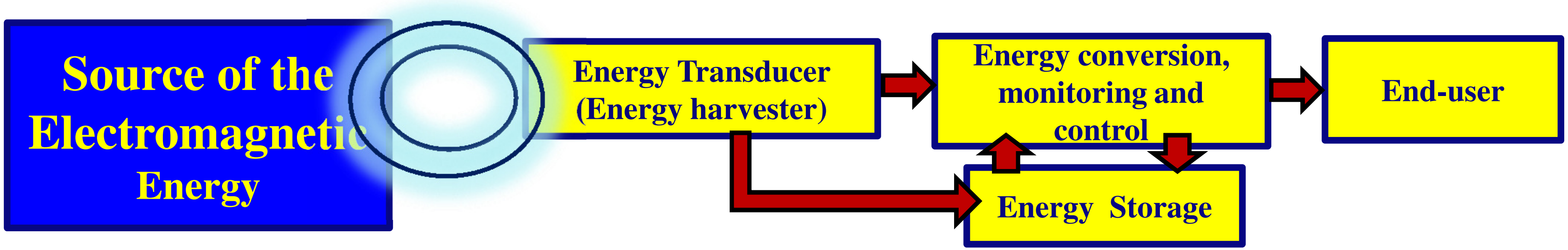

Two different classifications are possible

1) Type of the Source (intentional or not-intentional)

2) Coupling mechanism exploited by the transducer

A. Costanzo, M. Dionigi, D. Masotti, M. Mongiardo, G. Monti, L. Tarricone, R. Sorrentino, "**Electromagnetic Energy Harvesting and Wireless Power Transmission: A Unified Approach,**" *Proceedings of the IEEE* , Vol. 102 , Issue 11, pp. 1692–1711, Oct. 2014.

EAS based on EM Energy: Classifications

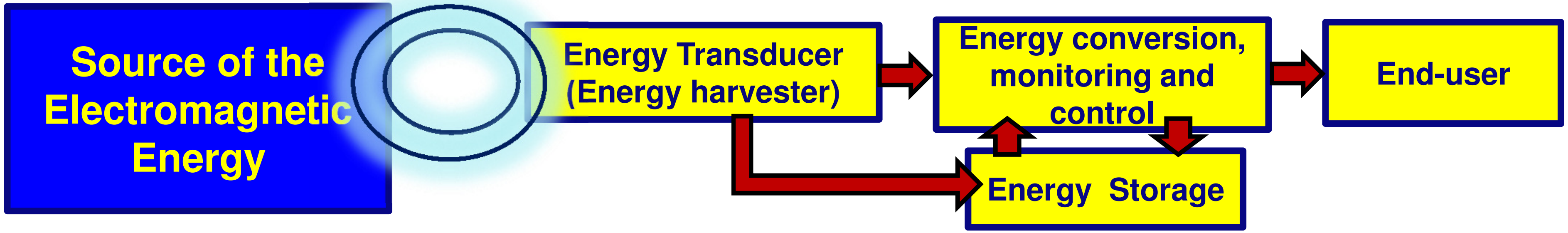

1) EM Source

Ad-hoc generated EM energy	EM energy available in the environment
WPT	**Energy Harvesting**

A. Costanzo, M. Dionigi, D. Masotti, M. Mongiardo, G. Monti, L. Tarricone, R. Sorrentino, "**Electromagnetic Energy Harvesting and Wireless Power Transmission: A Unified Approach,**" *Proceedings of the IEEE* , Vol. 102 , Issue 11, pp. 1692–1711, Oct. 2014.

EAS based on EM Energy: Classifications

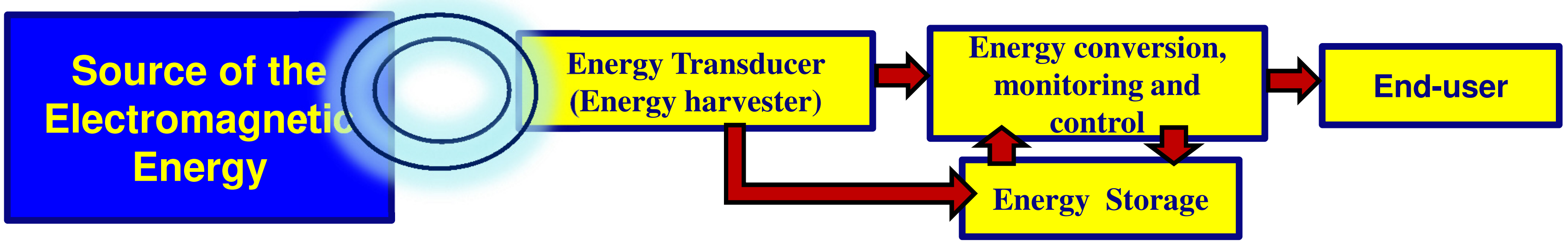

2) Coupling mechanism exploited by the transducer

Far-Field (Radiative)

Near-Field (Non-Radiative)

A. Costanzo, M. Dionigi, D. Masotti, M. Mongiardo, G. Monti, L. Tarricone, R. Sorrentino, "**Electromagnetic Energy Harvesting and Wireless Power Transmission: A Unified Approach,**" *Proceedings of the IEEE* , Vol. 102 , Issue 11, pp. 1692–1711, Oct. 2014.

Energy Harvesting vs WPT

Source of the Electromagnetic Energy → **Energy Transducer (Energy harvester)** → **Energy conversion, monitoring and control** → **End-user**

Energy Transducer (Energy harvester) → **Energy Storage** ⇄ **Energy conversion, monitoring and control**

Harvesting

Existing EM radiation *(e.g. GSM, FM, WiFi)* ***is used to power a wireless node***

Characteristics of the source unknown (position, frequency, bandwidth, polarization, etc.)

EAS

WPT (Wireless Power Transmission)

ad hoc generated EM radiation is **used to power a wireless node**

Characteristics of the source known (position, frequency, bandwidth, polarization, etc.)

EM power transmitter

EAS

EAS

Radiative vs non-radiative WPT

Far-Field radiative Coupling

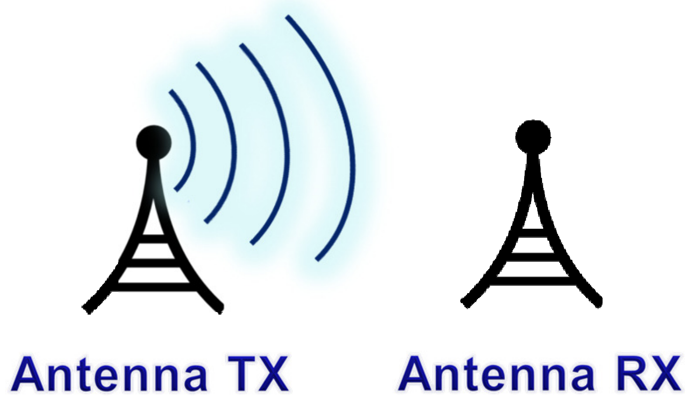

Near-Field non-radiative Coupling

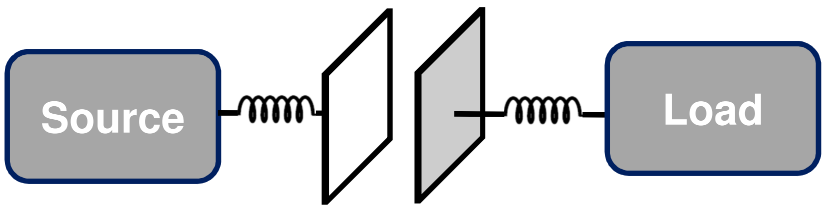

Far-Field radiative WPT

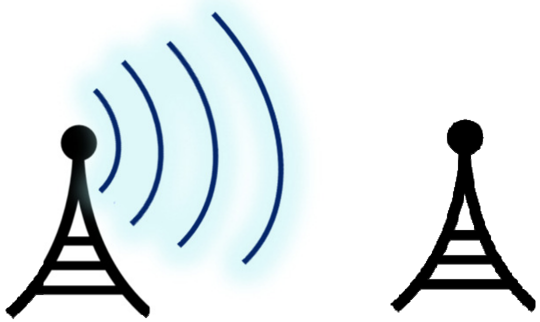

Antenna TX Antenna RX

Feature:

- ✓ **Long transfer distance**
- ✓ **High mobility**

Key devices:

Electromagnetically coupled Antennas

DESIGN OF CUSTOMIZED ANTENNAS
For energy harvesting applications broadband and circularly polarized antennas have to be preferred

Near-field non-radiative WPT

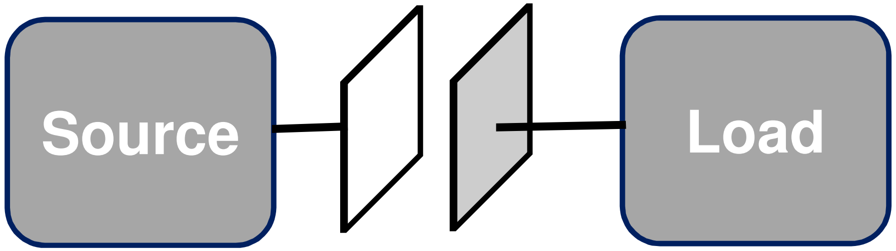

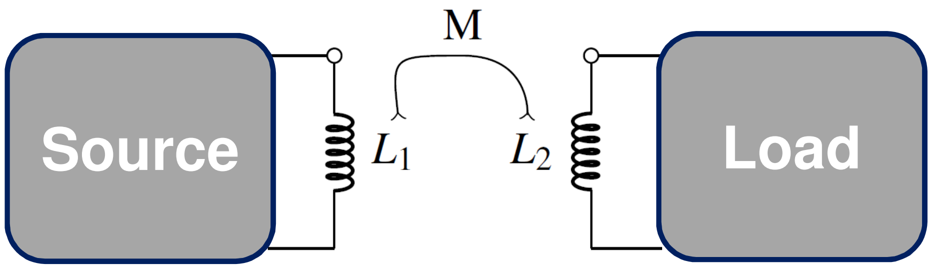

Electric Coupling:

- ✓ Sensitive to distance variations
- ✓ High interaction with the surrounding environment

Magnetic Coupling

- ✓ Low interaction with the surrounding environment
- ✓ Safer for humans

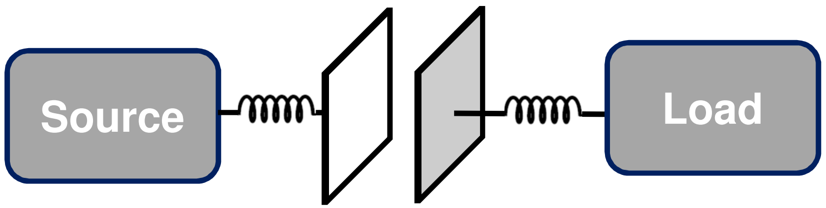

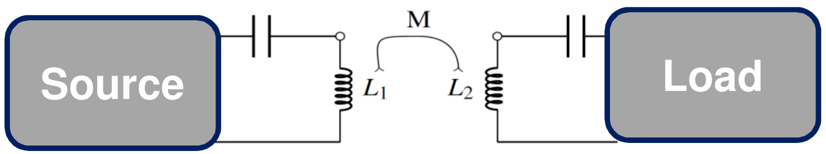

Efficient mid–range WPT links can be obtained by using resonant schemes based on magnetic coupling thus resulting in a so-called WIRELESS RESONANT ENERGY LINK

A. Kurs, et al., "Wireless Power Transfer via Strongly Coupled Magnetic Resonances." *Science* 317 (2007):

Network representation of a WPT link

How can we determine the parameters of the link for maximizing its performance?

A Network approach can be used for deriving useful design formulas

Network representation of a WPT link

The simplest implementation of a WPT occurs when a wireless link is adopted for power transmission from a single transmitter to a single receiver In this case, the link can be represented as a two-port network

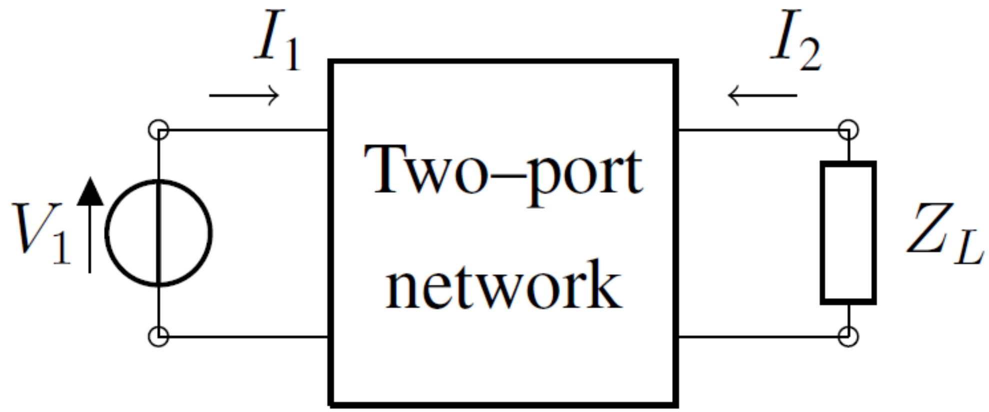

$$\bar{\bar{Z}}, \bar{\bar{Y}}$$

M. Dionigi, A. Costanzo and M. Mongiardo (2012). Network Methods for Analysis and Design of Resonant Wireless Power Transfer Systems, Wireless Power Transfer - Principles and Engineering Explorations, Dr. Ki Young Kim (Ed.), ISBN: 978-953-307-874-8, InTech.

Dionigi, M., Mongiardo, M., Perfetti, R.: Rigorous network and full-wave electromagnetic modeling of wireless power transfer links. Microwave Theory and Techniques, IEEE Transactions on 63(1), 65–75 (2015). DOI 10.1109/TMTT.2014.2376555

Network representation of a WPT link

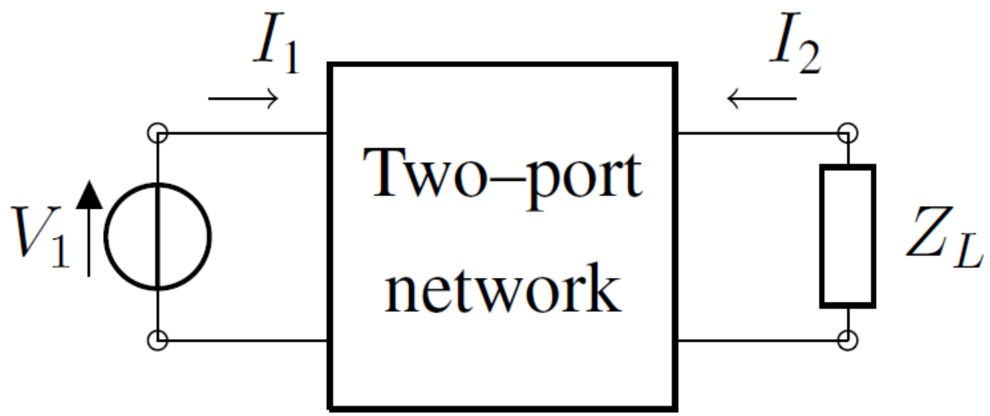

In order to introduce the variables of interest, it is assumed that a generator is on port 1 and that a load Z_L is on port 2.

active input power delivered from the generator to the two–port network

$$\bar{P}_{in} = \frac{1}{2} V_1 (I_1 \ )^*$$

active power on the load

$$\bar{P}_L = \frac{1}{2} V_2 (I_2 \ )^*$$

Network representation of a WPT link

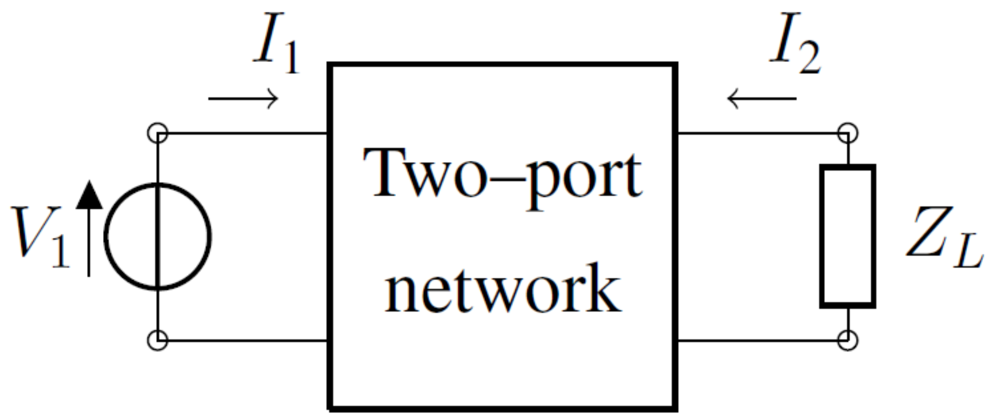

With regard to the use of the two-port network for WPT applications, two different solutions are of interest:

➔ the solution aiming at maximizing the active power delivered to the load **(MPDL solution)**;

➔ the solution aiming at maximizing the power transfer efficiency **(MPTE solution)**, η, defined as:

$$\eta = \frac{\bar{P}_L}{\bar{P}_{in}}$$

Network representation of a WPT link

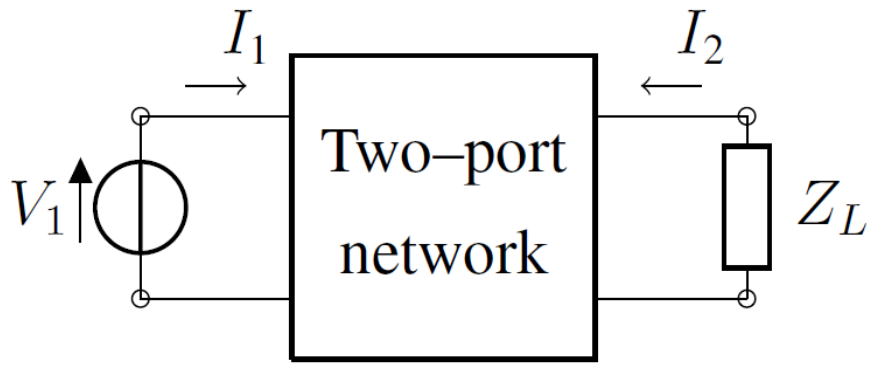

Depending on the network topology, an impedance or an admittance matrix can be more suited to model the two-port network

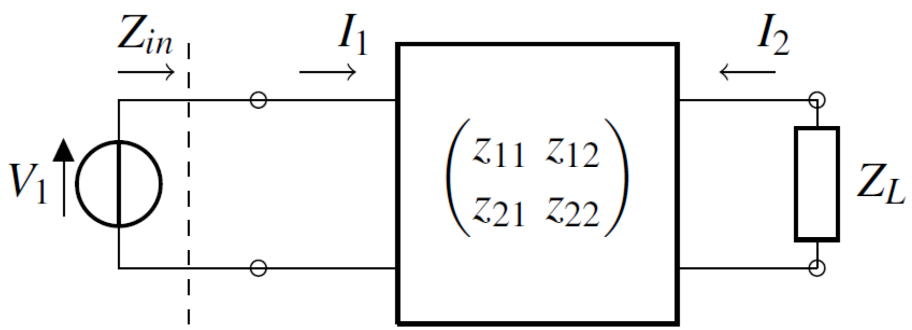

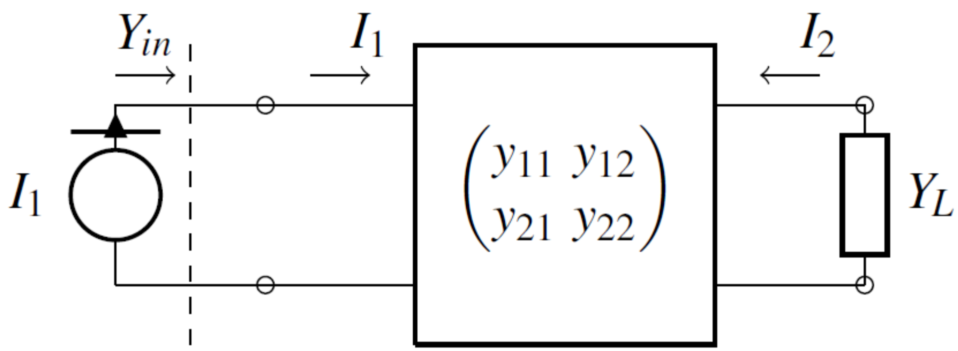

Impedance matrix representation of a two-port WPT link

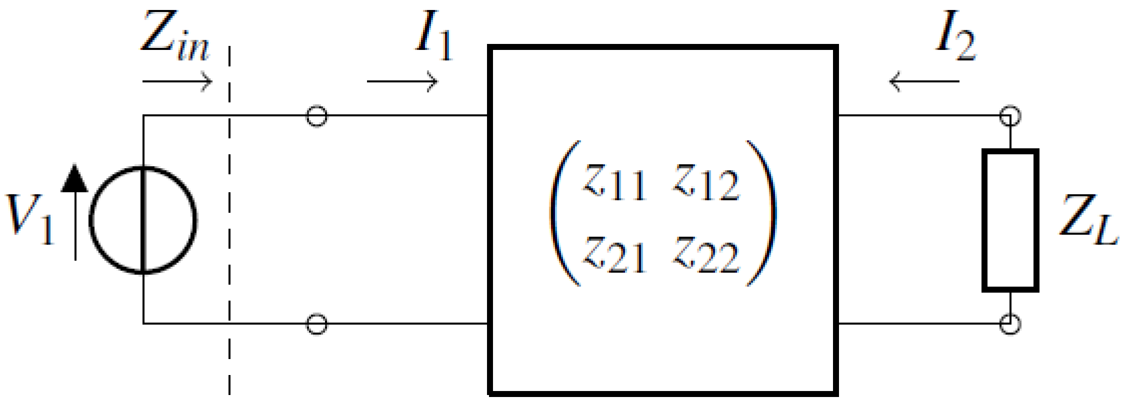

$$\mathbf{V} = \mathbf{ZI}$$

$$\mathbf{Z} = \begin{pmatrix} z_{11} & z_{12} \\ z_{21} & z_{22} \end{pmatrix}$$

$$z_{ij} = r_{ij} + jx_{ij}, (i, j = 1,2)$$

Input impedance of the network	$Z_{in} = R_{in} + jX_{in} = z_{11} - \frac{{z_{12}}^2}{z_{22} + Z_L}$
Active power delivered by the voltage generator to the network	$\bar{P}_{in} = \frac{R_{in}}{2\lvert Z_{in}\rvert^2} \lvert V_{in}\rvert^2$
Available active power assuming that the internal resistance of the generator at port 1 is r_{11}	$P_0 = \frac{\lvert V_{in}\rvert^2}{8r_{11}}$

Impedance matrix representation of a two-port WPT link

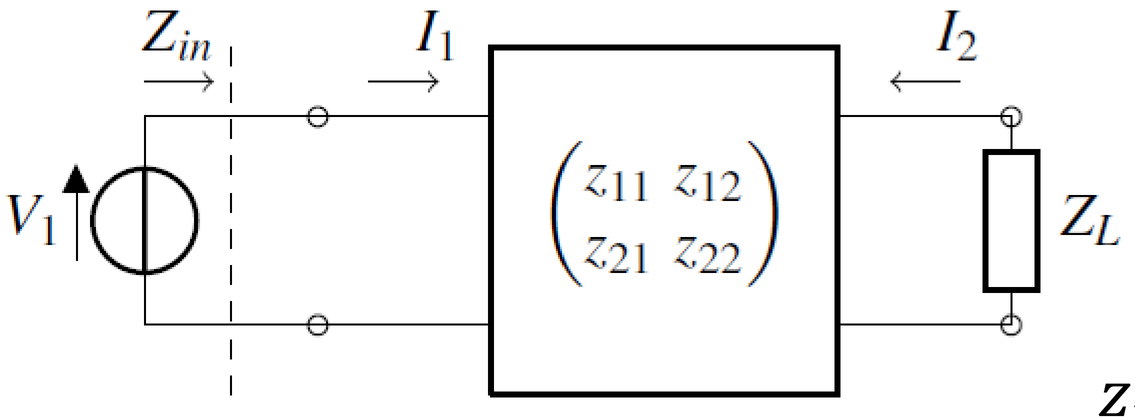

$$\mathbf{V} = \mathbf{Z}\mathbf{I}$$

$$\mathbf{Z} = \begin{pmatrix} z_{11} & z_{12} \\ z_{21} & z_{22} \end{pmatrix}$$

$$z_{ij} = r_{ij} + jx_{ij}, (i, j = 1,2)$$

Goal:

Determine the expression of the load $Z_L = R_L + j X_L$ that maximizes either the efficiency or the active power on the load

$$\bar{P}_L = \frac{R_L}{2|Z_L|^2}|V_2|^2$$

$$\eta = \frac{\bar{P}_L}{\bar{P}_{in}} = \frac{R_L}{R_{in}} \frac{|Z_{in}|^2}{|Z_L|^2} \frac{|V_2|^2}{|V_1|^2}$$

Impedance matrix representation of a two-port WPT link

It is convenient to define the parameters

$$\chi_z^2 = \frac{x_{12}^2}{r_{11} r_{22}} \qquad \xi_z^2 = \frac{r_{12}^2}{r_{11} r_{22}}$$

$$\mu_z = \frac{x_{11}}{r_{11}} \qquad \nu_z = \frac{x_{22}}{r_{22}}$$

$$\theta_{r,z} = \sqrt{1+\chi_z{}^2}\sqrt{1-\xi_z{}^2},$$
$$\theta_{x,z} = \chi_z \xi_z\,.$$

By using these parameters the Z-matrix can be expressed as

$$\mathbf{Z} = \begin{pmatrix} r_{11}\,(j\,\mu_z+1) & \sqrt{r_{11}\,r_{22}}\,(\xi_z + j\,\chi_z) \\ \sqrt{r_{11}\,r_{22}}\,(\xi_z + j\,\chi_z) & r_{22}\,(j\,\nu_z+1) \end{pmatrix}$$

The MPDL solution

The load impedance that realizes the maximum power condition is the complex conjugate of the input impedance ($Z_{2,sc}$) seen at port 2 when the generator on port 1 is short circuited

$$Z_{2,sc} = \frac{V_2}{I_2}_{|V_1=0} = \frac{1}{y_{22}} = r_{22}\left(1 + j\,v_z\right) - \frac{r_{22}\left(\xi_z + j\,\chi_z\right)^2}{\left(1 + j\mu_z\right)}$$

$$Z_L^p = R_L^p + jX_L^p$$

$$R_L^p = r_{22}\frac{\left(\mu_z^{\,2} + \chi_z^{\,2} + 1 - \xi_z^{\,2} - 2\,\chi_z\,\mu_z\,\xi_z\right)}{\mu_z^{\,2} + 1}$$

$$X_L^p = r_{22}\frac{\left(\chi_z^{\,2}\,\mu_z - \mu_z\,\xi_z^{\,2} + 2\,\chi_z\,\xi_z - \mu_z^{\,2}\,v_z - v_z\right)}{\mu_z^{\,2} + 1}$$

The MPDL solution

the active power delivered to the load, normalized with respect to $P_0 = \frac{|V_1|^2}{8r_{11}}$

$$P_L^p = \frac{\left(\xi_z^{\ 2} + \chi_z^{\ 2}\right)}{\left(1 - \xi_z^{\ 2} - 2\chi_z \mu_z \xi_z + \mu_z^{\ 2} + \chi_z^{\ 2}\right)}$$

By equating to zero the derivative of P_L with respect to μ_z it can be derived that the following relation must be satisfied:

$$\mu_z = \theta_{x,z} \quad \Rightarrow \quad x_{11} = x_{12}\frac{r_{12}}{r_{22}} \qquad z_{ij} = r_{ij} + jx_{ij},\ (i,j = 1,2)$$

This condition can be satisfied by adding a compensating reactance X_{c1} in series to port 1

$$\boxed{X_{c1} = x_{12}\frac{r_{12}}{r_{22}} - x_{11}}$$

The MPDL solution

When the compensating reactance is added to the network the following expressions can be derived for the MPDL solution

$$Z_L^p = R_L^p + jX_L^p$$

$$R_L^p = r_{22}\frac{\theta_{r,z}^2}{\theta_{x,z}^2+1}$$

$$X_L^p = -x_{22} + r_{22}\theta_{x,z} + r_{22}\frac{\theta_{x,z}\theta_{r,z}^2}{1+\theta_{x,z}^2}$$

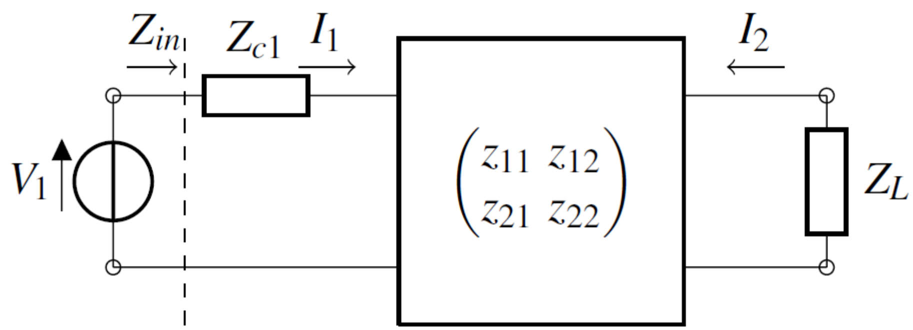

$$Z_{c1} = jX_{c1} = jx_{12}\frac{r_{12}}{r_{22}} - x_{11}$$

$$R_{in}^p = 2r_{11}\frac{\theta_{r,z}^2}{1+\theta_{r,z}^2+\theta_{x,z}^2}$$

$$\eta^p = \frac{1}{2}\frac{\chi_z^2+\xi_z^2}{1+\theta_{r,z}^2+\theta_{x,z}^2}$$

$$P_{in}^p = 2\frac{1+\theta_{r,z}^2+\theta_{x,z}^2}{\theta_{r,z}^2}$$

$$P_L^p = \frac{\chi_z^2+\xi_z^2}{\theta_{r,z}^2}$$

The MPDL solution

when $r_{12}=0$ (i.e., $Z_{12}= j\, x_{12}$) the MPDL solution simplifies as follows

Optimal load

$$Z_L^p = R_L^p + jX_L^p$$
$$R_L^p = r_{22}\theta_{r,z}^2$$
$$X_L^p = -x_{22}$$

Power on the load and efficiency

$$P_L^p = \frac{\chi_z^2}{\left(1+\chi_z^2\right)}$$

$$\eta^p = \frac{\chi_z^2}{2\left(2+\chi_z^2\right)}$$

The MPTE solution

The power transfer efficiency is expressed as the ratio between the active power delivered to the load (i.e., the power dissipated on the load impedance Z_L) and the active power delivered to the network by the generator

$$\eta = \frac{\bar{P}_L}{\bar{P}_{in}} = \frac{R_L}{R_{in}} \frac{|Z_{in}|^2}{|Z_L|^2} \frac{|V_2|^2}{|V_1|^2}$$

By using the elements of the impedance matrix to express the voltages V_1 and V_2, the following expression can be obtained for the efficiency

$$\eta = \frac{R_L}{R_{in}} \left| \frac{z_{12}}{z_{22} + Z_L} \right|^2$$

The MPTE solution

The value of the MPTE solution can be obtained by solving the following system of equations

$$\frac{\partial \eta}{\partial \{R_L\}} = 0 \qquad \frac{\partial \eta}{\partial \{X_L\}} = 0$$

$$\Downarrow$$

$$Z_L^e = R_L^e + jX_L^e$$

$$R_L^e = r_{22}\theta_{r,z}$$

$$X_L^e = r_{22}\theta_{x,z} - x_{22}$$

The MPTE solution

When port 2 is terminated on the load corresponding to the MPTE solution, the following expressions can be derived for the efficiency and the power on the load normalized to P_0 (i.e., the active power available from the generator)

$$\eta^e = \frac{{\xi_z}^2 + {\chi_z}^2}{(\theta_{r,z}+1)^2 + \theta_{x,z}^2} \qquad P_L^e = 4\frac{\theta_{r,z}\left({\xi_z}^2 + {\chi_z}^2\right)}{\left((\theta_{x,z}-\mu_z)^2 + \theta_{r,z}^2\right)\left((\theta_{r,z}+1)^2 + \theta_{x,z}^2\right)}$$

The input impedance and the normalized active input power are given by

$$Z_{in}^e = r_{11}\theta_{r,z} - j\left(r_{11}\theta_{x,z} - x_{11}\right) \qquad P_{in}^e = \frac{4\theta_{r,z}}{(\theta_{x,z}-\mu_z)^2 + \theta_{r,z}^2}$$

The MPTE solution

By observing the expressions of the power on the load and the active input power

$$P_L^e = 4\frac{\theta_{r,z}\left(\xi_z{}^2+\chi_z{}^2\right)}{\left(\left(\theta_{x,z}-\mu_z\right)^2+\theta_{r,z}^2\right)\left(\left(\theta_{r,z}+1\right)^2+\theta_{x,z}^2\right)} \qquad P_{in}^e = \frac{4\theta_{r,z}}{\left(\theta_{x,z}-\mu_z\right)^2+\theta_{r,z}^2}$$

It can be seen that they are both maximized when the following condition is satisfied

$$\mu_z = \theta_{x,z} \Rightarrow x_{11} = x_{12}\frac{r_{12}}{r_{22}}$$

This condition can be satisfied by adding in series to port 1 a compensating reactance X_{c1}

$$X_{c1} = x_{12}\frac{r_{12}}{r_{22}} - x_{11}$$

$$Z_{in}^e = r_{11}\theta_{r,z}$$

This is the same condition that has been derived for the MPDL solution: the same compensating reactance is necessary for the MPTE and the MPDL solution!

The MPTE solution

When the compensating reactance is added to the network the following expressions can be derived for the MPTE solution

$$Z_L^e = R_L^e + jX_L^e$$
$$R_L^e = r_{22}\theta_{r,z}$$
$$X_L^e = r_{22}\theta_{x,z} - x_{22}$$

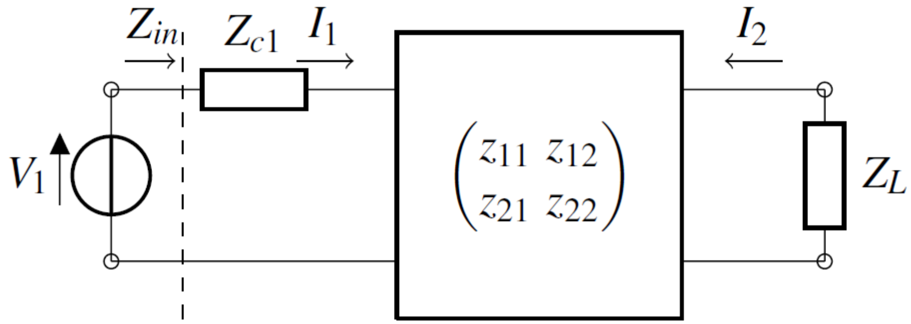

$$Z_{c1} = jX_{c1} = jx_{12}\frac{r_{12}}{r_{22}} - x_{11}$$

$$Z_{in}^e = r_{11}\theta_{r,z} \qquad \eta^e = \frac{\xi_z{}^2 + \chi_z{}^2}{(\theta_{r,z}+1)^2 + \theta_{x,z}^2}$$

$$P_{in}^e = \frac{4}{\theta_{r,z}} \qquad P_L^e = \frac{4\eta^e}{\theta_{r,z}}$$

MPTE solution case r_{12}=0

Case r_{12} =0 (i.e., Z_{12}= j x_{12})

In the case where r_{12} =0 (i.e., Z_{12}= j x_{12}), the expressions of the power on the load and of the efficiency corresponding to the MPTE solution become

$$
\begin{aligned}
Z_L^e &= R_L^e + jX_L^e \\
R_L^e &= r_{22}\theta_{r,z} \\
X_L^e &= -x_{22}
\end{aligned}
\Rightarrow
$$

$$
\eta^e = \frac{{\chi_z}^2}{(1+\sqrt{1+{\chi_z}^2})^2}
$$

$$
P_L^e = \frac{4\chi_z^2}{\sqrt{1+\chi_z^2}\left(1+\sqrt{1+\chi_z^2}\right)^2}
$$

MPDL vs MPTE solution

MPDL solution

$$Z_L^p = R_L^p + jX_L^p$$

$$R_L^p = r_{22}\frac{\theta_{r,z}^2}{\theta_{x,z}^2 + 1}$$

$$X_L^p = -x_{22} + r_{22}\theta_{x,z} + r_{22}\frac{\theta_{x,z}\theta_{r,z}^2}{1+\theta_{x,z}^2}$$

MPTE solution

$$Z_L^e = R_L^e + jX_L^e$$

$$R_L^e = r_{22}\theta_{r,z}$$

$$X_L^e = r_{22}\theta_{x,z} - x_{22}$$

it is evident that, in the general case, the MPTE solution has both the real and the imaginary parts different from the ones corresponding to the MPDL solution

MPDL vs MPTE solution

Case $r_{12} = 0$ (i.e., $Z_{12} = j\, x_{12}$)

MPDL solution

$$\boxed{\begin{aligned} Z_L^p &= R_L^p + jX_L^p \\ R_L^p &= r_{22}\theta_{r,z}^2 \\ X_L^p &= -x_{22} \end{aligned}}$$

MPTE solution

$$\boxed{\begin{aligned} Z_L^e &= R_L^e + jX_L^e \\ R_L^e &= r_{22}\theta_{r,z} \\ X_L^e &= -x_{22} \end{aligned}}$$

In this case the MPTE and the MPDL solutions have the same imaginary part: the reactive part of the optimal load is the same for both the MPDL and the MPTE solution

Optimal design of a WPT link: the MPTE and MPDL solution

Table 1 Impedance matrix representation of a two-port WPT link: a summary of the parameters' values for the approaches that maximize efficiency and power. The parameters have the following meanings: $\chi_z = x_{12}/\sqrt{r_{11}r_{22}}$, $\xi_z = r_{12}/\sqrt{r_{11}r_{22}}$, $\theta_{r,z} = \sqrt{1+\chi_z{}^2}\sqrt{1-\xi_z{}^2}$, $\theta_{x,z} = \chi_z\xi_z$. The power has been normalized w.r.t. $P_0 = |V_1|^2/(8r_{11})$.

Parameter	maximum efficiency	maximum power
R_L	$r_{22}\theta_{r,z}$	$r_{22}\theta_{r,z}^2/(\theta_{x,z}^2+1)$
X_L	$r_{22}\theta_{x,z} - x_{22}$	$-x_{22} + r_{22}\theta_{x,z} + r_{22}\theta_{x,z}\theta_{r,z}^2/(\theta_{x,z}^2+1)$
R_{c1}	0	0
X_{c1}	$x_{12}r_{12}/r_{22} - x_{11}$	$x_{12}r_{12}/r_{22} - x_{11}$
R_{in}	$r_{11}\theta_{r,z}$	$2r_{11}\theta_{r,z}^2/(1+\theta_{r,z}^2+\theta_{x,z}^2)$
X_{in}	0	0
P_{in}	$4/\theta_{r,z}$	$2(1+\theta_{r,z}^2+\theta_{x,z}^2)/\theta_{r,z}^2$
P_L	$4\eta^e/\theta_{r,z}$	$(\xi_z^2+\chi_z^2)/\theta_{r,z}^2$
η	$\eta^e = (\xi_z^2+\chi_z^2)/((1+\theta_{r,z})^2+\theta_{x,z}^2)$	$(\xi_z^2+\chi_z^2)/(2(1+\theta_{r,z}^2+\theta_{x,z}^2))$

MPDL solution vs MPTE solution power on the load behaviour

Power on the load corresponding to the MPDL solution

$$P_L^p = \frac{\chi_z^2}{(1+\chi_z^2)}$$

$$\chi_z \to \infty$$

$$P_L^p \to 1$$

This means that the power on the load approaches the generator available power

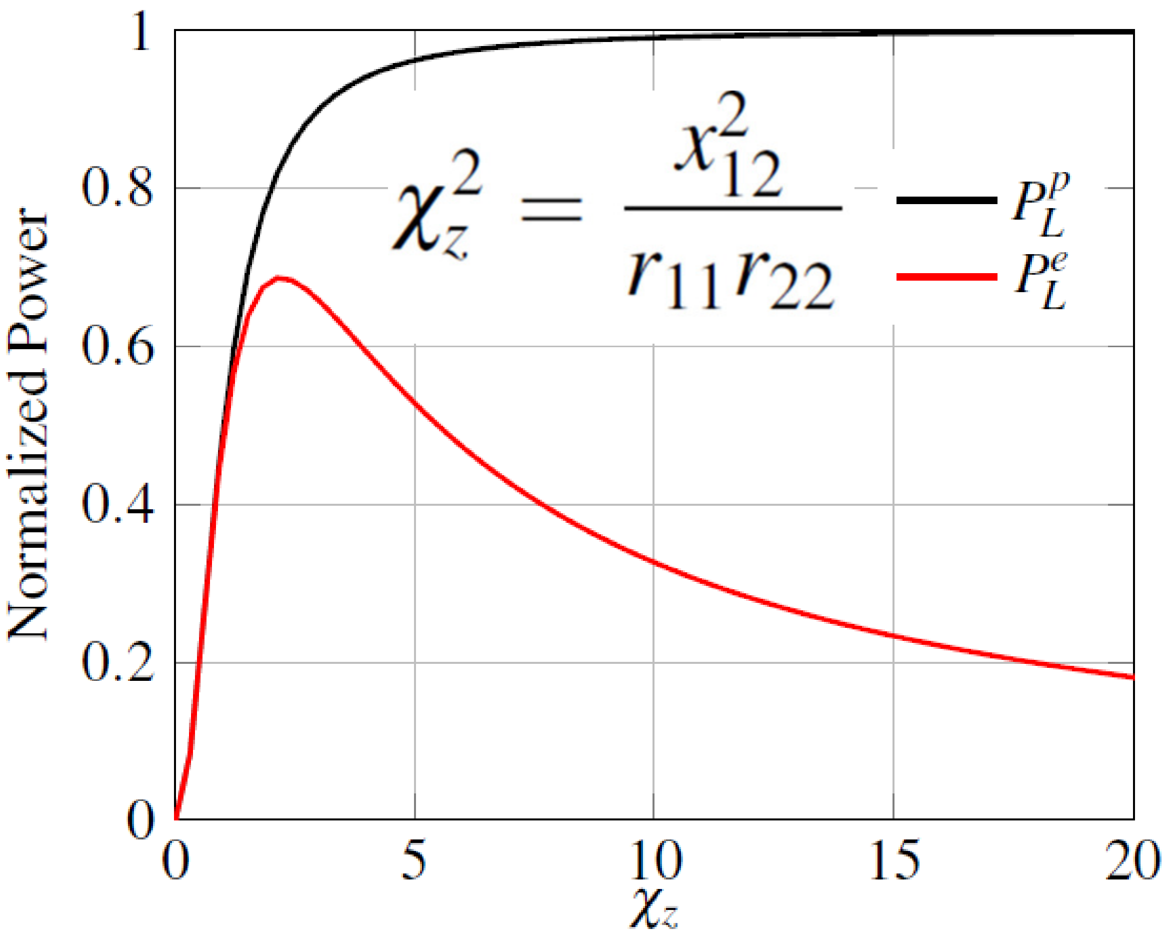

MPDL solution vs MPTE solution power on the load behaviour

Power on the load corresponding to the MPTE solution

$$P_L^e = \frac{4\chi_z^2}{\sqrt{1+\chi_z^2}\left(1+\sqrt{1+\chi_z^2}\right)^2}$$

$$\chi_z \to \infty$$

$$P_L^e \to P_0/\chi_z$$

As a consequence, for the MPTE solution, when the efficiency tends to one the output power reduces to zero

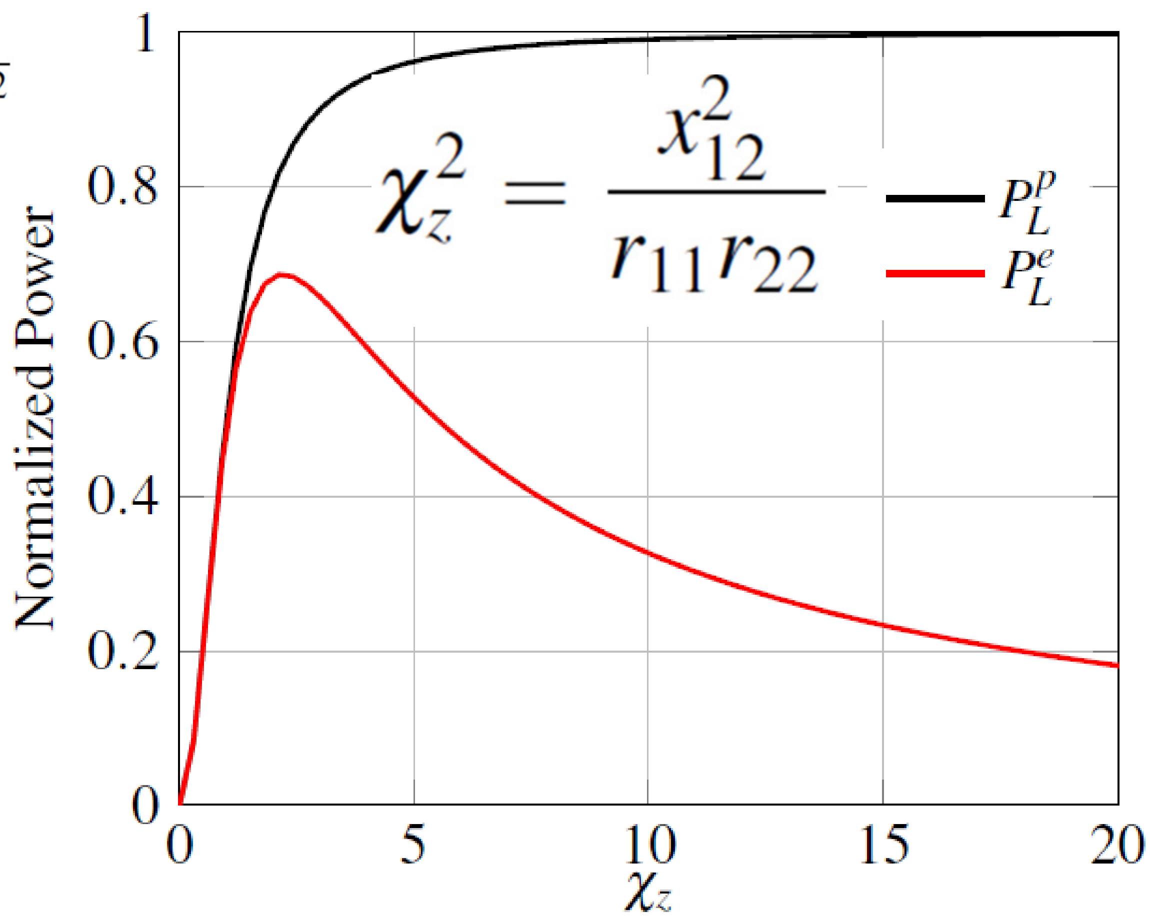

MPDL solution vs MPTE solution efficiency behaviour

Efficiency corresponding to the MPDL solution

$$\eta^p = \frac{\chi_z^2}{2\left(2+\chi_z^2\right)}$$

$$\chi_z \rightarrow \infty$$

$$\eta_\infty^p \rightarrow 1/2$$

in this case the asymptotic value of the efficiency is 0.5, and thus lower that the maximum achievable value of 1

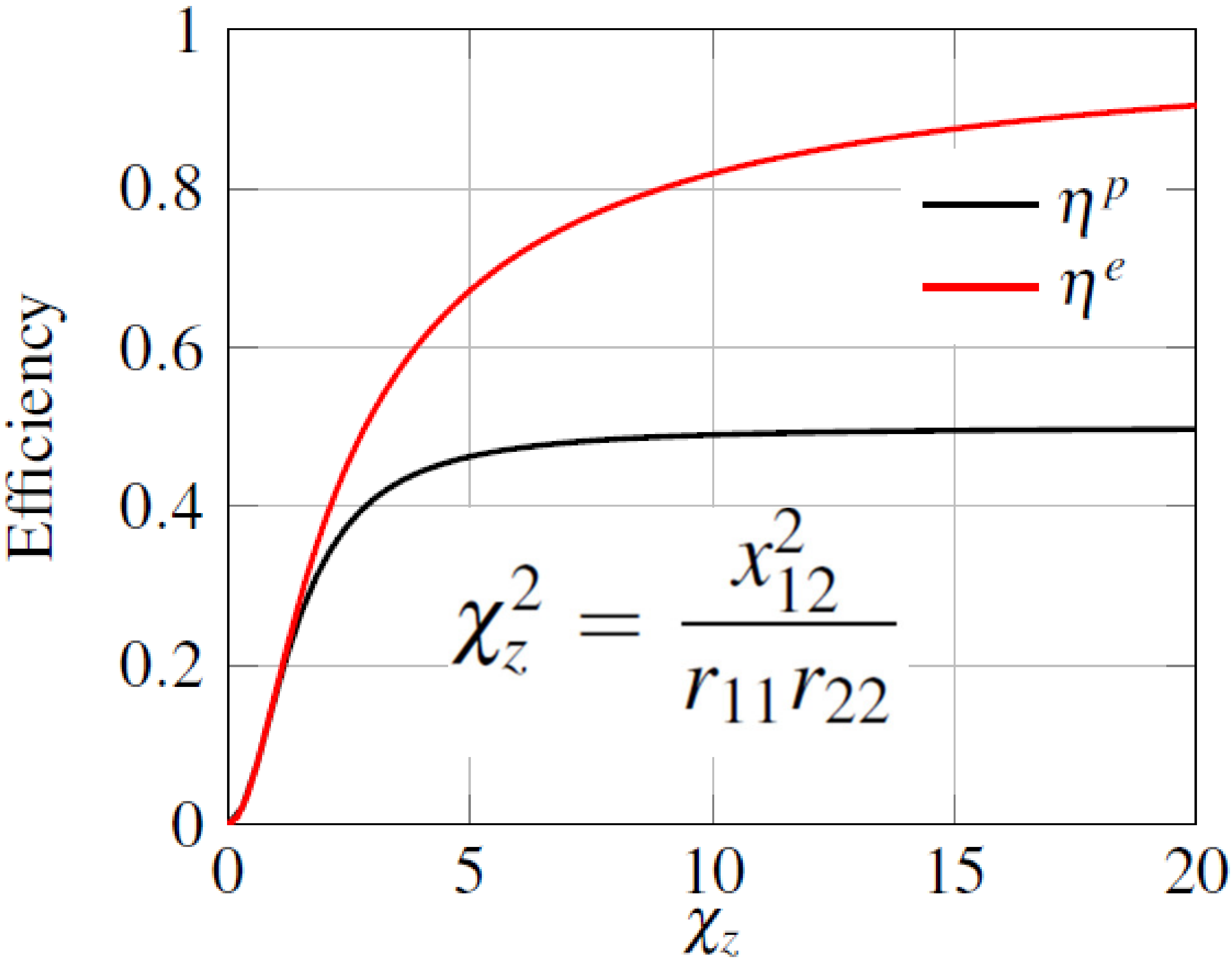

MPDL solution vs MPTE solution efficiency behaviour

Efficiency corresponding to the MPTE solution

$$\eta^e = \frac{\chi_z{}^2}{(1+\sqrt{1+\chi_z{}^2})^2}$$

$$\chi_z \rightarrow \infty$$

$$\eta^e_\infty \rightarrow 1$$

in this case the asymptotic value is the maximum achievable value

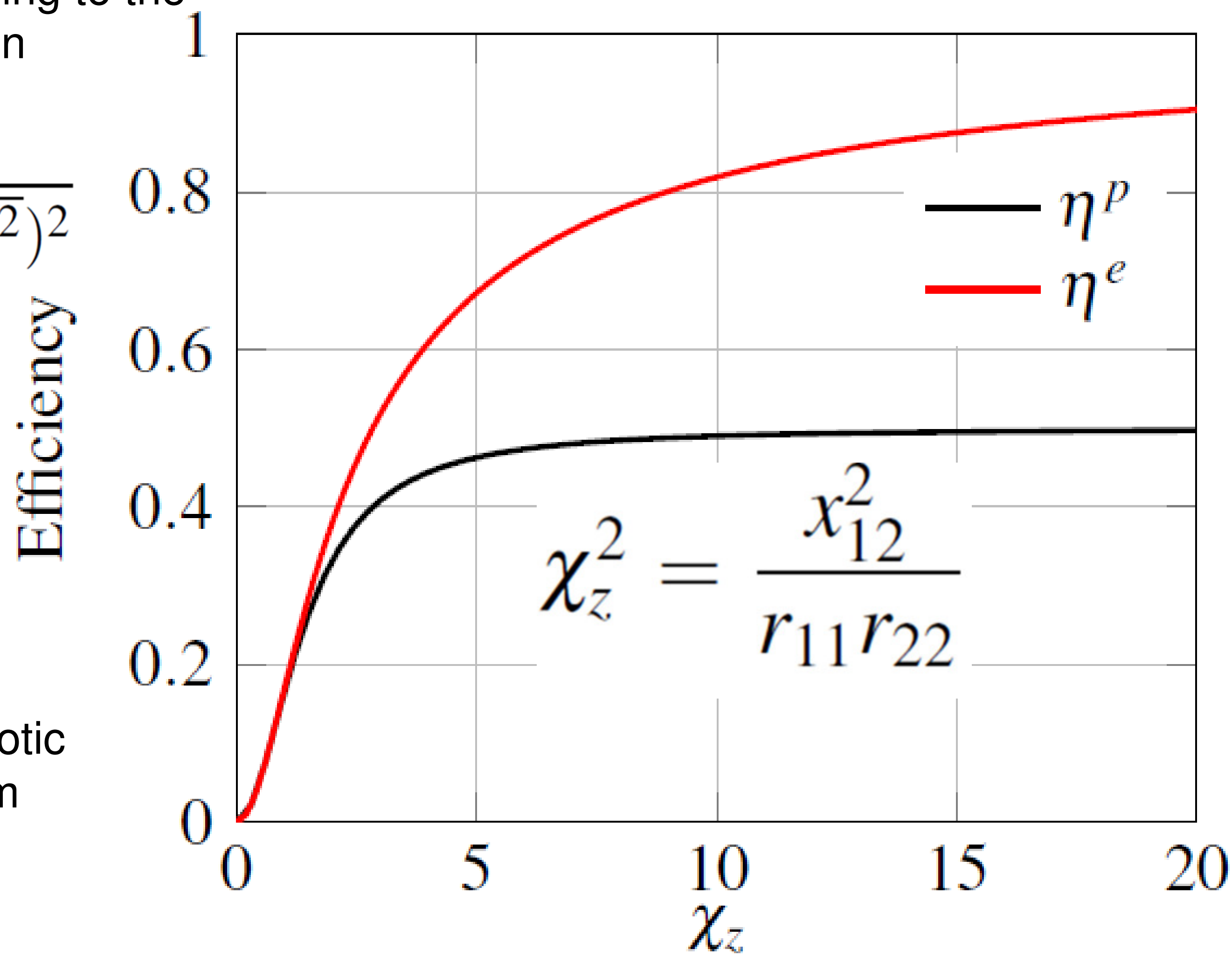

The case of two coupled inductors

The simplest case of WPT that can be conveniently described by using an impedance matrix approach is provided by two coupled inductors.

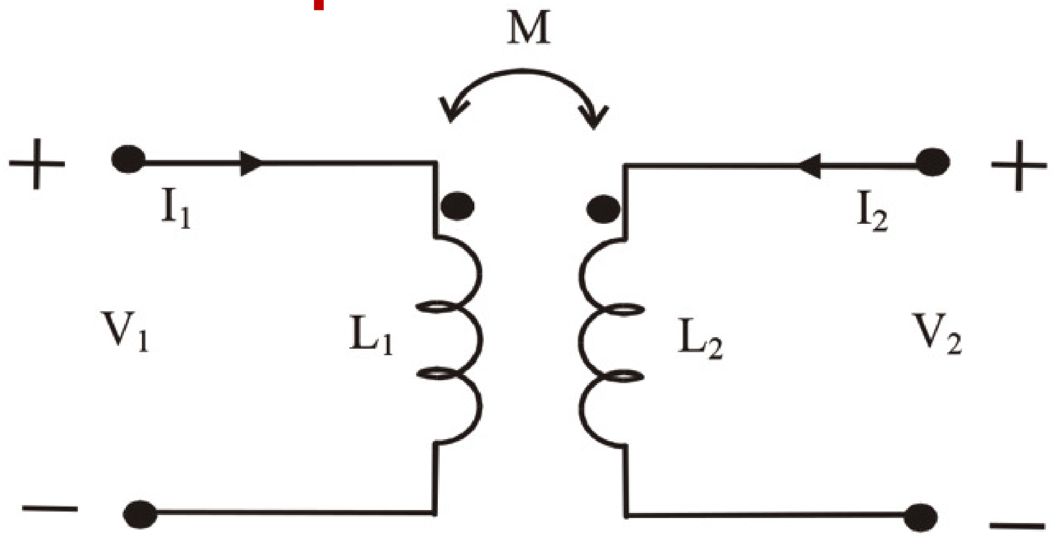

The coupling coefficient *k* is typically used to represent the efficiency of energy transfer from the transmitter coil to the receiver coil; this coupling coefficient is given by the expression in terms of the mutual inductance and the self-inductances

mutual inductance

$$M = k\sqrt{L_1 L_2}$$

The case of two coupled inductors

The impedance matrix of the two coupled inductors is

$$z_{ij} = r_{ij} + jx_{ij}, (i, j = 1{,}2)$$

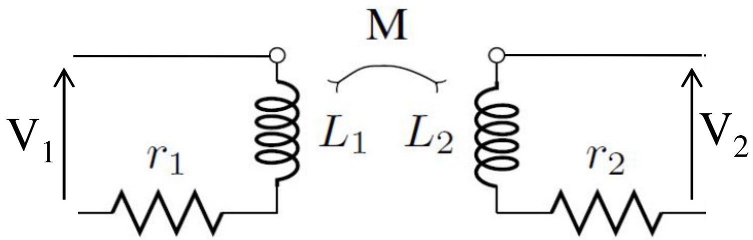

$$\begin{bmatrix} z_{11} & z_{12} \\ z_{21} & z_{21} \end{bmatrix} = \begin{bmatrix} r_1 + j\omega L_1 & j\omega M \\ j\omega M & r_2 + j\omega L_2 \end{bmatrix}$$

r_1 and r_2 are series resistances representing the system loss and are related to the Q factor of the inductors

$$r_i = \frac{\omega_0 L_i}{Q_i} \; (i = 1{,}2)$$

The case of two coupled inductors

The impedance matrix of the two coupled inductors is

$$\begin{bmatrix} z_{11} & z_{12} \\ z_{21} & z_{21} \end{bmatrix} = \begin{bmatrix} r_1 + j\omega L_1 & j\omega M \\ j\omega M & r_2 + j\omega L_2 \end{bmatrix}$$

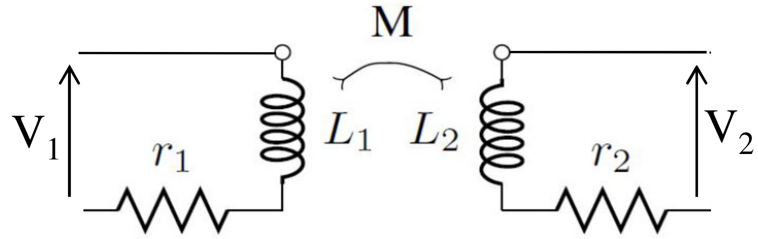

$$\chi_z^2 = \frac{x_{12}^2}{r_{11} r_{22}}$$

$$\xi_z^2 = \frac{r_{12}^2}{r_{11} r_{22}}$$

$$\theta_{r,z} = \sqrt{1+\chi_z{}^2}\sqrt{1-\xi_z{}^2},$$
$$\theta_{x,z} = \chi_z \xi_z \,.$$

It can be seen that in this case the term $Z_{12} = j\, x_{12}$, i.e. we are in the case $r_{12} = 0$

$$\chi_z^2 = k_0^2 Q_1 Q_2 \qquad \theta_{r,z} = \sqrt{1+\chi_z^2}$$
$$\xi_z^2 = 0 \qquad \theta_{x,z} = 0$$

The case of two coupled inductors

The compensating reactance to be added at port 1 is given by

$$X_{c1} = x_{12}\frac{r_{12}}{r_{22}} - x_{11} = -\omega L_1$$

Assuming that the operating frequency of the link is ω_0, the compensating reactance is the capacitance to be added in series to L_1 for realizing the resonance condition at ω_0

$$C_1 = 1/(\omega_0^2 L_1)$$

Similarly, the reactive part of the load impedance of both the MPDL and the MPTE solution, is given by

$$X_L = X_L^p = X_L^e = -x_{22} = -\omega L_2$$

X_L is the capacitance C_2 to be added in series to L_2 for realizing the resonance condition at ω_0

$$C_2 = 1/(\omega_0^2 L_2).$$

The reactances to be added in series to port 1 and port 2 for the MPDL and the MPTE solutions are the same: these reactances are the ones realizing a resonat coupling

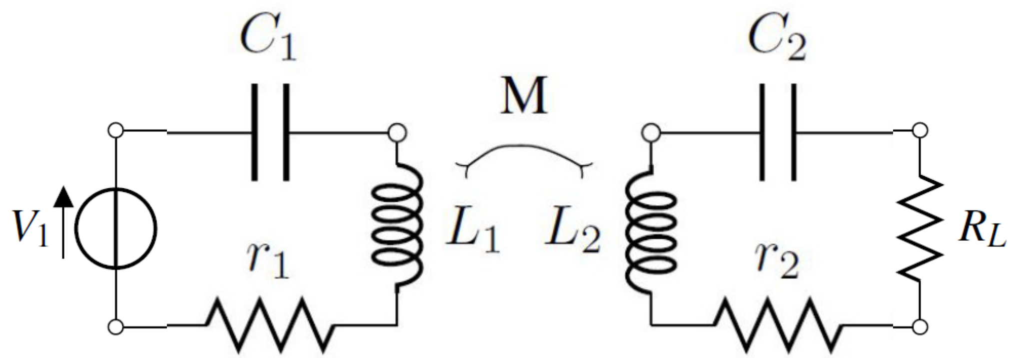

The case of two coupled inductors

The MPTE solution

$$R_L{}^e = r_{22}\sqrt{1+{\chi_z}^2} = r_2\sqrt{1+{k_0}^2 Q_2 Q_1} \qquad Z_{in}{}^e = R_{in} = r_{11}\sqrt{1+{\chi_z}^2} = r_1\sqrt{1+{k_0}^2 Q_2 Q_1}$$

$$\eta^e = \frac{{\xi_z}^2 + {\chi_z}^2}{\left(1+{\vartheta_{r,z}}^2\right)^2 + {\vartheta_{x,z}}^2} = \frac{{k_0}^2 Q_2 Q_1}{1+{k_0}^2 Q_2 Q_1} \qquad P_L{}^e = 4\frac{\eta^e}{\vartheta_{r,z}} = \frac{4}{\sqrt{1+{k_0}^2 Q_2 Q_1}}\frac{{k_0}^2 Q_2 Q_1}{1+{k_0}^2 Q_2 Q_1}$$

The MPDL solution

$$R_L{}^p = r_{22}(1+{\chi_z}^2) = r_2(1+{k_0}^2 Q_2 Q_1) \qquad Z_{in}{}^p = R_{in} = r_{11}\left(1+{\chi_z}^2\right) = r_1\left(1+{k_0}^2 Q_2 Q_1\right)$$

$$\eta^p = \frac{{\xi_z}^2 + {\chi_z}^2}{2\left(1+{\vartheta_{r,z}}^2 + {\vartheta_{x,z}}^2\right)} = \frac{{k_0}^2 Q_2 Q_1}{2\left(1+{k_0}^2 Q_2 Q_1\right)} \qquad P_L{}^p = \frac{{\xi_z}^2 + {\chi_z}^2}{{\vartheta_{r,z}}^2} = \frac{{k_0}^2 Q_2 Q_1}{1+{k_0}^2 Q_2 Q_1}$$

The case of two coupled inductors: MPDL solution vs MPTE solution

$$\chi_z^2 = k_0^2 Q_1 Q_2$$

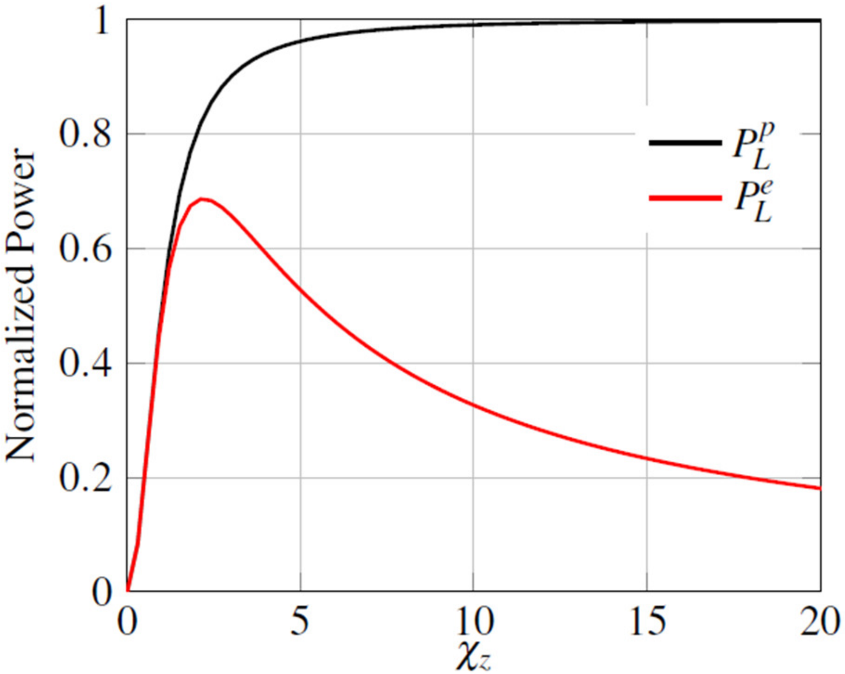

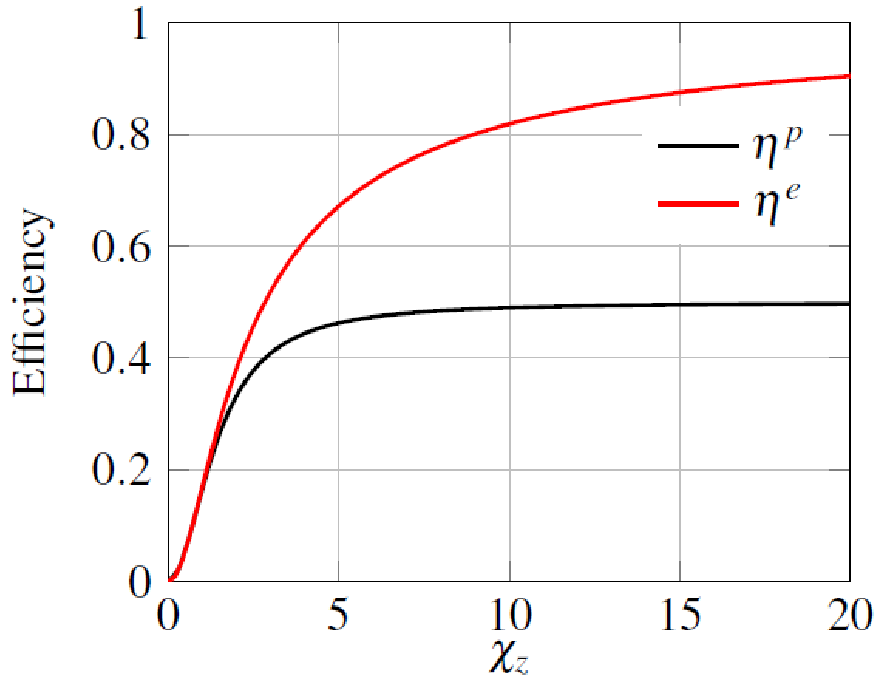

$$P_L{}^p = \frac{k_0{}^2 Q_2 Q_1}{1 + k_0{}^2 Q_2 Q_1}$$

$$P_L{}^e = \frac{4}{\sqrt{1 + k_0{}^2 Q_2 Q_1}} \frac{k_0{}^2 Q_2 Q_1}{1 + k_0{}^2 Q_2 Q_1}$$

$$\eta^p = \frac{k_0{}^2 Q_2 Q_1}{2\left(1 + k_0{}^2 Q_2 Q_1\right)}$$

$$\eta^e = \frac{k_0{}^2 Q_2 Q_1}{1 + k_0{}^2 Q_2 Q_1}$$

MPDL or MPTE solution?

An alternative could be the introduction of a figure of merit (FOM) defined taking into account both the efficiency of the link and the power on the load

$$FOM = \eta^{\alpha} \times P_L$$

Where α is the prioritization number, which depends on the importance of η over P_L for the specific application of interest .

J. P. K. Sampath, A. Alphones, and D. M. Vilathgamuwa, "Tunable Metamaterials for Optimization of Wireless Power Transfer Systems," in *Antennas and Propagation Society International Symposium (APSURSI), 2015 IEEE*, 2015

WPT links: Applications

WPT links for wearable and implantable devices

Motivations

On-Body

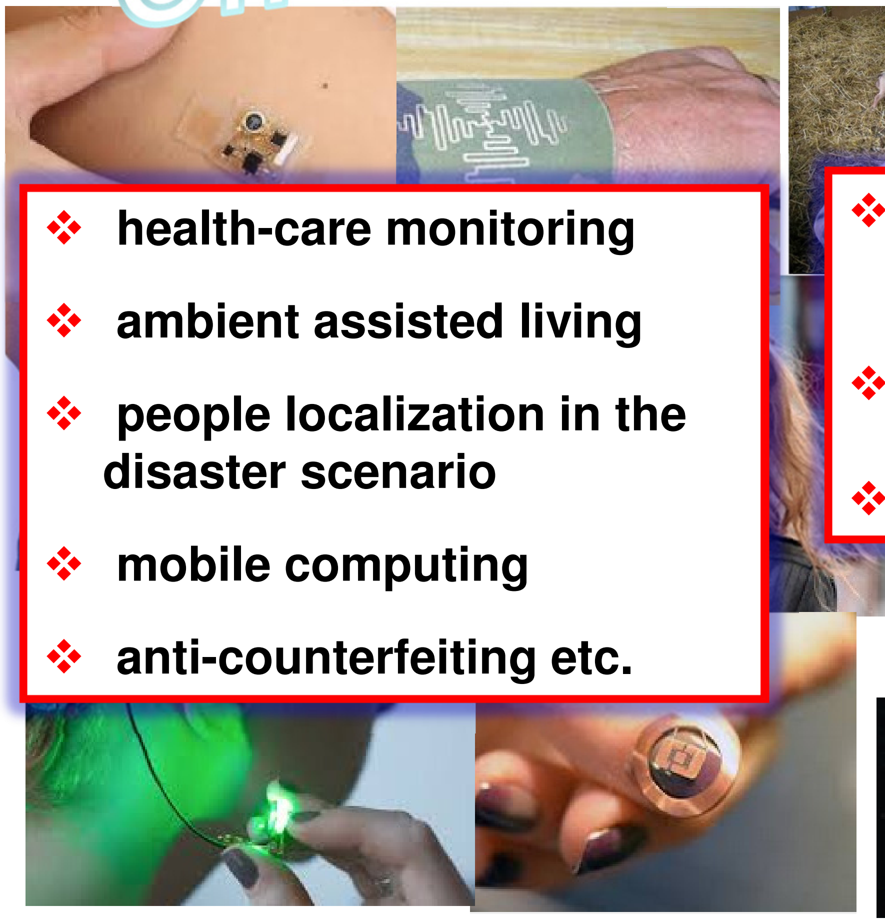

- health-care monitoring
- ambient assisted living
- people localization in the disaster scenario
- mobile computing
- anti-counterfeiting etc.

In-Body

- Medical Implants for the treatment of important diseases
- Tracking and tracing in agro-food chain
- Livestocks monitoring

Enabling Technologies

ON-Body/wearable solutions
In-Body/implanted solutions

KEYWORDS

- Energy autonomy
- Non-intrusive
- Effective
- Seamless integration

- Wireless technology for data and power transmission
- Non-conventional materials and fabrication techniques
- Customized solutions

Enabling Technologies

Contactless Power and Data transfer → **Wearable/Implantable Devices for power and data transmission**

WPT and EH for wearable applications

G. Monti, L. Corchia, L. Tarricone, “**Fabrication Techniques for Wearable antennas**,” *in Proc. of 42th EuRAD*, Nuremberg, pp.: 435-438, Oct. 9-11, 2013.

G. Monti, L. Corchia, L. Tarricone, “**Logo Antenna on Textile Materials,**” *2014 EUMC*, Rome, Italy, Oct. 2014.

Materials and Fabrication Techniques

- Cutting Plotter & Adhesive Copper Tape


- Hand Embroidery & Conductive Thread


- Cutting plotter & Adhesive Conductive Non Woven


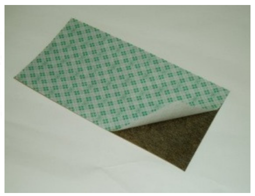

Fabrication Techniques for Wearable devices

Cutting Plotter & Adhesive Copper Tape

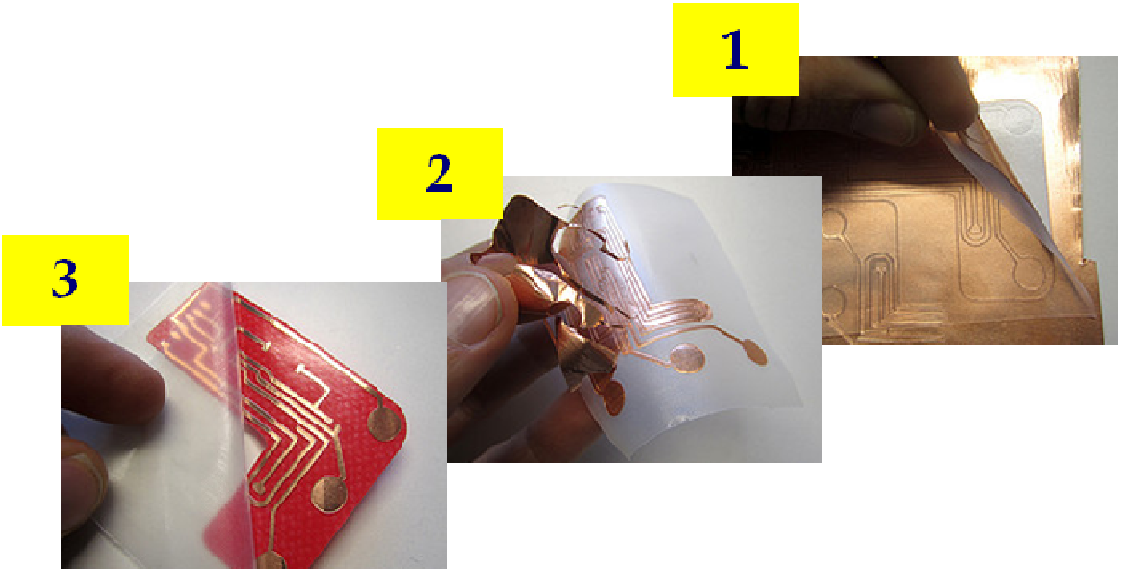

- Time-saving, low cost and easy industrial implementation
- NO stretching, NO washing and NO ironing

Fabrication Techniques for Wearable Devices

Hand Embroidery & Conductive Thread

YES stretching, YES washing YES ironing; antenna with very complex layout.

An accurate numerical model of the embroidered pattern requires a great computational efforts. Often, a simplified model must be used at the cost of the results accuracy.

Fabrication Techniques for Wearable Devices

Cutting plotter & Adhesive Conductive Non-Woven

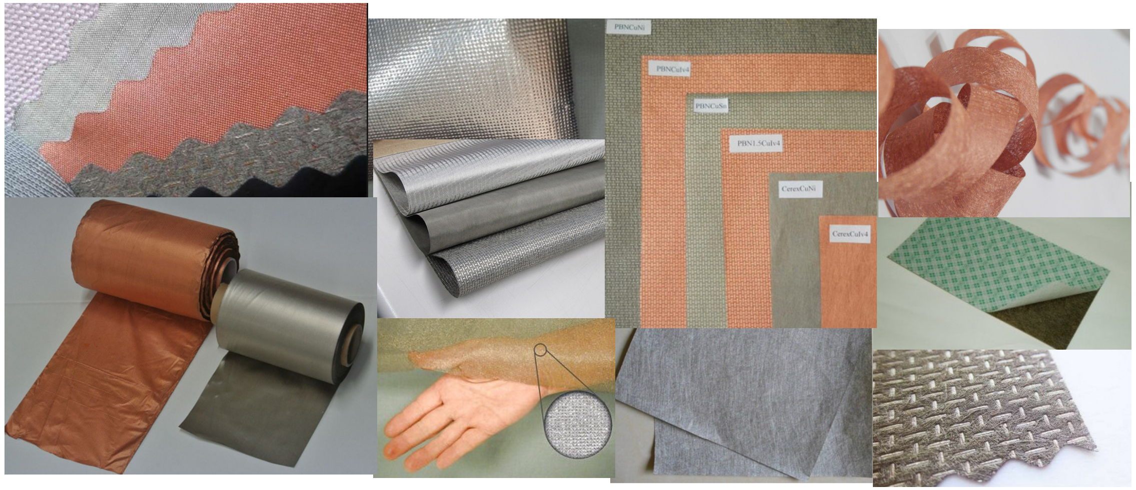

Easy industrial implementation, complex antennas layout, flexible, wearable, NO problem with washing and ironing; <u>Low-cost, Mechanical resistance, NO fraying problem</u>.

The flexibility depends on fabric and adhesive thickness.

Fabrication Techniques for Wearable Devices

Cutting plotter & Adhesive Conductive Non-Woven

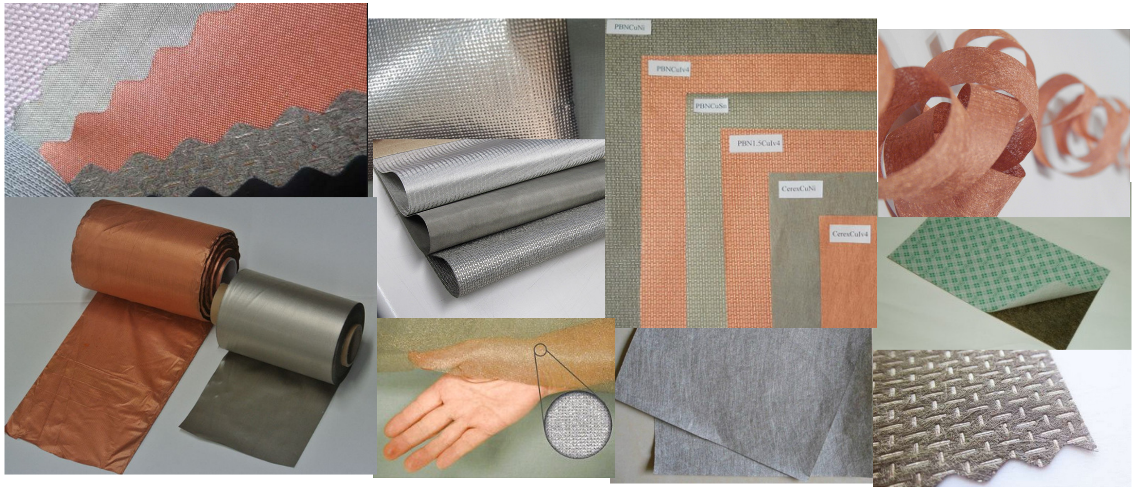

This solution appears as a good trade-off between performance and efforts required by the design and fabrication process.

Examples of application

UHF Wearable Rectenna for harvesting the electromagnetic energy associated to RFID systems

UHF Wearable Rectenna on Textile Materials

Schematic representation of a RECTENNA (Rectifying Antenna)

$$\eta_{RF-DC} = \frac{P_{OUT,DC}}{S_{RF} A_{eff}} = \left(\frac{V_{DC}^2}{R_L} \right) \frac{1}{S_{RF} A_{eff}}$$

S_{RF} = *power density incident on the antenna*

V_{DC} = *DC output voltage*

R_L = *resistive load*

A_{eff} = *effective area of patch*

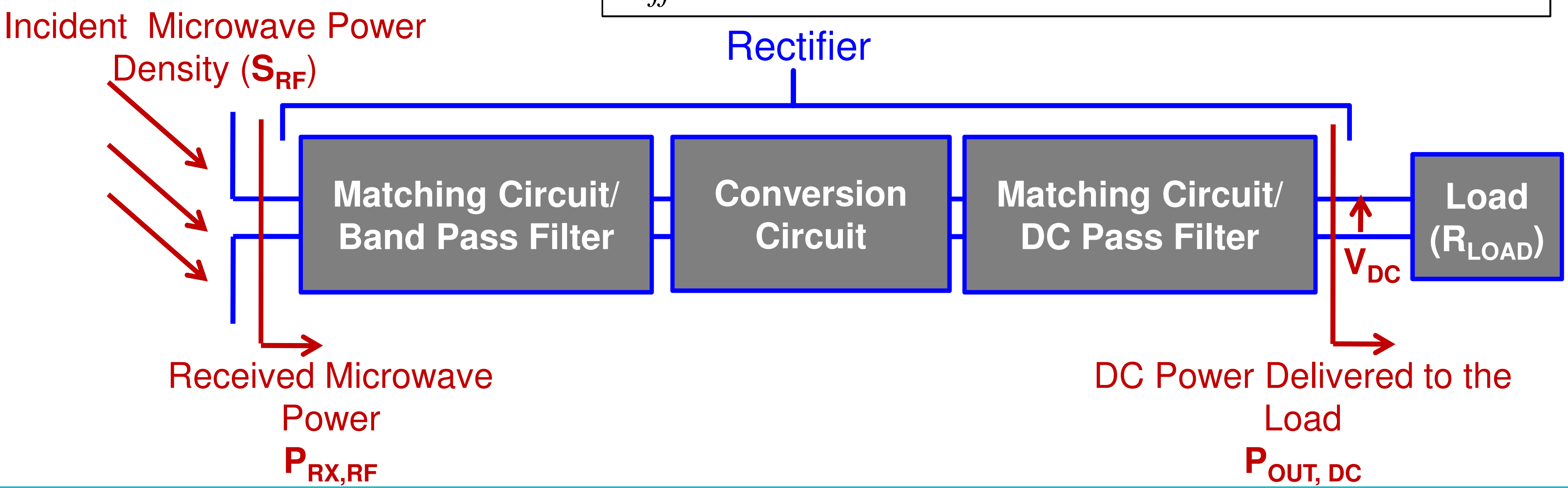

UHF Wearable Rectenna on Textile Materials

G. Monti, L. Corchia, L. Tarricone, “UHF Wearable Rectenna on Textile Materials,” IEEE Transactions on Antennas and Propagation published by IEEE , Vol. 61, Issue 7, pp. 3869–3873, 2013.

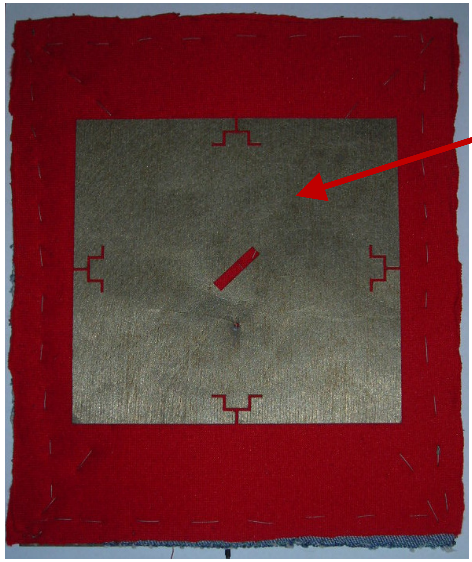

Front View

BackView

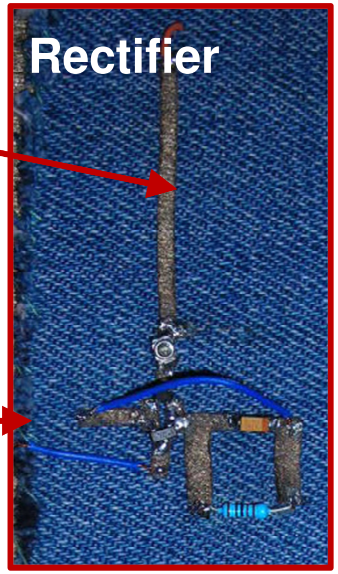

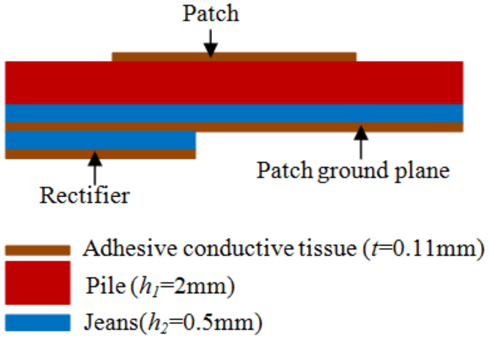

UHF Wearable Rectenna on Textile Materials

G. Monti, L. Corchia, L. Tarricone, “UHF Wearable Rectenna on Textile Materials,” IEEE Transactions on Antennas and Propagation, Vol. 61, Issue 7, pp. 3869–3873, 2013.

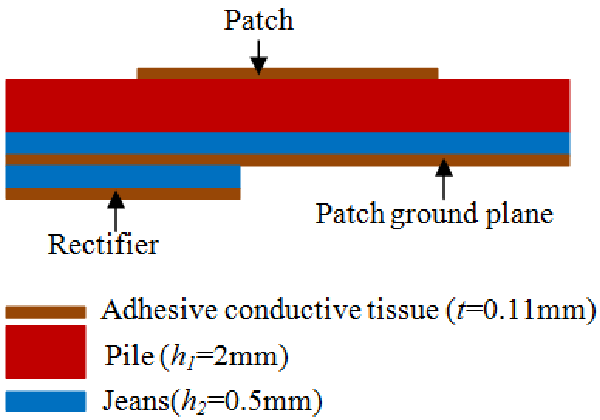

Conductive fabric:
Resistivity: 0.04Ω/square
Thickness: 0.11mm

Substrates:
ε_{pile}= 1.12
ε_{jeans} = 1.67

UHF Wearable Rectenna on Textile Materials

G. Monti, L. Corchia, L. Tarricone, “UHF Wearable Rectenna on Textile Materials,” IEEE Transactions on Antennas and Propagation Vol. 61, Issue 7, pp. 3869–3873, 2013.

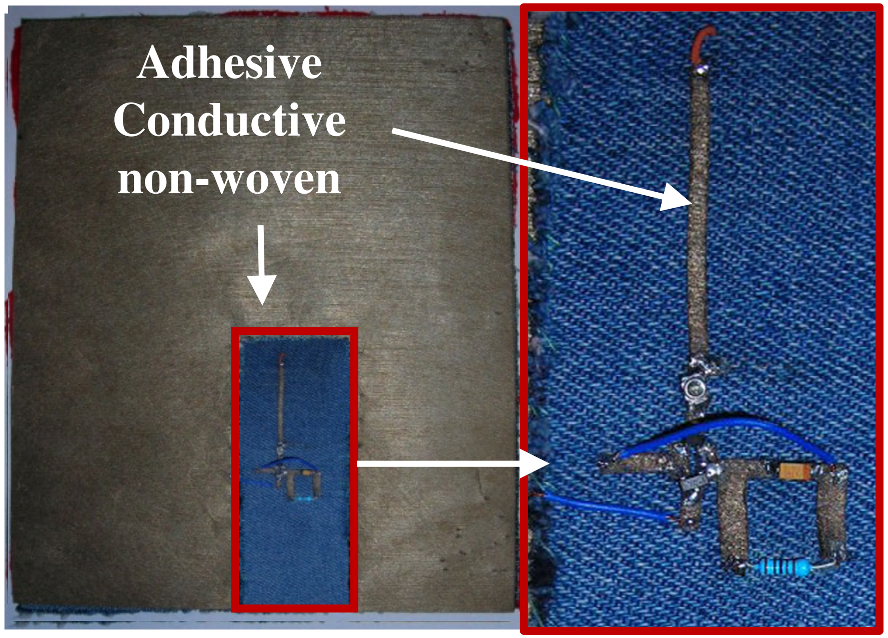

BackView

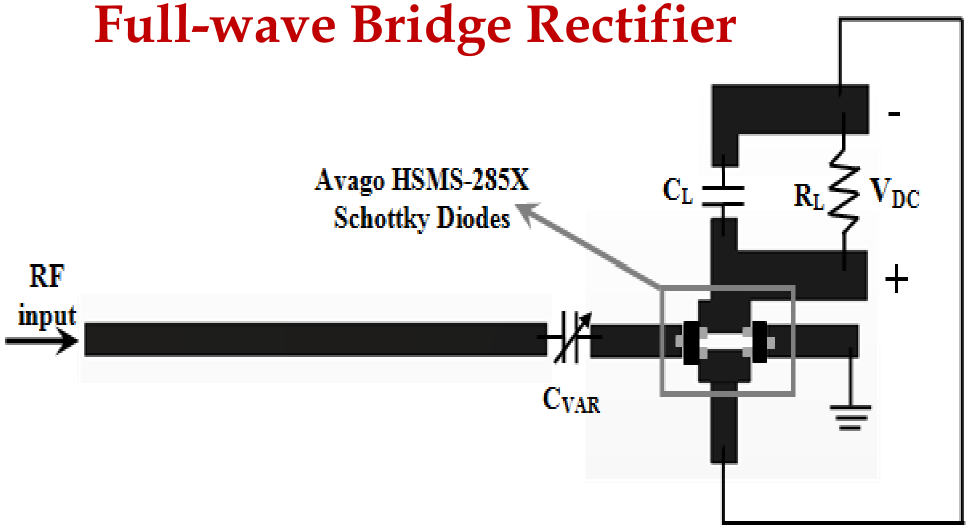

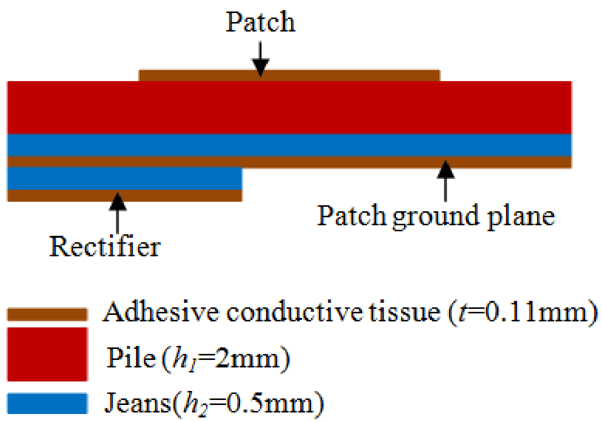

Conductive fabric:
Resistivity: 0.04Ω/square
Thickness: 0.11mm

Substrates:

$\varepsilon_{pile} = 1.12$
$\varepsilon_{jeans} = 1.67$

UHF Wearable Rectenna on Textile Materials

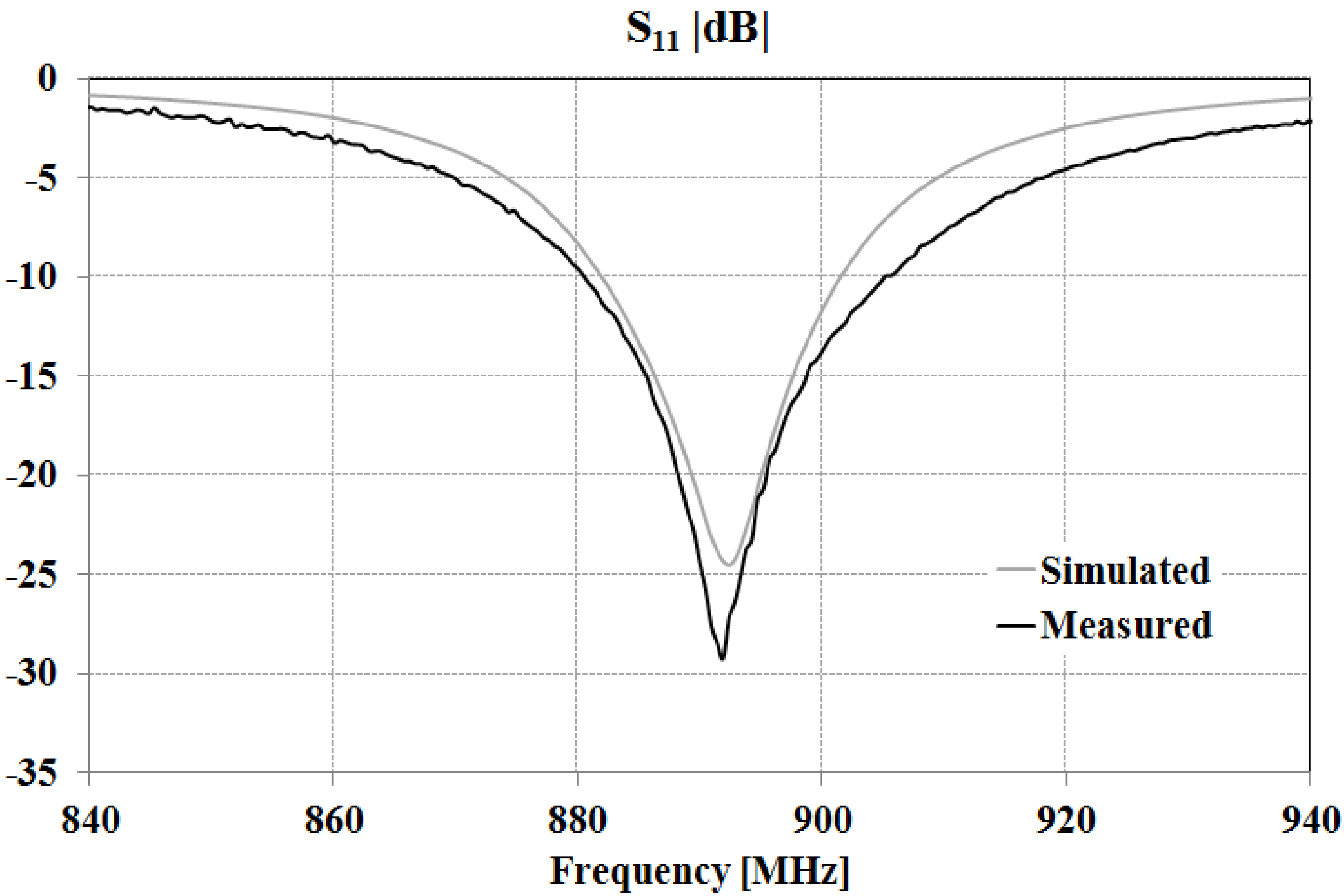

$BW_{-10\ dB}$: 880-905 MHz

UHF Wearable Rectenna on Textile Materials

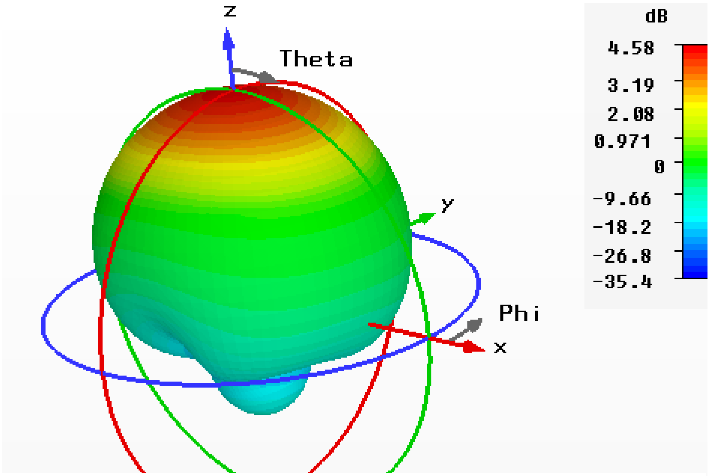

Front-to-Back ratio = 20 dB

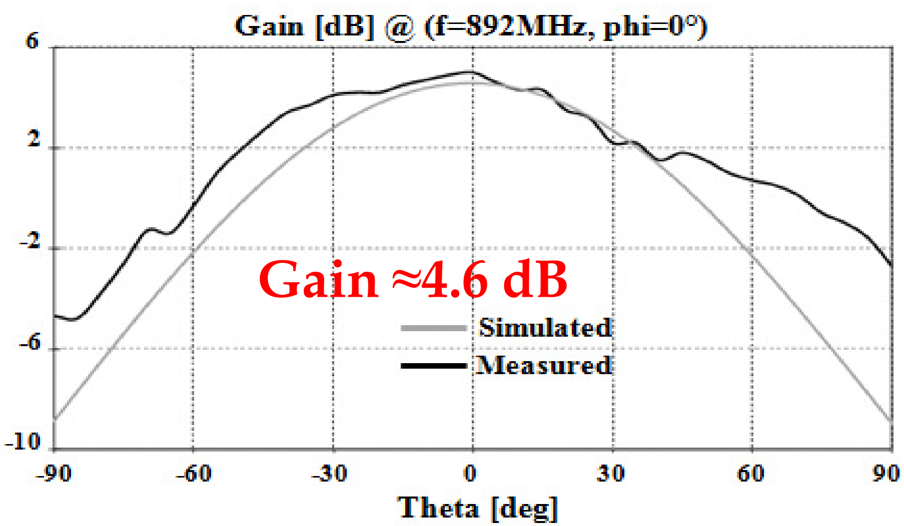

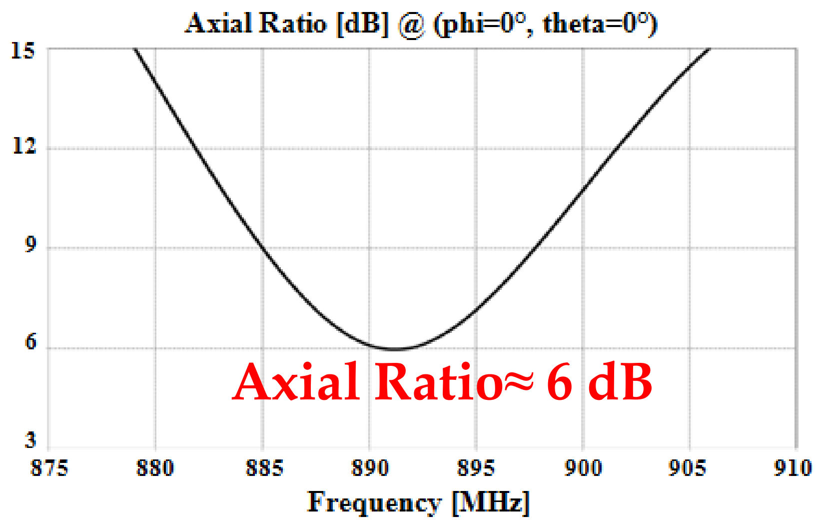

UHF Wearable Rectenna on Textile Materials

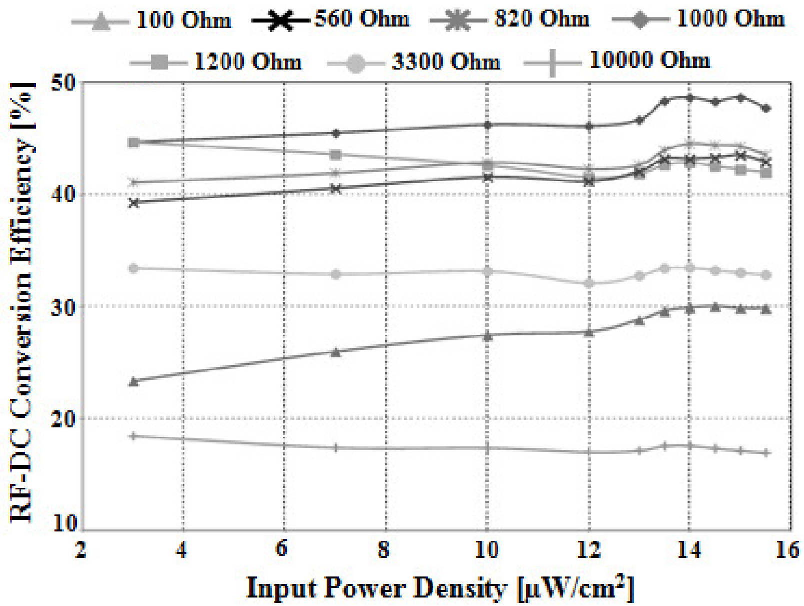

$$\eta_{RF-DC} = \frac{P_{OUT,DC}}{S_{RF} A_{eff}} = \left(\frac{V_{DC}^2}{R_L}\right) \frac{1}{S_{RF} A_{eff}}$$

S_{RF} = power density incident on the antenna

V_{DC} = DC output voltage

R_L = resistive load

A_{eff} = effective area of patch

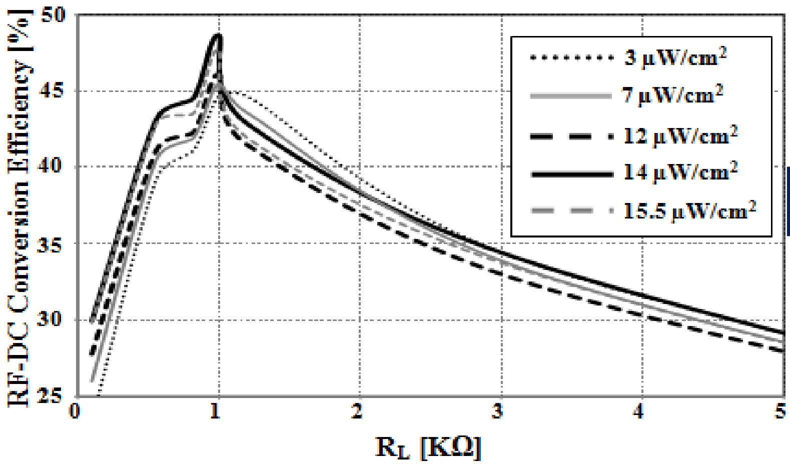

$\eta_{RF\text{-}DC} \approx 50\%$ @ 876 MHz, $R_L = 1\ k\Omega$, $S_{RF} = 14\ \mu W/cm^2$

UHF Wearable Rectenna on Textile Materials

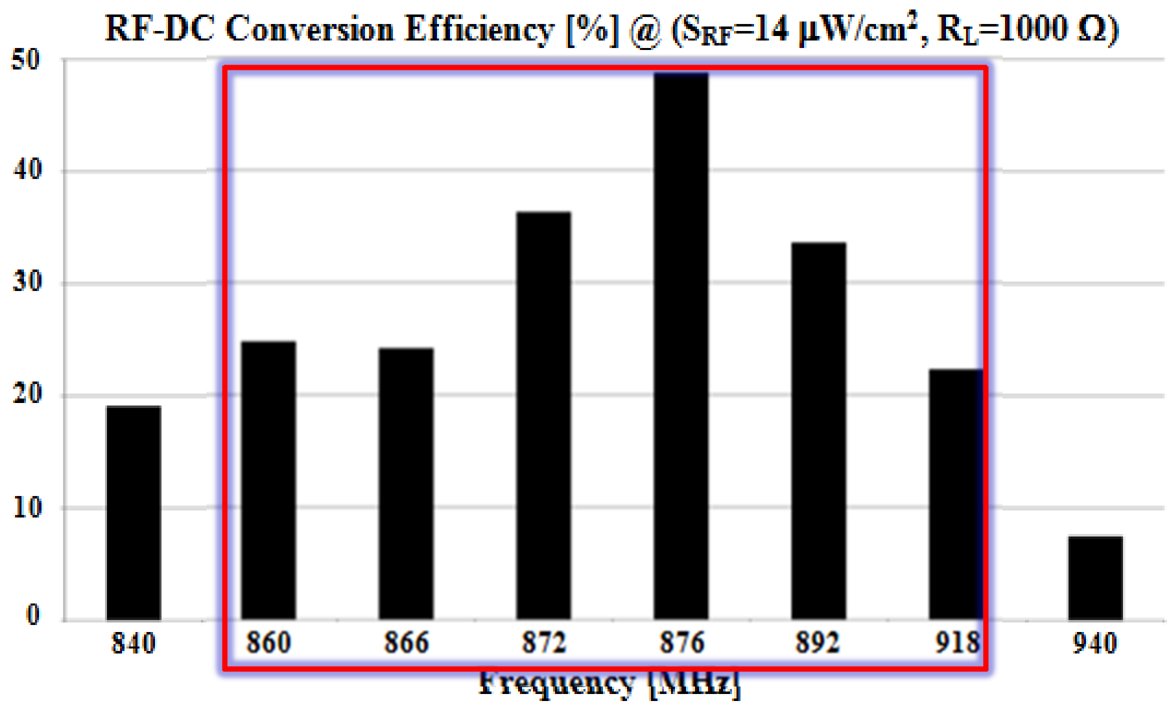

$\eta_{RF\text{-}DC}$> 20% @ BW=860-918 MHz,
R_L= 1 kΩ, S_{RF}= 14 µW/cm^2

Examples of application

Portable Charger on Leather for Thin-Film Batteries

A Portable Energy Link for Charging Thin-Film Batteries

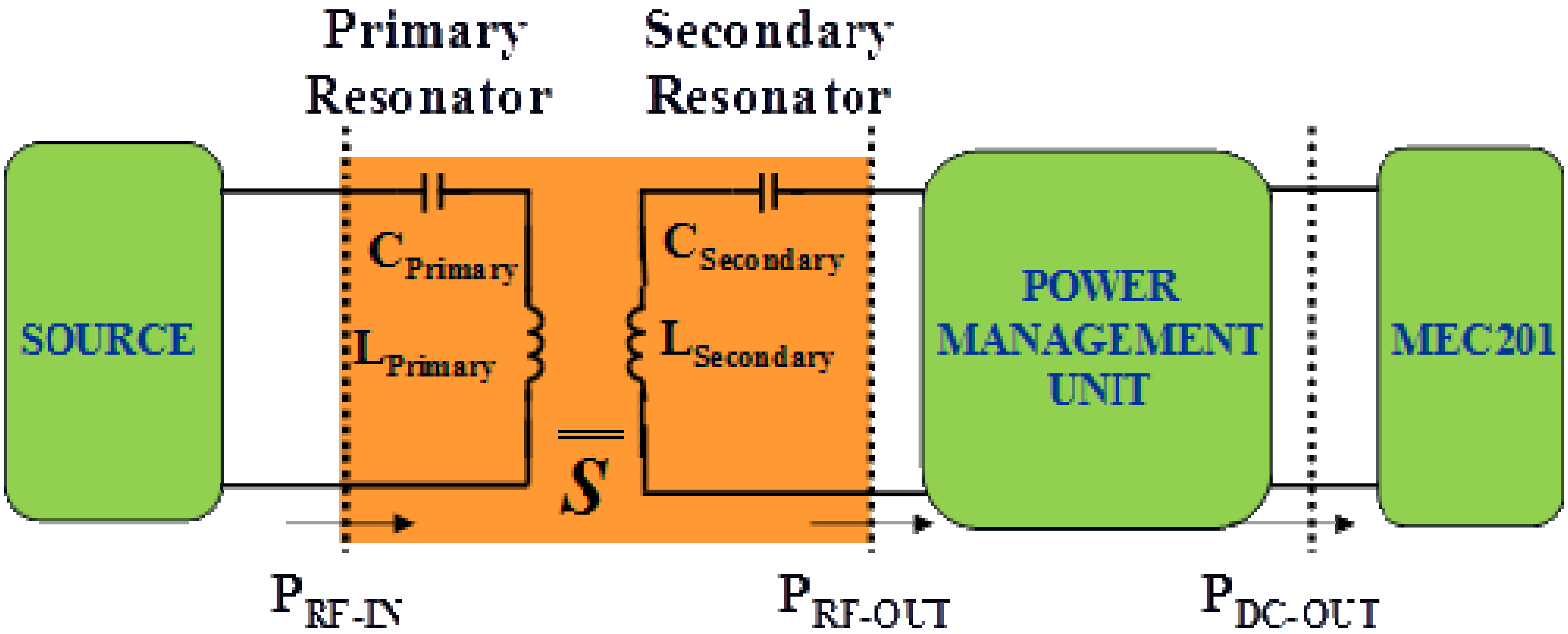

G. Monti, L. Corchia, E. De Benedetto and L. Tarricone, “A Wearable Wireless Energy Link for Thin-Film Batteries Charging", International Journal of Antennas and Propagation, 2016.

A Portable Energy Link for Charging Thin-Film Batteries

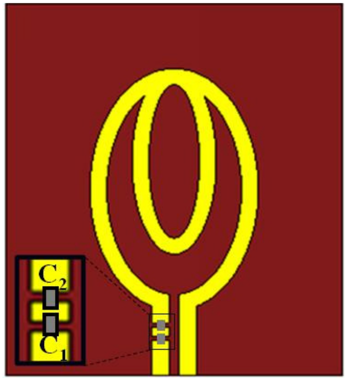

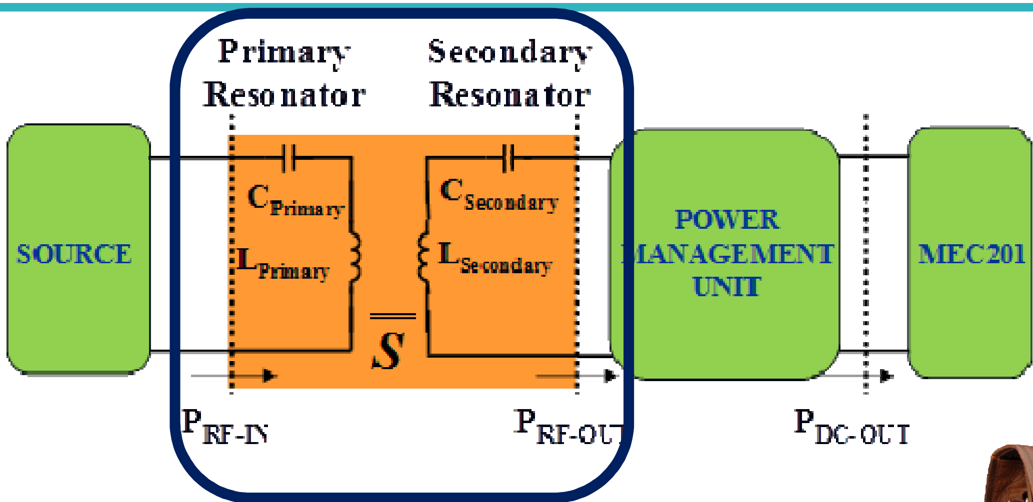

The WPT link operates in the ISM band centered at 434 MHz

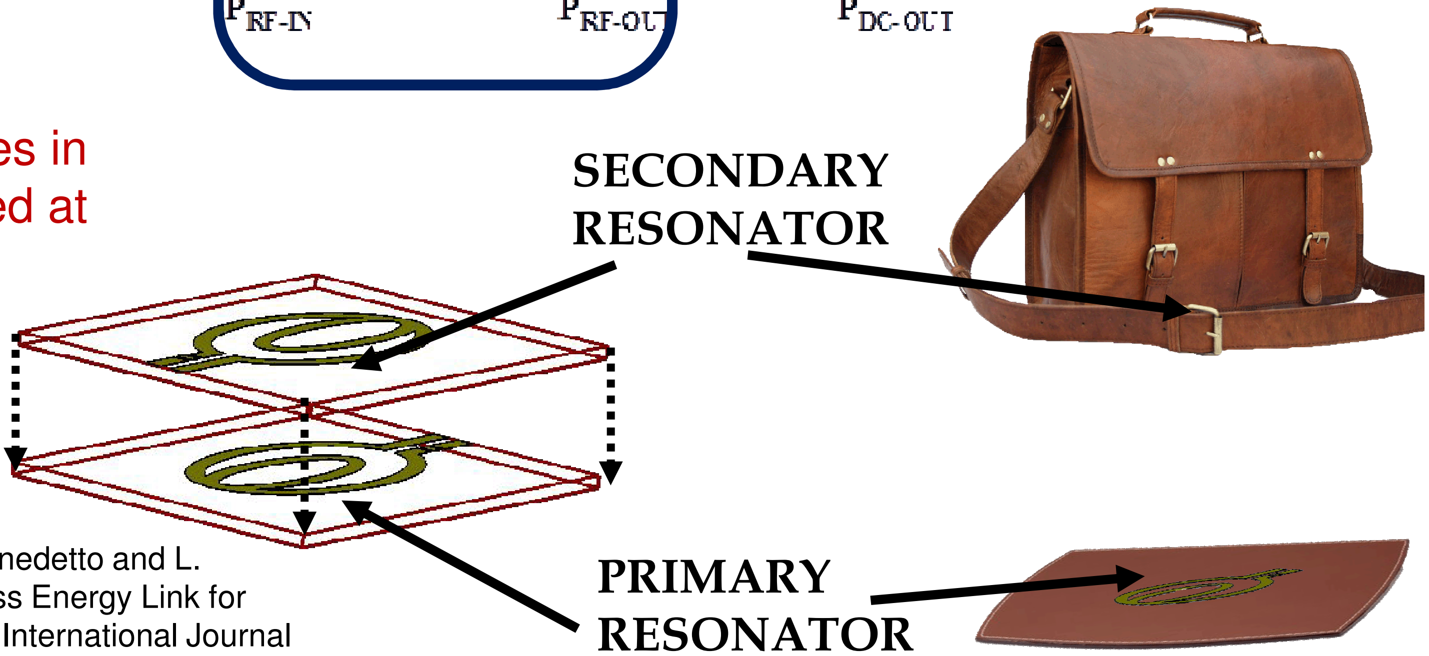

G. Monti, L. Corchia, E. De Benedetto and L. Tarricone, “A Wearable Wireless Energy Link for Thin-Film Batteries Charging", International Journal of Antennas and Propagation, 2016.

Portable Battery Charger: Power Link

Parameter of the leather substrate:
thickness = 1.65 mm
relative dielectric permittivity (ε_r) = 3
tg δ= 0.06

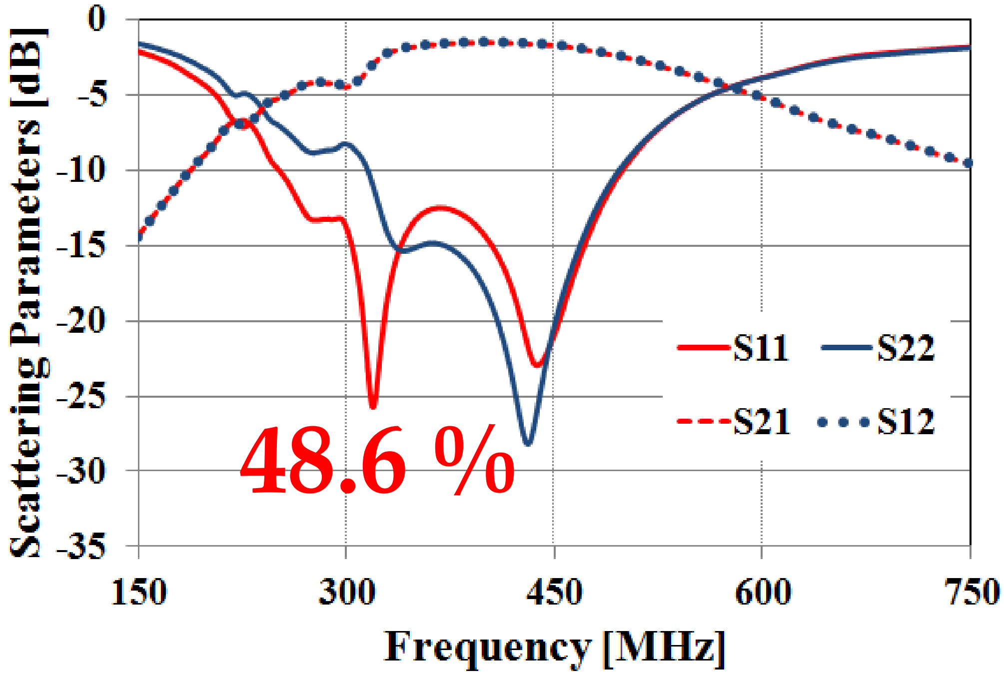

S_{11}= -22.6 dB
S_{21}= -1.6 dB
S_{22}= -27.6 dB
S_{12}= -1.6 dB

@ 434 MHz

Portable Battery Charger: RF-to-RF Efficiency

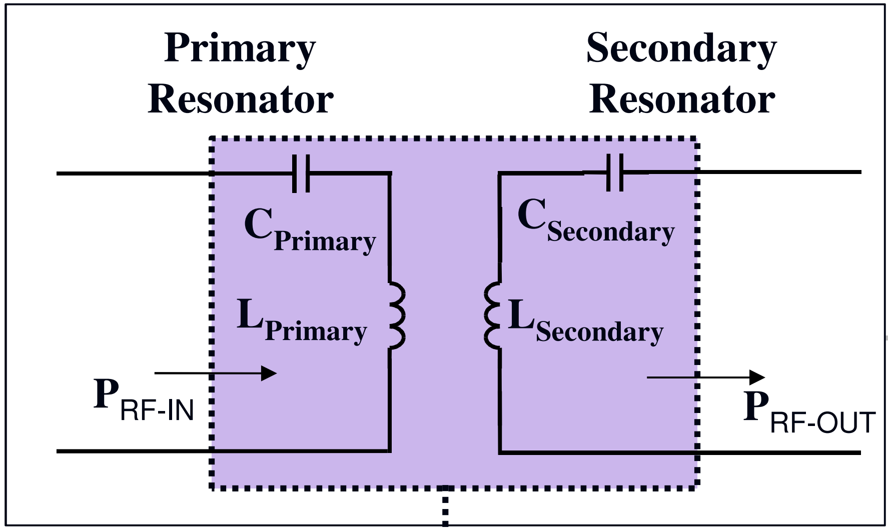

$$\eta_{RF-RF} = \frac{P_{RF\_OUT}}{P_{RF\_IN}} \times 100 =$$

$$= |S_{21}|^2 \times 100$$

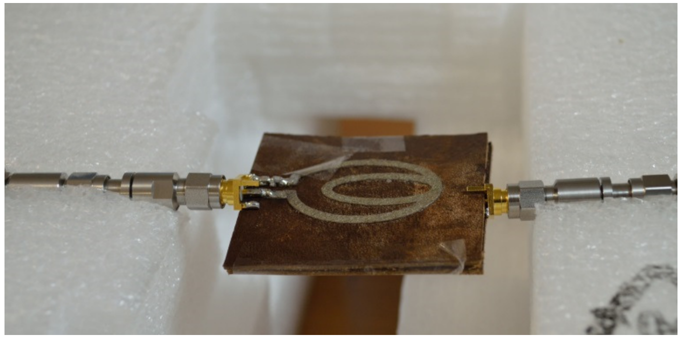

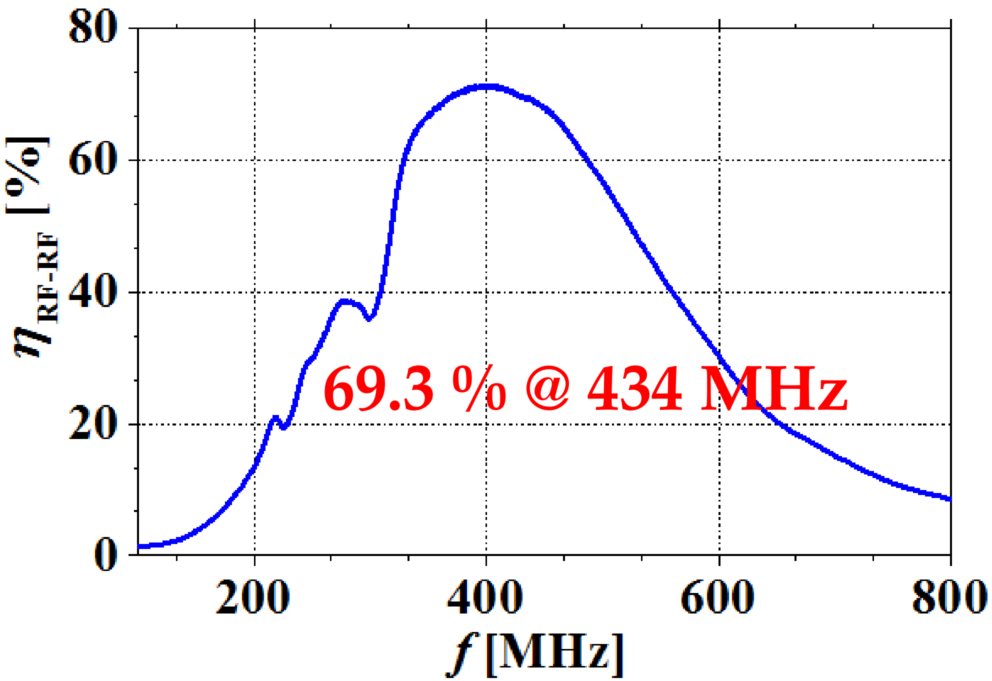

Portable Battery Charger: Power Management Unit

Texas Instruments LM2767

LTC4071 chip by Linear Technologies

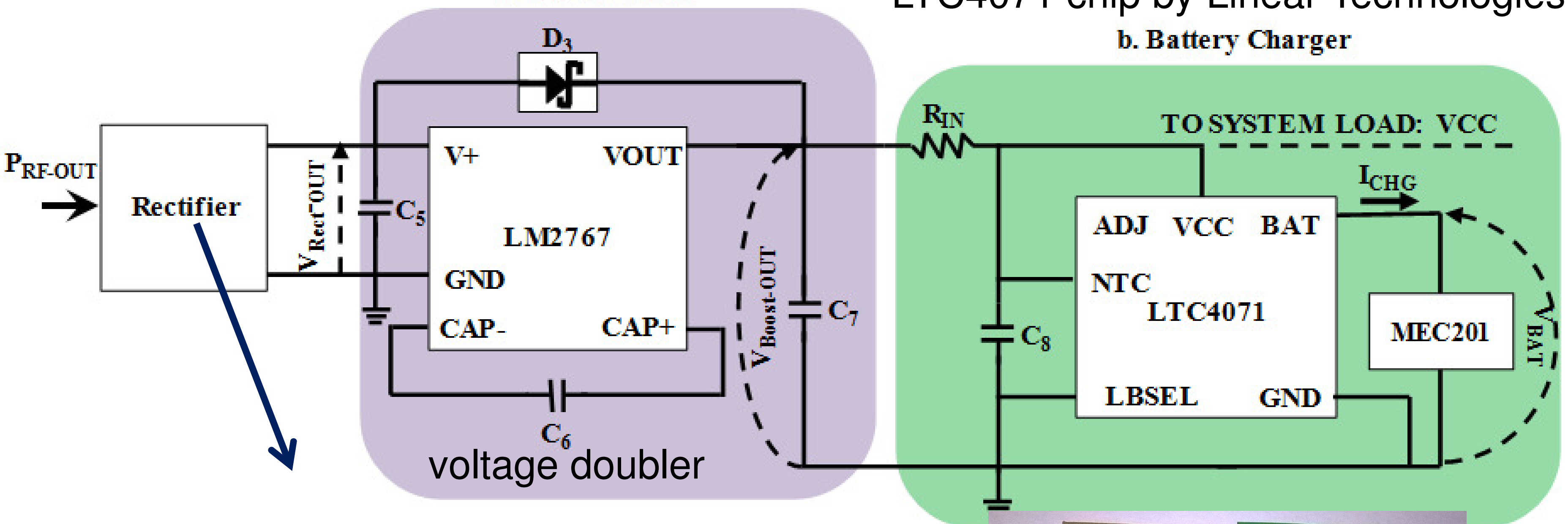

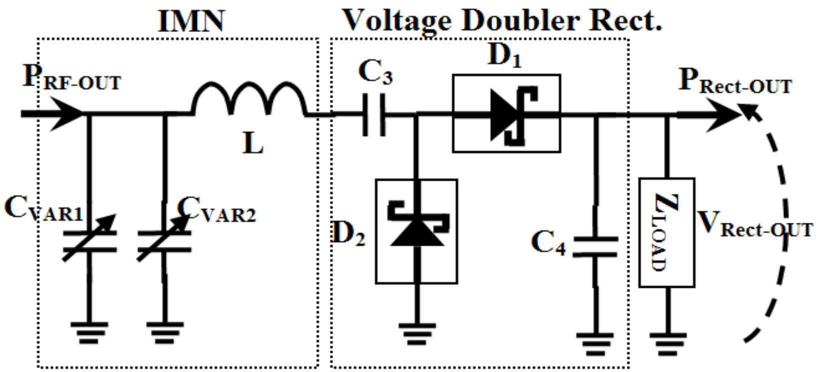

The schottky diodes are the HSMS-2820 by Avago Technologies

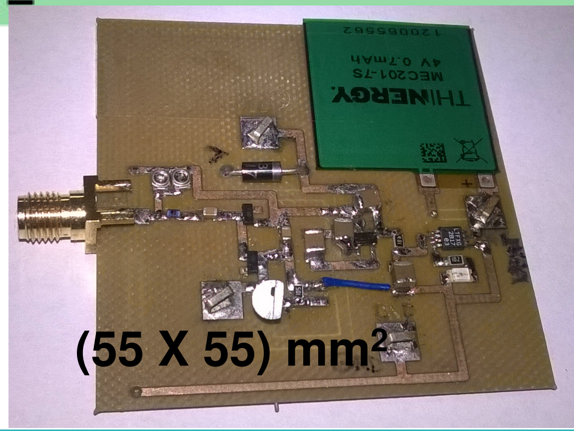

Portable Battery Charger: Power Management Unit

Recharge mode
User mode

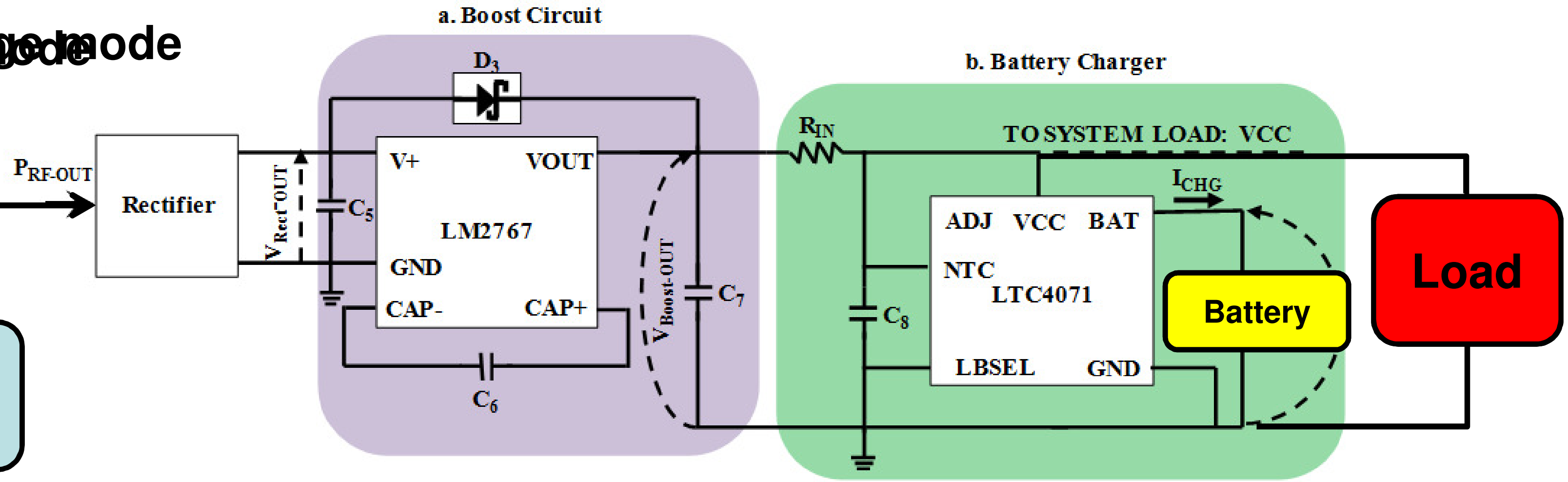

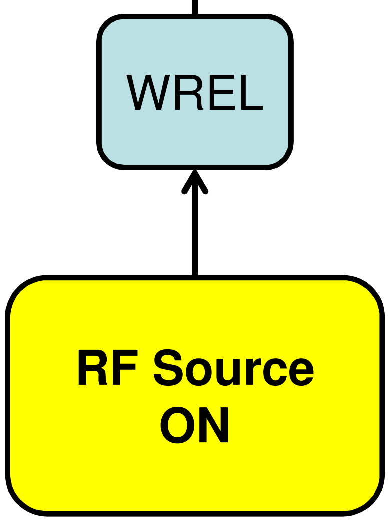

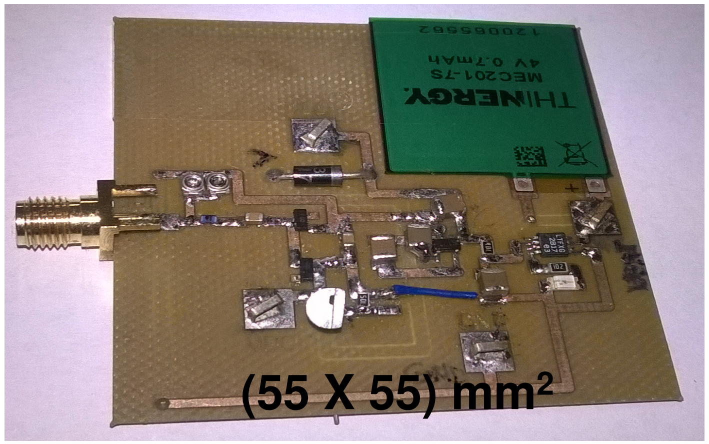

Portable Battery Charger: Performance

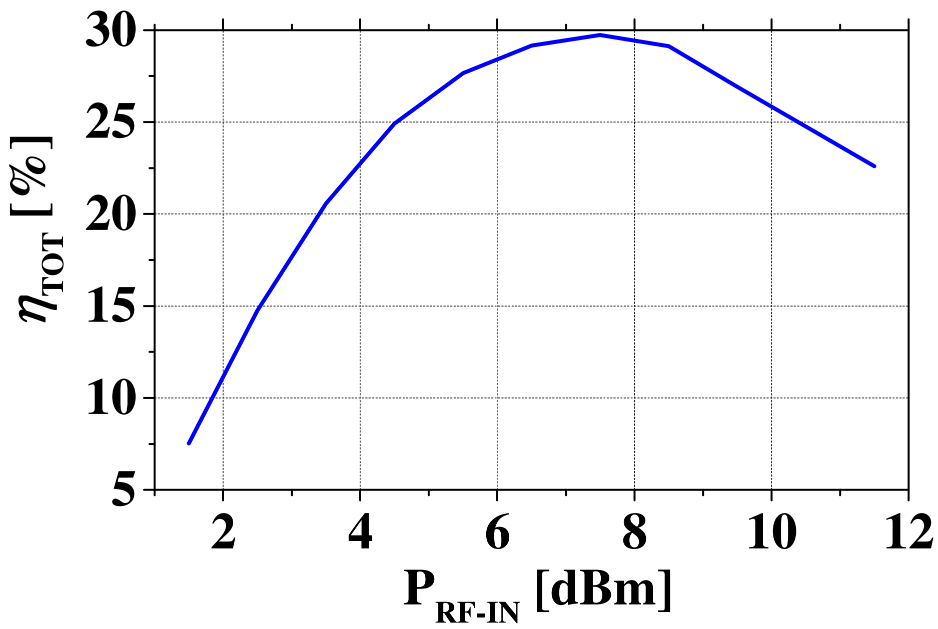

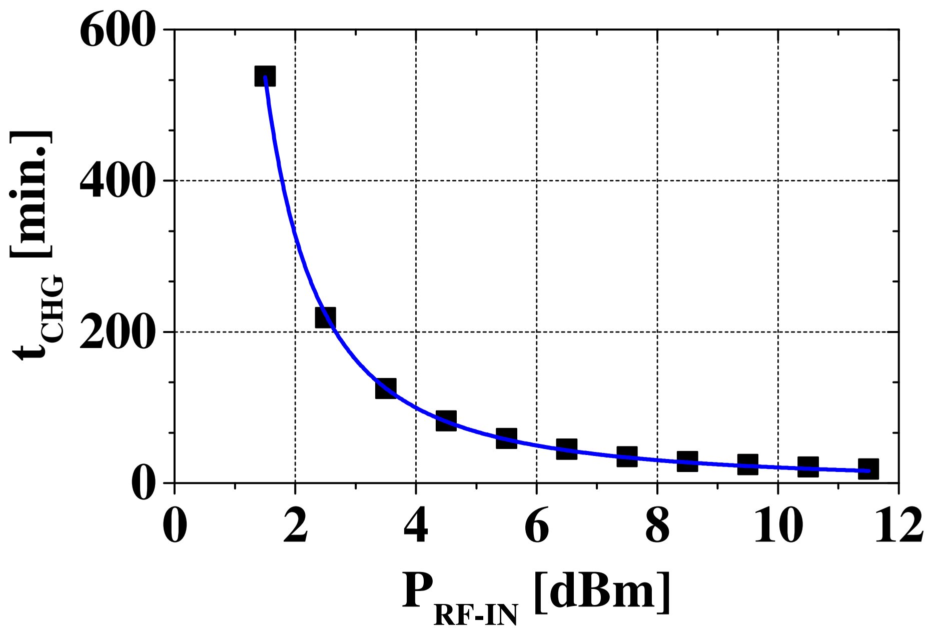

$$\eta_{TOT} = \frac{P_{DC-OUT}}{P_{RF-IN}} = \frac{V_{BAT} \cdot I_{CHG}}{P_{RF-IN}}$$

for $P_{RF\text{-}IN}$ higher than 6 dBm, the time necessary to recharge the THINERGY MEC201 battery (by Infinite Power Solutions, battery capacity = 0.7 mAh) is shorter than 50 minutes

Resonator on leather for inductive WPT and far-field data links

Parameter of the leather substrate:

thickness = 1.9 mm

ε_r = 2.45

tg δ= 0.07

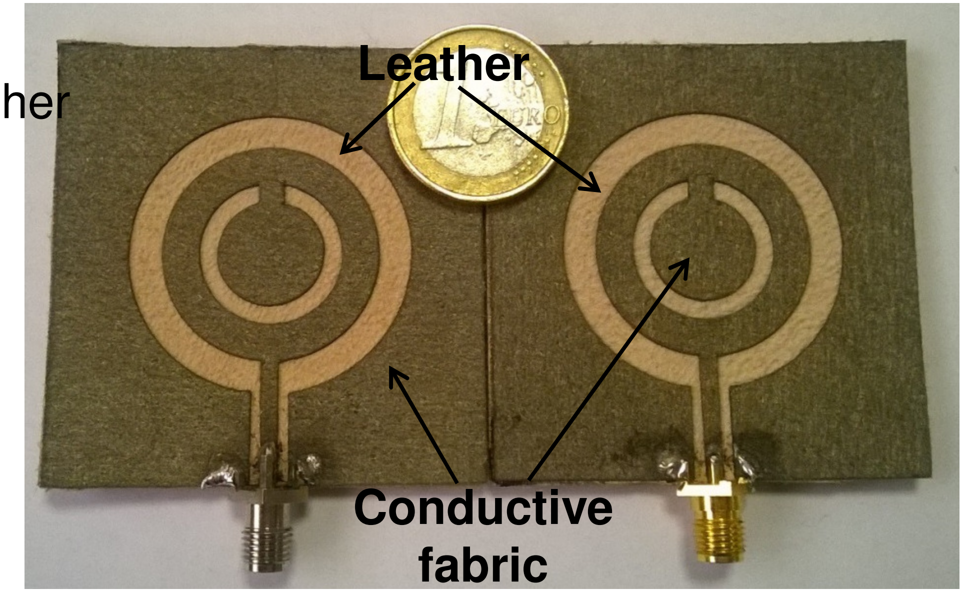

Dipole-like antenna behaviour at 2.45 GHz

Resonator of an inductive power link in the UHF band

Resonator on leather for inductive WPT and far-field data links

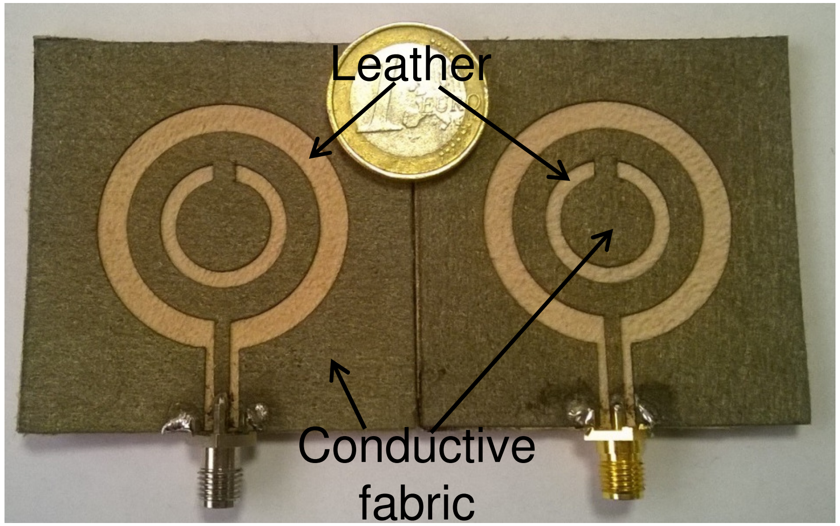

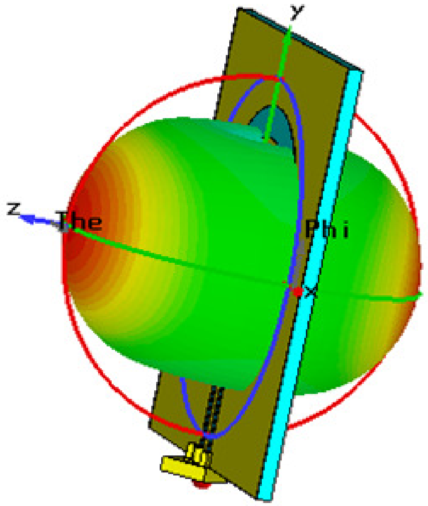

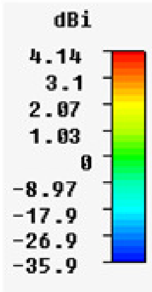

Dipole-like antenna behaviour at 2.45 GHz

Antenna Behaviour

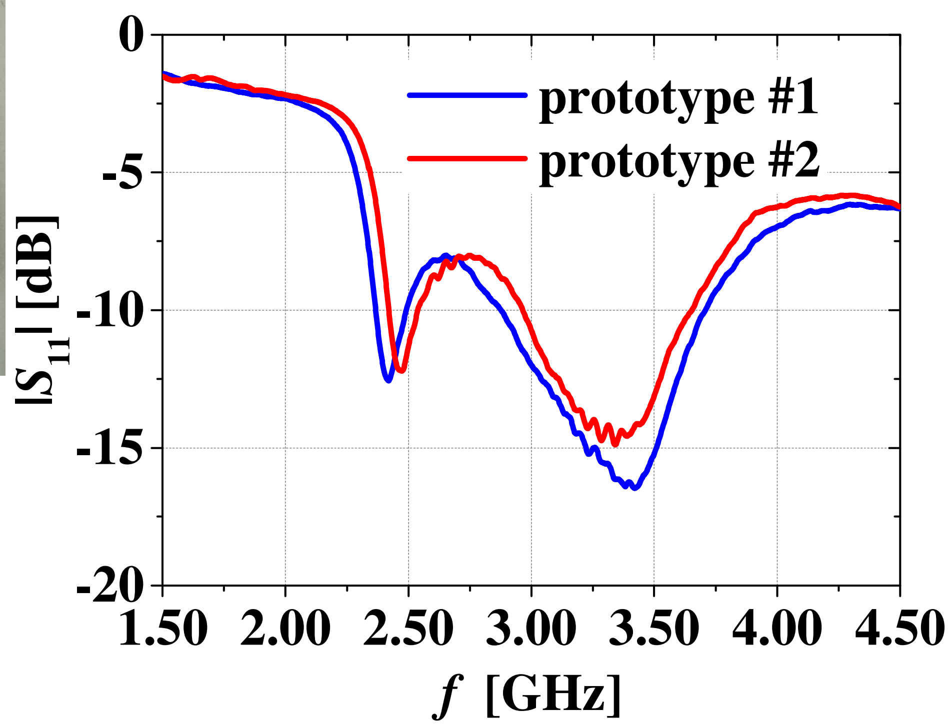

Resonator on leather for inductive WPT and far-field data links

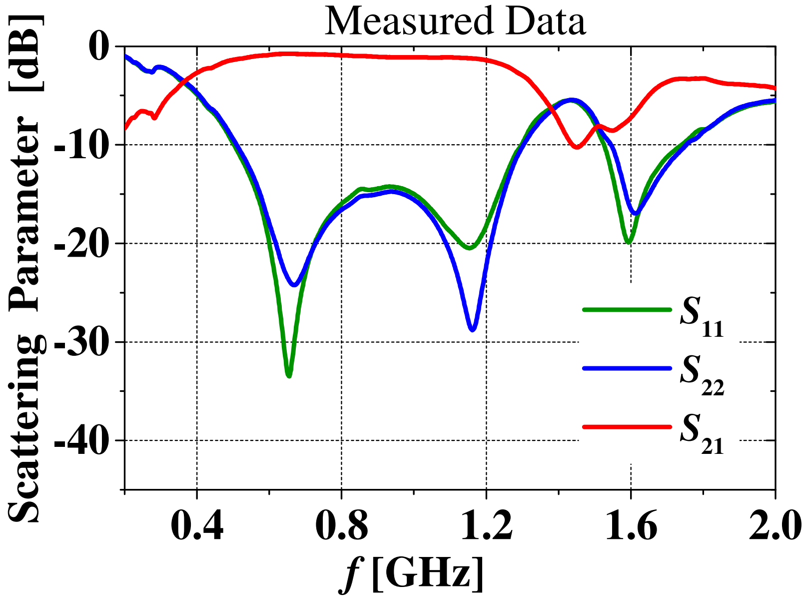

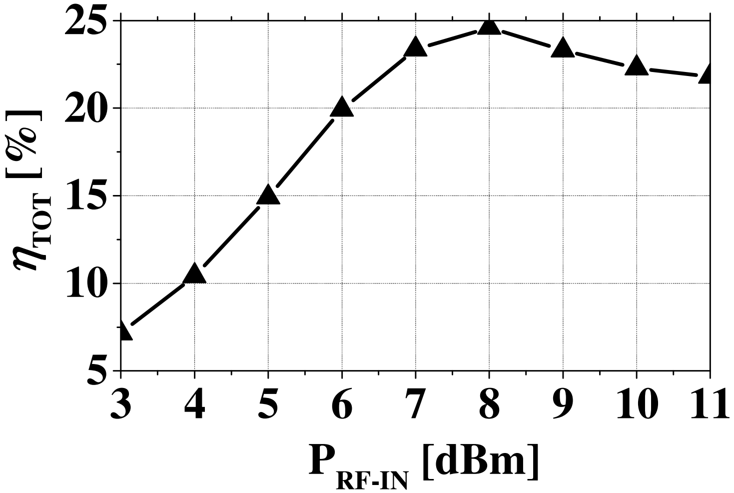

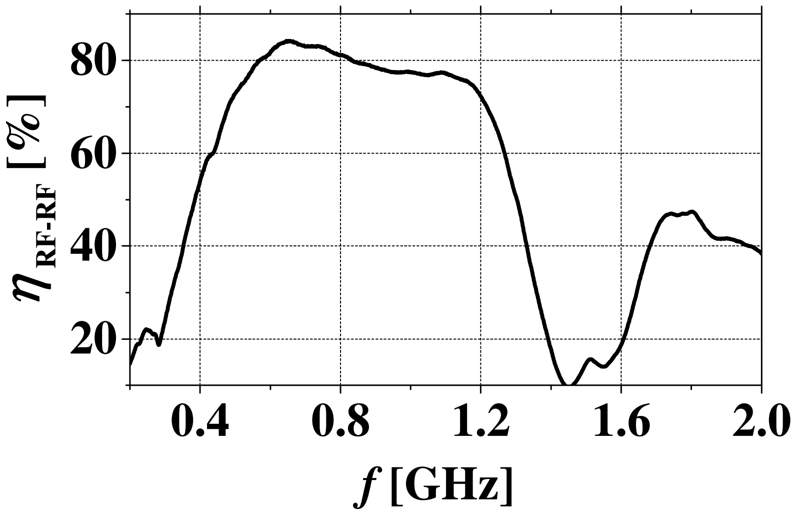

WPT links: Applications

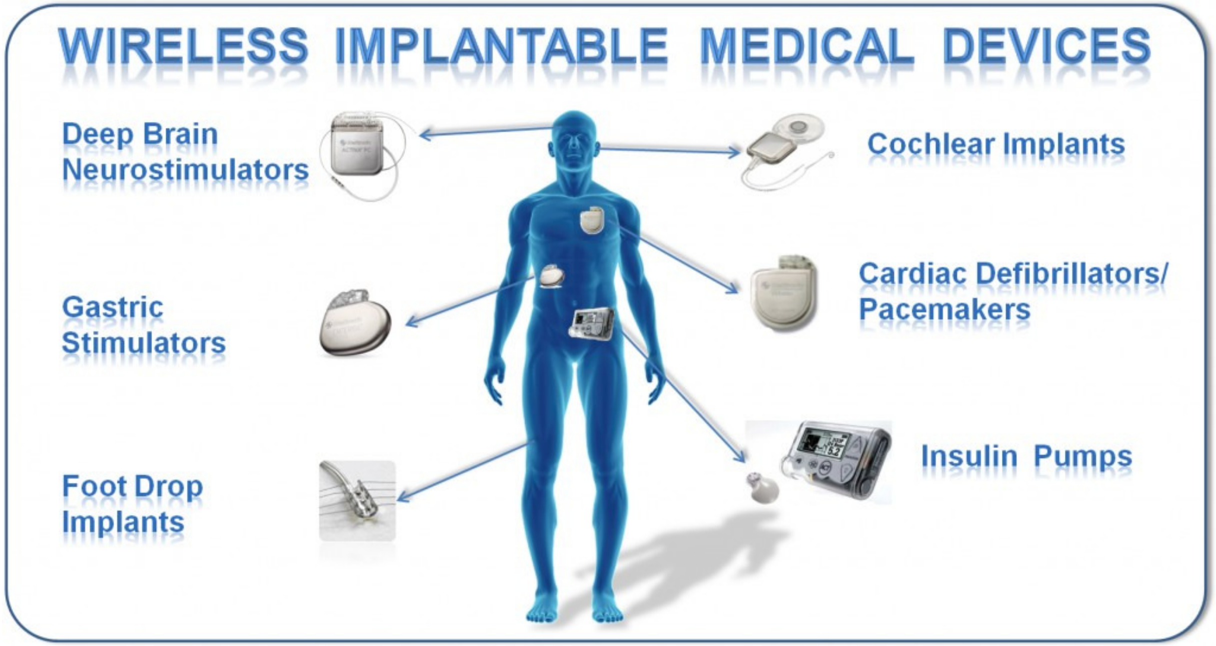

WPT for implantable devices

Motivations:
extend the lifetime of medical implants

WPT for Implantable devices

WPT LINK FOR DEEP BRAIN STIMULATION SYSTEMS

http://journal.frontiersin.org/article/10.3389/fnint.2011.00046/full

CONVENTIONAL DBS SYSTEM

typical lifetime 2~5 years

DBS SYSTEM WITH RECHARGEABLE BATTERY

Expected lifetime up to 10~20 years

http://www.vercise.com/vercise-and-guide-dbs-systems/vercise-dbs/
https://www.youtube.com/watch?v=sGn-honS8MQ
http://www.epda.eu.com/en/x-parkinsons/x-medinfo/neurosurgery/deep-brain-stimulation-dbs/

Examples of application

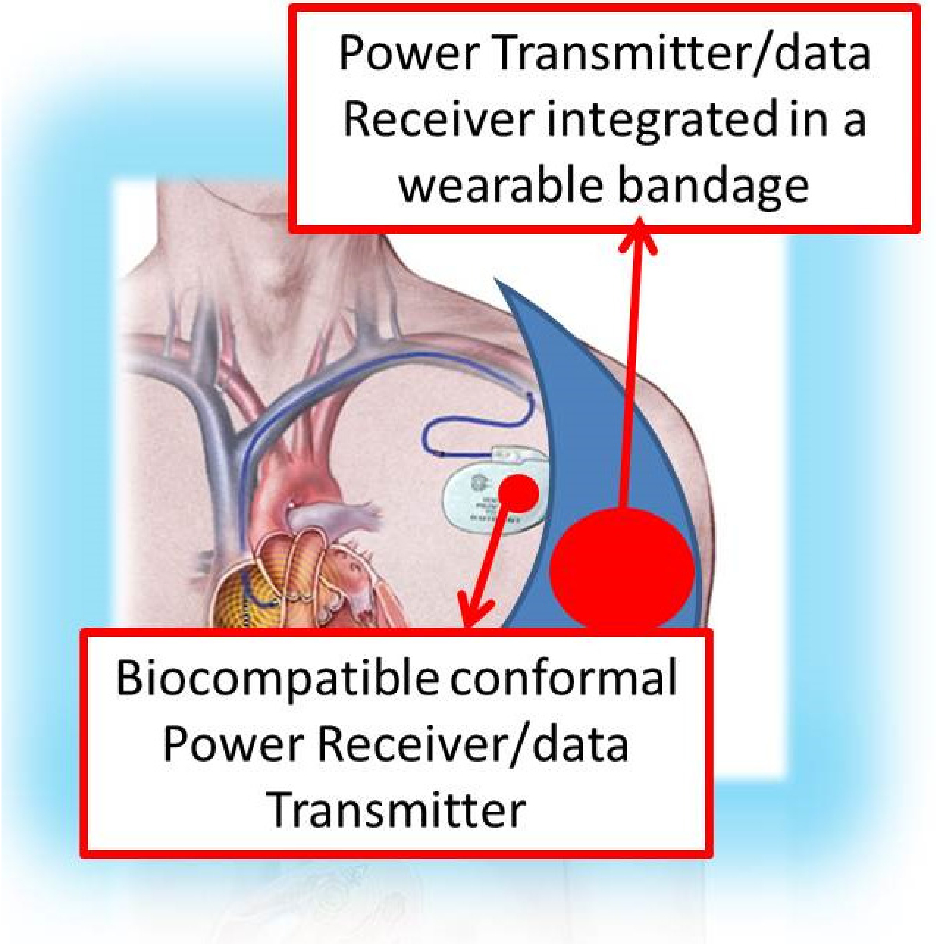

Inductive WPT link for medical devices implanted in the chest

Selection of the operating frequency

Electromagnetic energy absorption in human tissues increases as the frequency increases

Most of WPT links for medical medical implants operate at very low frequency

- **A different link is necessary for power and data transmission**
- **The WPT link is exposed to interferences**

Selection of the operating frequency

the Medradio band (401-406 MHz) reserved to medical devices

- **The same wireless link can be used for data and power transmission**
- **No interferences**

G. Monti, M. V. De Paolis, L. Tarricone,**"Wireless Energy Link for Deep Brain Stimulation"**, Microwave Conference (EuMC), 2015 European, Paris, 7-10 Sept. 2015, pp.64-67.

Selection of strategy for WPT

Resonant Magnetic Coupling

- **Low interaction with the surrounding environment**
- **Safer for humans**
- **Maximize the efficiency for Medium/Long transfer distances**

G. Monti, M. V. De Paolis, L. Tarricone,**"Wireless Energy Link for Deep Brain Stimulation"**, Microwave Conference (EuMC), 2015 European, Paris, 7-10 Sept. 2015, pp.64-67.

WPT for medical implants: configuration

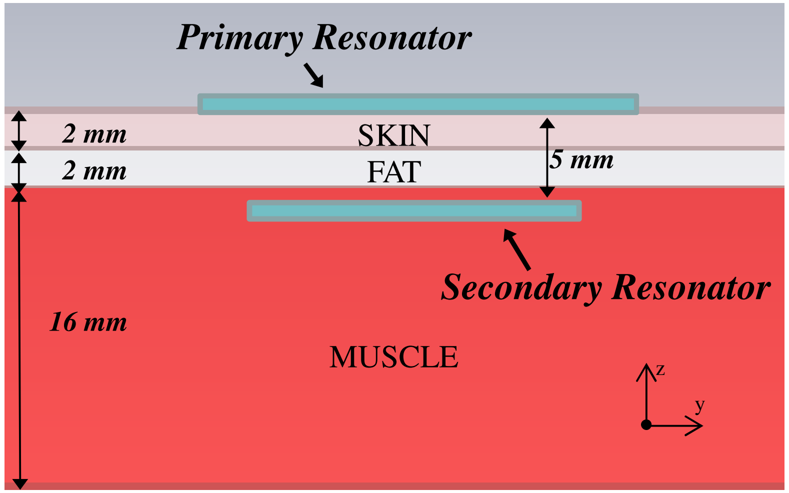

f_{ris} = 403 MHz	Skin	Fat	Muscle
ε_r	46.7	11.6	57.1
σ [S/m]	0.68	0.081	0.797
ρ [kg/m^3]	1090	1109	911

http://www.itis.ethz.ch/itis-for-health/tissue-properties/database/

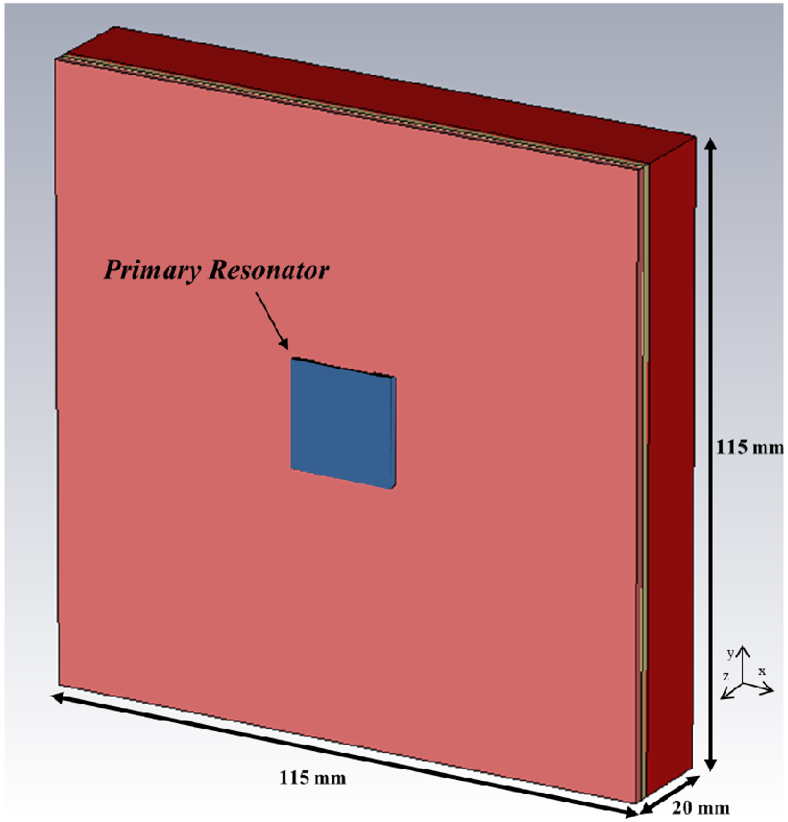

WPT for medical implants: geometry

PRIMARY RESONATOR

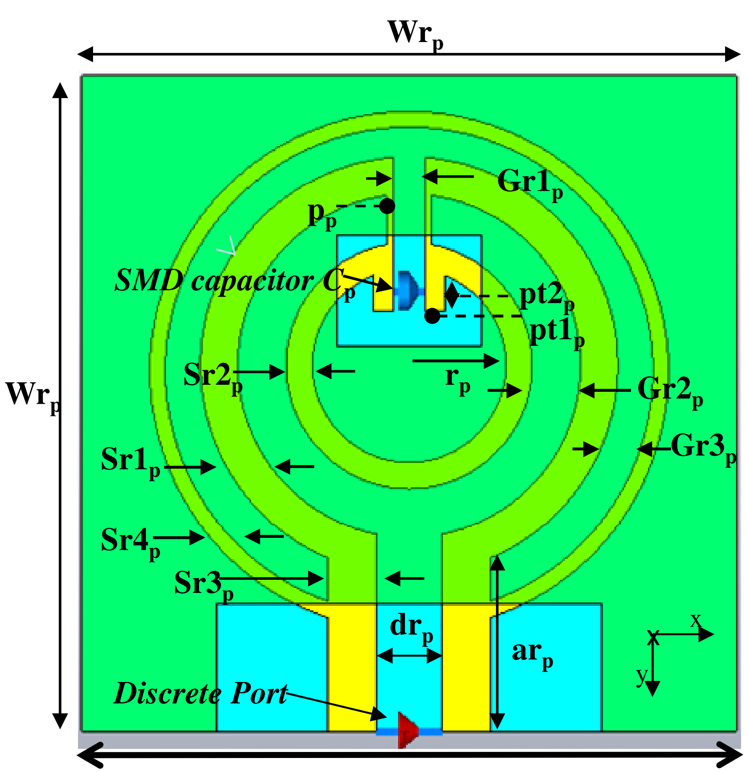

SECONDARY RESONATOR

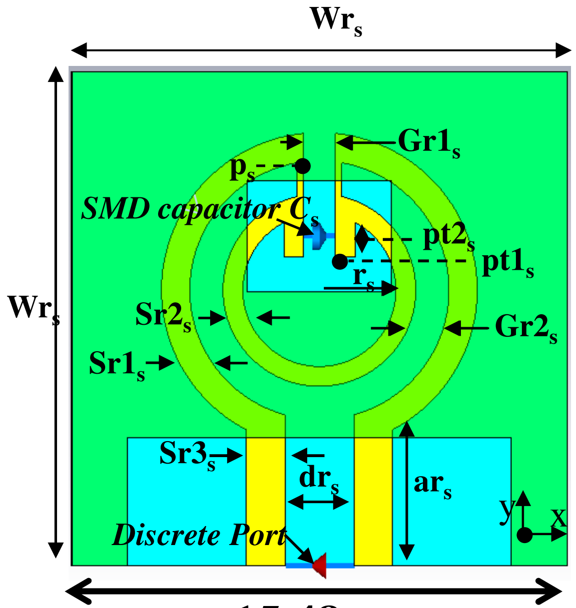

Front view

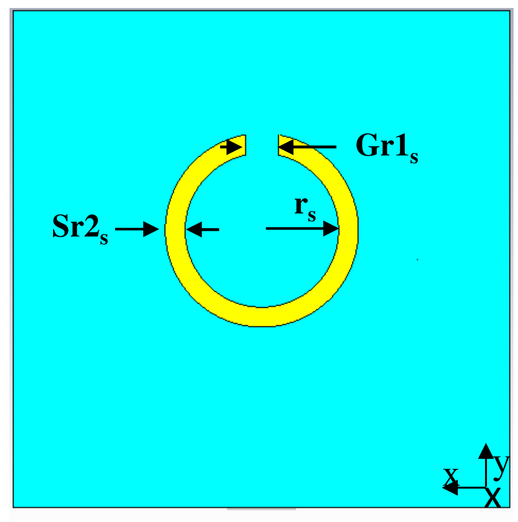

Back view

Substrate→ Arlon DiClad 880 (ε_r= 2.17, tanδ= 0.0009, and h= 0.508 mm)
Superstrate →Arlon AR1000 (ε_r=9.7, and tanδ= 0.003, and h= 0.610 mm)

WPT for medical implants: experimental setup

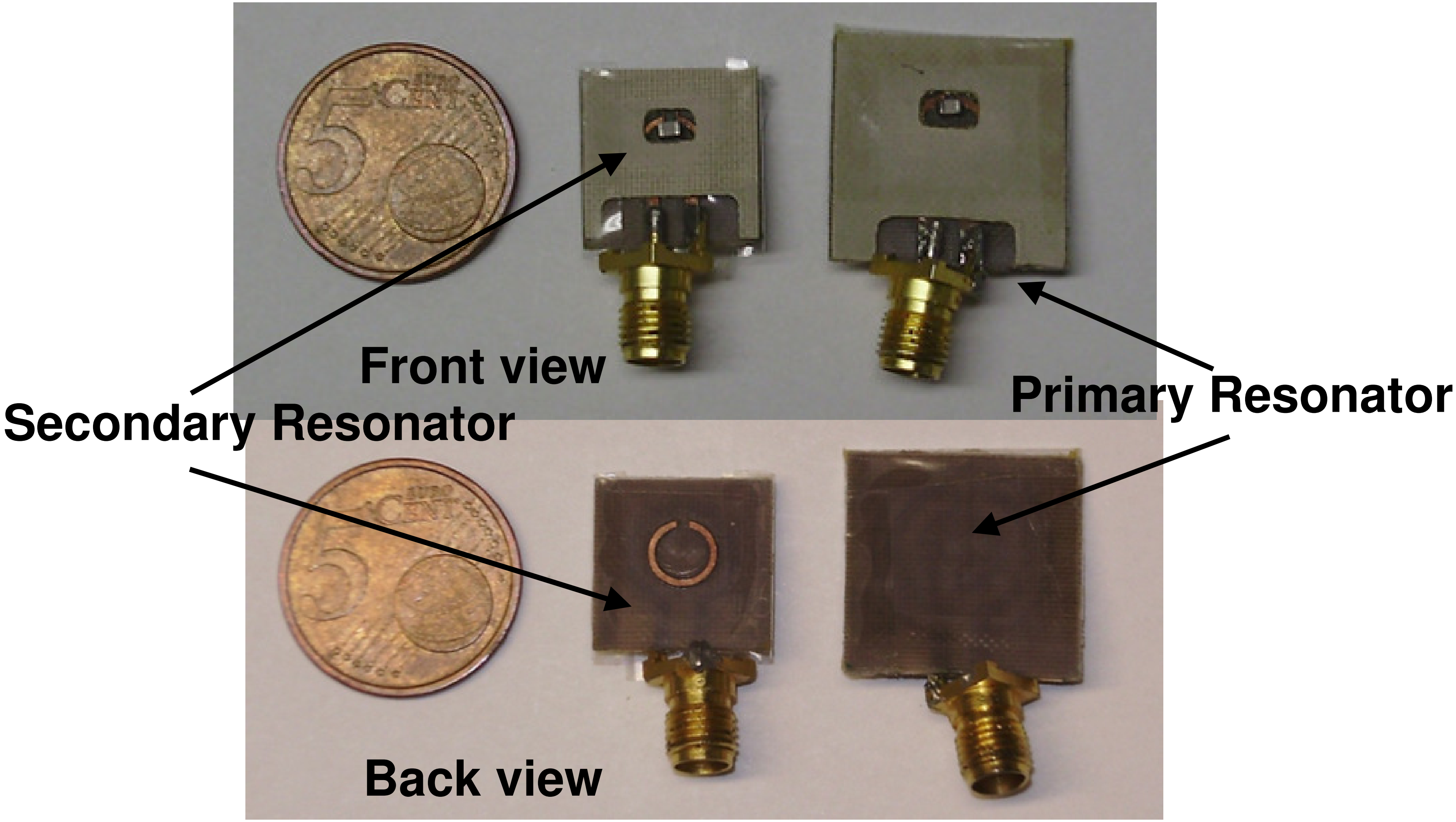

WPT for medical implants: experimental setup

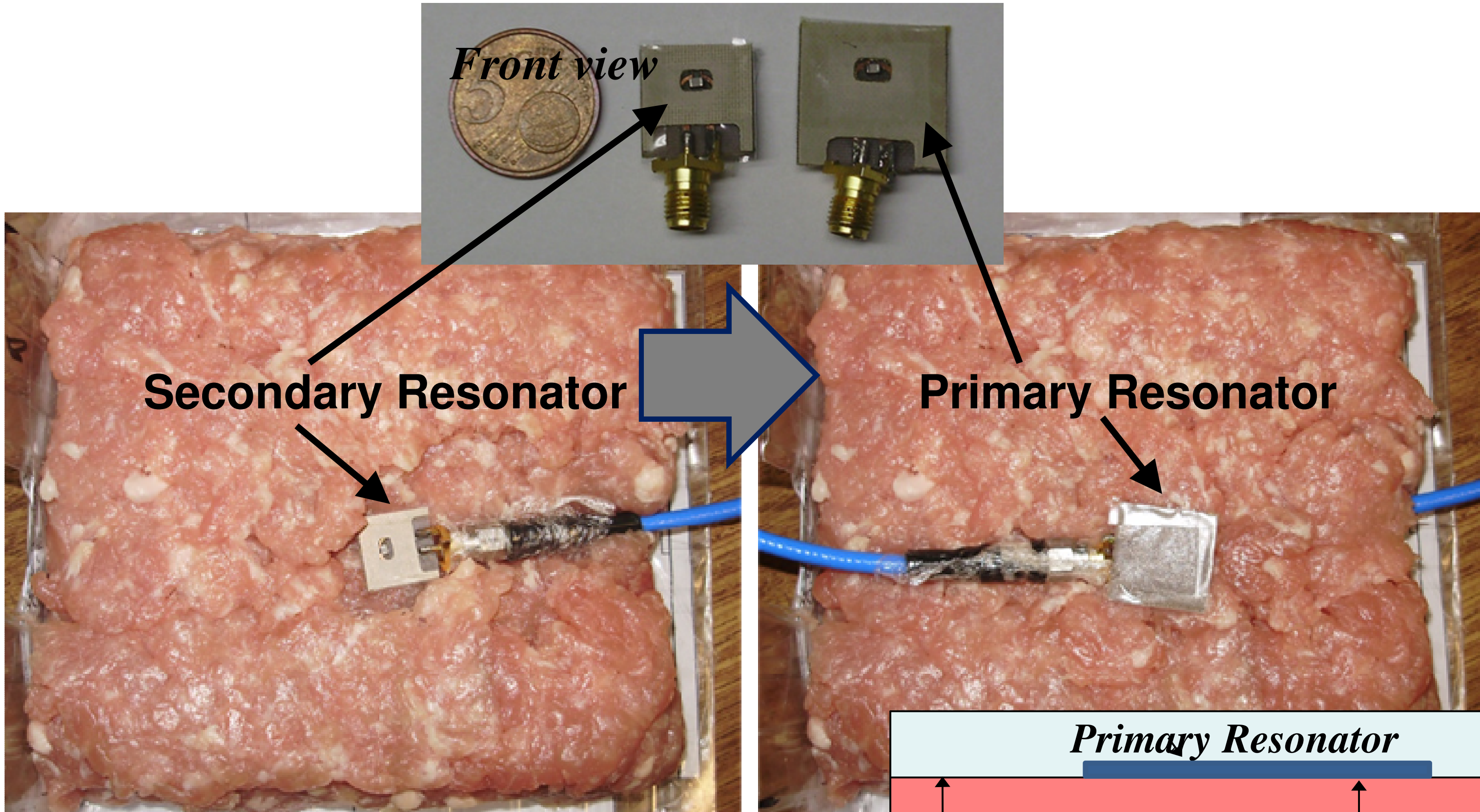

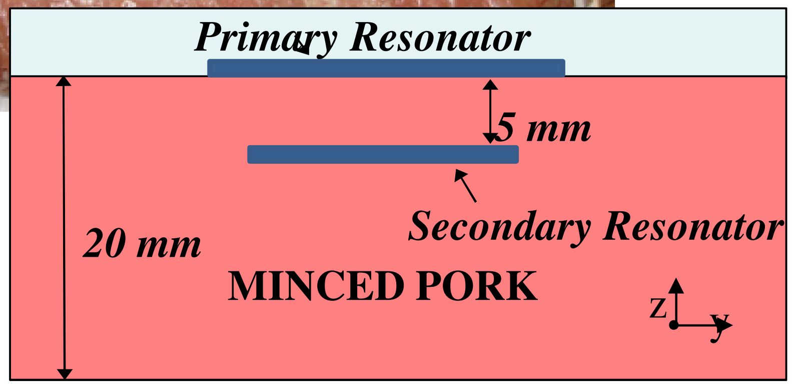

WPT for medical implants: experimental results

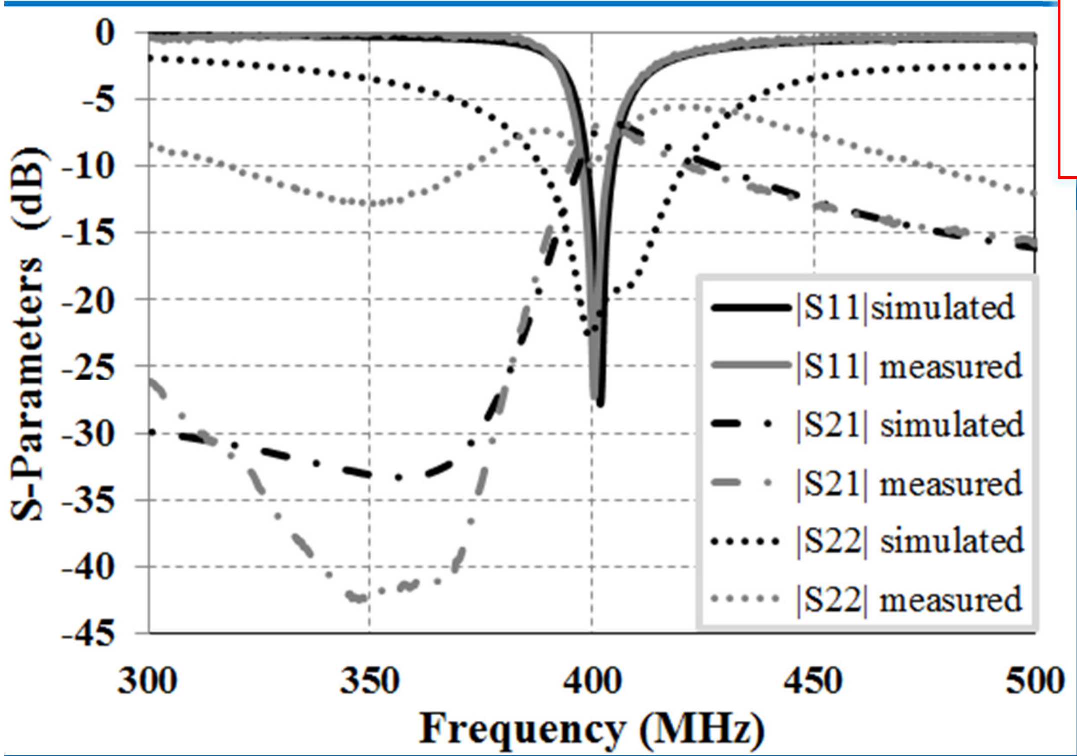

SIMULATED

At 403 MHz:
$|S_{11}|$= -17,10 dB
$|S_{21}|$= -6.83 dB
$|S_{22}|$= -20,04 dB

MEASURED

At 403 MHz:
$|S_{11}|$= -11,96 dB
$|S_{21}|$= -6,87 dB
$|S_{22}|$= -8,84 dB

$$\eta_{RF-RF}[\%] = \frac{P_{RX}}{P_G} \times 100 == |S_{21}|^2 x100$$

@ 403MHz

$\eta_{RF\text{-}RF\ simulated}$ = 20.74 %
$\eta_{RF\text{-}RF\ measured}$ = 20.54 %

WPT for medical implants:
Compliance with safety regulations

At the operating frequency of the proposed WPT link the IEEE (Institute of Electrical and Electronic Engineers) and the ICNIRP (International Commission on Non-Ionizing Radiation Protection) guidelines provide basic restrictions for electromagnetic fields in terms of the peak spatial-averaged Specific Absorption Rate (SAR)

The SAR measures the rate at which energy is absorbed by the human body when exposed to an RF EM field; it is defined as the power absorbed per mass unit of tissue:

$$SAR\left(\frac{W}{kg}\right) = \frac{d}{dt}\left(\frac{dW}{dm}\right) = \frac{d}{dt}\left(\frac{dW}{\rho dV}\right)$$

where *dW* is the incremental energy absorbed by, or dissipated in, an incremental mass *dm* contained in a volume element *dV* of density *ρ*.

In the trunk area, the exposure limit considering a mass of 10-g is 2 W/kg

Compliance with safety regulations

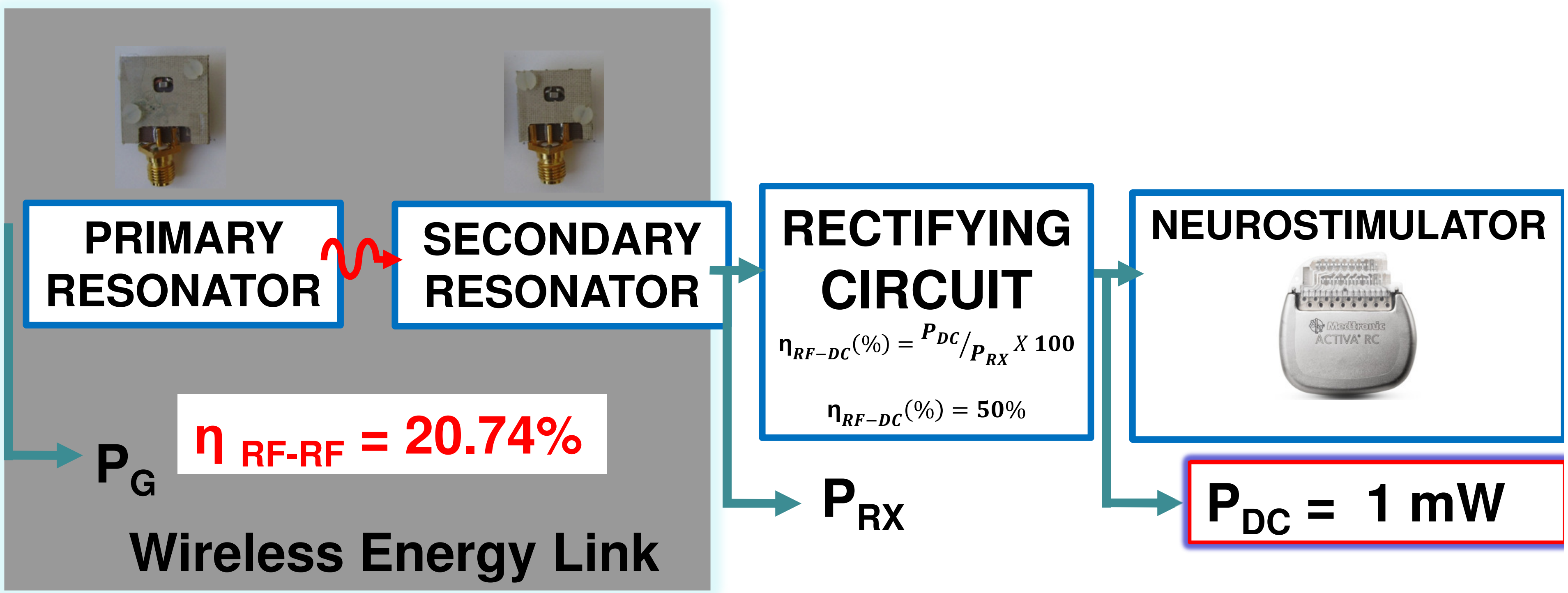

$$P_G = P_{DC} / (\eta_{\ RF\text{-}RF}\ X\ \eta_{\ RF\text{-}DC}) = 9.64\ mW$$

Compliance with safety regulations

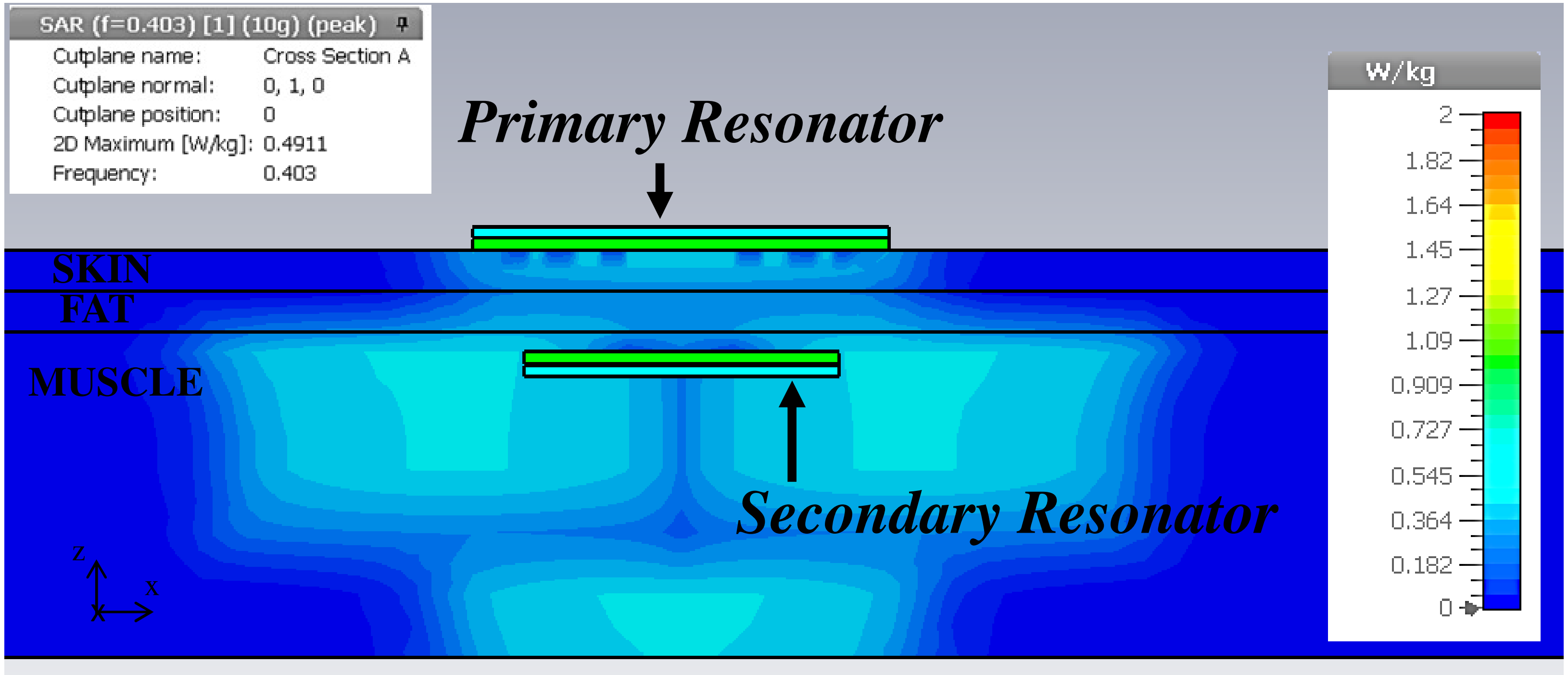

P_G = 10.52 mW 10-g average SAR → SAR < 0.49 W/kg → √ **REGULATION LIMITS** (2 W/Kg)

Examples of application

LAMPHAR

Energy harvester for power generation by spurious emissions from compact fluorescent lamps (CFL)

LAMPHAR

A CFL consists of a tube curved so to occupy a smaller volume and an electronic ballast which provides the proper starting and operating electrical conditions.

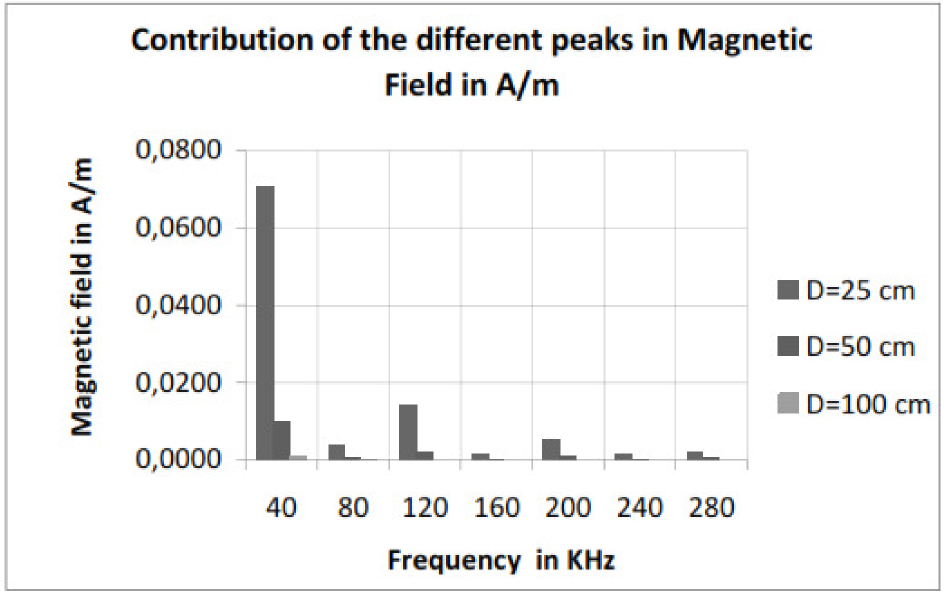

Due to the high frequency solid state electronic circuitry used in the ballast, CFLs emit a relatively strong electromagnetic field

LAMPHAR

Energy harvester for power generation by spurious emissions from compact fluorescent lamps

The harvester is a resonant loop placed in the near-field region of the CFL: the operating frequency is 41 kHz which corresponds to a peak of the EM emissions from common CFLs

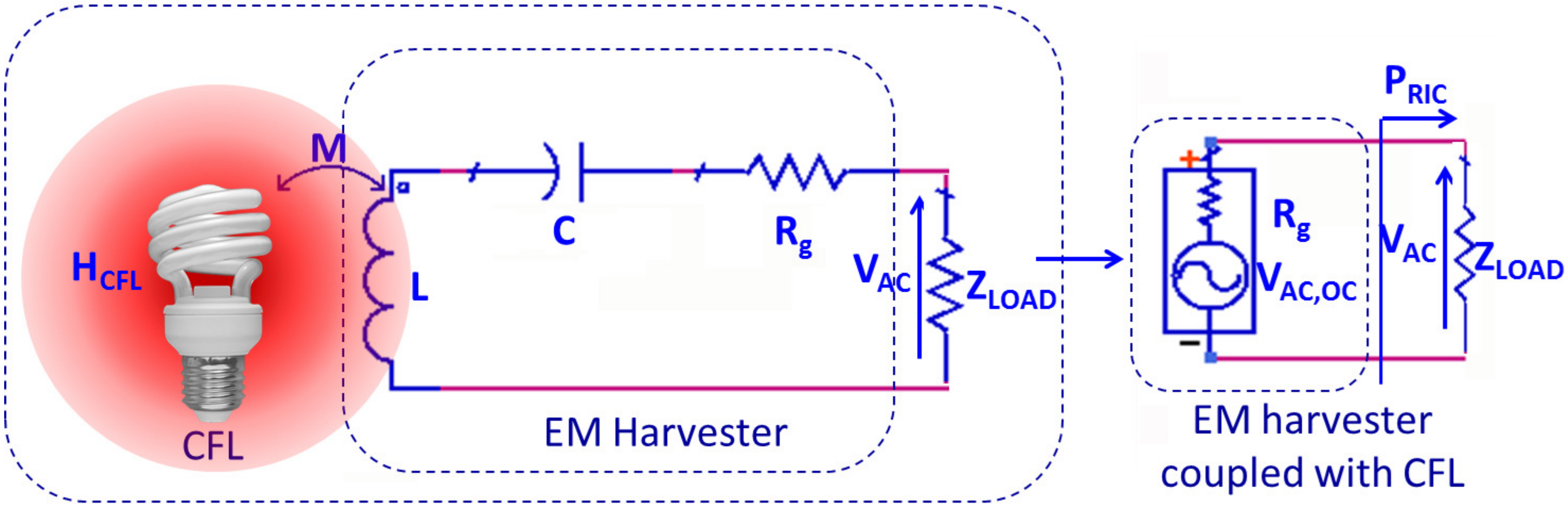

G. Monti, F. Congedo, P. Arcuti, L. Tarricone, "Resonant Energy Scavenger for Sensor Powering by Spurious Emissions from Compact Fluorescent Lamps," IEEE Sensors Journal published by IEEE (Piscataway, NJ, USA), Vol. 14, Issue 7, pp. 2347-2354.

LAMPHAR

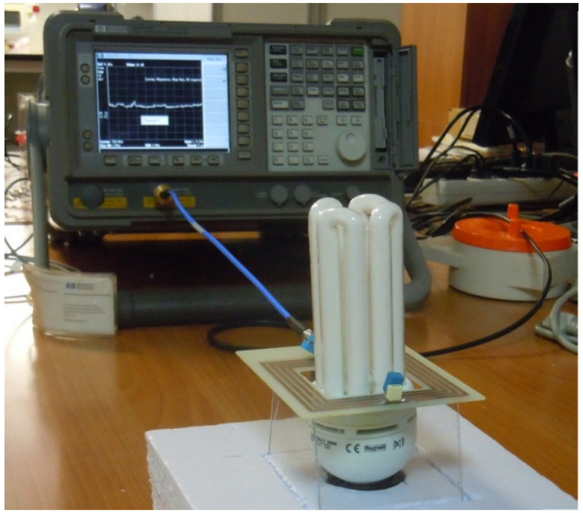

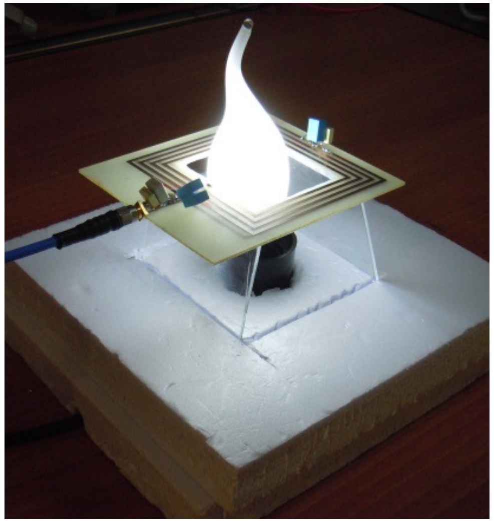

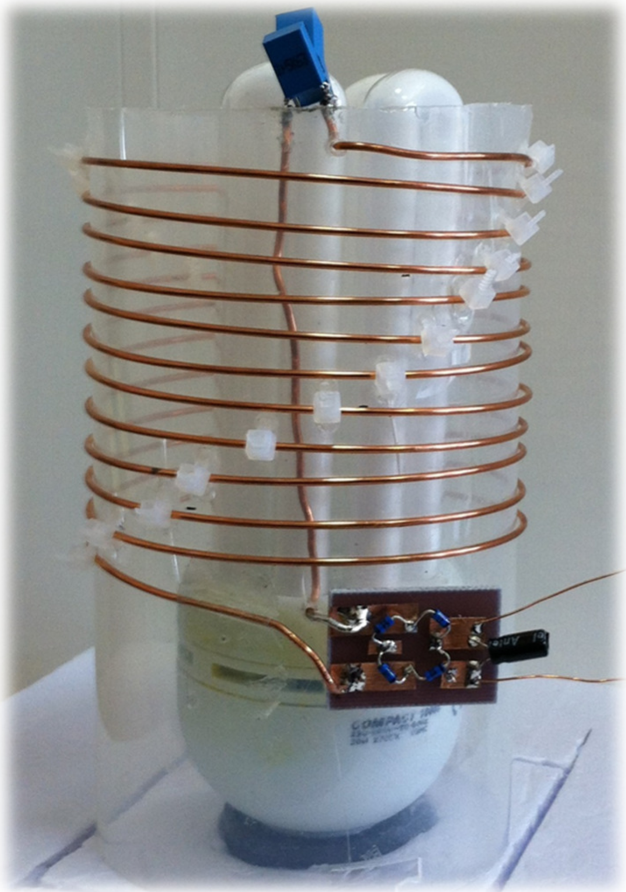

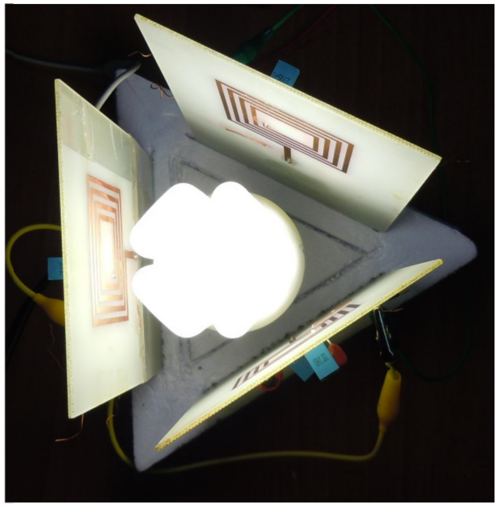

LAMPHAR

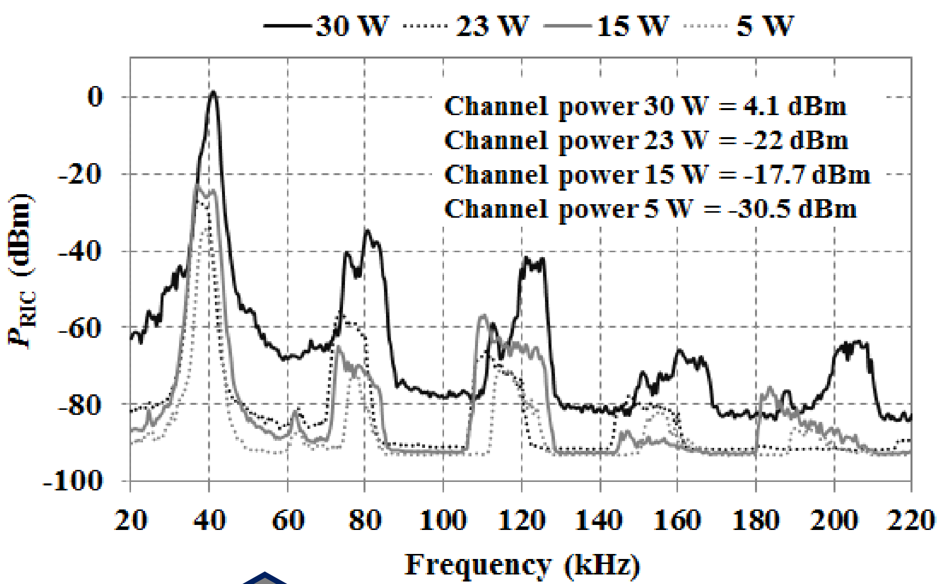

DC output power generated by coupling the Lamphar with a 30W CFL

RF Spectrum received by the resonator

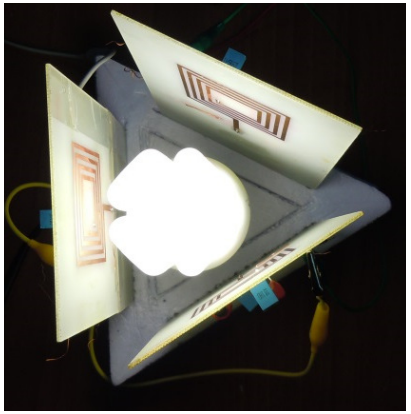

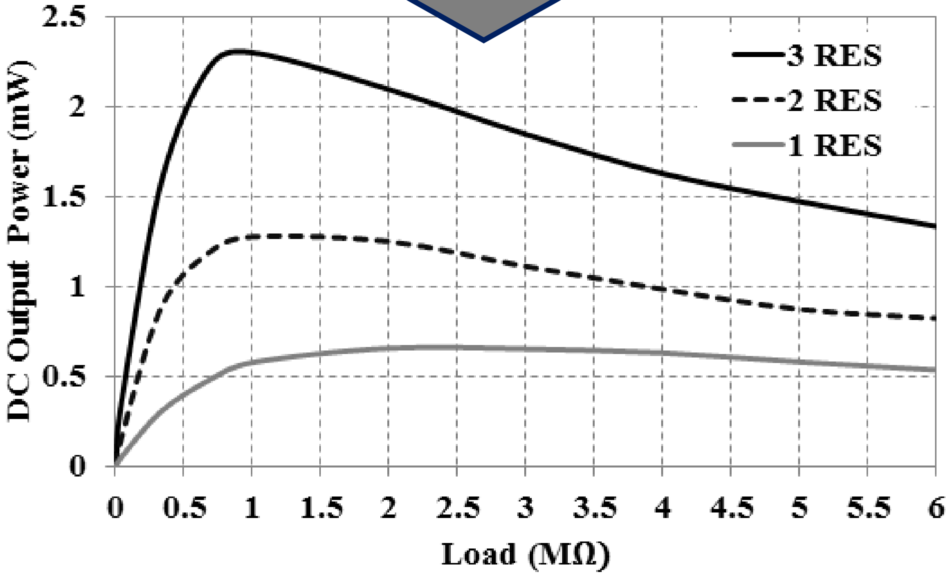

Conclusion

- Optimal design of a single transmitter-single receiver WPT link: a network approach has been used for deriving closed form design formulas for the load that maximizes either the power transfer efficiency or the power on the load

- Example of applications: WPT links for wearable and implantable devices

THANK YOU FOR YOUR ATTENTION!

Suggested readings

- Karalis, A., R. Moffatt, J. D. Joannopoulos, P. Fisher, and M. Soljacic A. Kurs. “Wireless Power Transfer via Strongly Coupled Magnetic Resonances.” *Science* 317 (2007): 83–86.
- Joannopoulos, J.D., M. Soljacic, and A. Karalis. “Efficient Wireless Non-Radiative Mid-range Energy Transfer.” Annals of Physics 323 (2008): 24–48.
- Tomassoni, C., P. Russer, R. Sorrentino, and M. Mongiardo. “Rigorous Computer-Aided Design of Spherical Dielectric Resonators for Wireless Non-Radiative Energy Transfer.” In MTT-S International Microwave Symposium, Boston, 2009, pp. 1–4.
- M. Dionigi, A. Costanzo and M. Mongiardo (2012). Network Methods for Analysis and Design of Resonant Wireless Power Transfer Systems, Wireless Power Transfer - Principles and Engineering Explorations, Dr. Ki Young Kim (Ed.), ISBN: 978-953-307-874-8, InTech, Available from:http://www.intechopen.com/books/wireless-power-transferprinciples-and-engineering-explorations/networksmethods-for-theanalysis-and-design-of-wireless-power-transfer-systems.
- Dionigi, M., Mongiardo, M., Perfetti, R.: Rigorous network and full-wave electromagnetic modeling of wireless power transfer links. Microwave Theory and Techniques, IEEE Transactions on 63(1), 65–75 (2015). DOI 10.1109/TMTT.2014.2376555
- A. Costanzo, M. Dionigi, D. Masotti, M. Mongiardo, G. Monti, L. Tarricone, R. Sorrentino, “**Electromagnetic Energy Harvesting and Wireless Power Transmission: A Unified Approach,**” *Proceedings of the IEEE* published by IEEE (Piscataway, NJ, USA), Vol. 102 , Issue 11, pp. 1692–1711, DOI: 10.1109/JPROC.2014.2355261, INSPEC Accession Number: 14682530, ISSN: 0018-9219, Oct. 2014.
- Giuseppina Monti, Wenquan Che, Qinghua Wang, Marco Dionigi, Mauro Mongiardo, Renzo Perfetti, and Yumei Chang, “**Wireless Power Transfer Between One Transmitter and Two Receivers: Optimal Analytical Solution**,” Wireless Power Transfer, 2016.

Suggested readings

- Ping, Hu, A.P., S. Malpas, D. Budgett Si. “A frequency control method for regulating wireless power to implantable devices.” Transactions on Biomedical Circuits and Systems 2, no. 1 (2008): 22–29.
- Xuelin Liu, Hao Li, G. Shao, Qi Li, Hongyi Fang. “Wireless Power Transfer System for Capsule Endoscopy Based on Strongly Coupled Magnetic Resonance Theory.” in International Conference on Mechatronics and Automation, 2011, pp. 232–236.
- G. Monti, P. Arcuti, L. Tarricone, “Resonant Inductive Link for Remote Powering of Pacemakers,” IEEE Transactions on Microwave Theory and Techniques published by IEEE (Piscataway, NJ, USA), Vol. 63, Issue 11, pp.: 3814 – 3822, Nov. 2015.
- Giuseppina Monti, Laura Corchia, Egidio De Benedetto and Luciano Tarricone, “A Wearable Wireless Energy Link for Thin-Film Batteries Charging", International Journal of Antennas and Propagation, 2016.
- F. Congedo, G. Monti, L. Tarricone, V. Bella, “A 2.45-GHz Vivaldi Rectenna for the Remote Activation of an End Device Radio Node,” IEEE Sensors Journal published by IEEE (Piscataway, NJ, USA), Vol. 13, Issue 9, pp. 3454 – 3461, DOI: 10.1109/JSEN.2013.2265081, ISSN: 1530-437X, May 2013.
- G. Monti, F. Congedo, P. Arcuti, L. Tarricone, “Resonant Energy Scavenger for Sensor Powering by Spurious Emissions from Compact Fluorescent Lamps,” IEEE Sensors Journal published by IEEE (Piscataway, NJ, USA), Vol. 14, Issue 7, pp. 2347-2354, DOI: 10.1109/JSEN.2014.2310235, INSPEC Accession Number:14331856, ISSN:1530-437X, July 2014.
- Leonardo Sileo, Luigi Martiradonna, Paola Arcuti, Giuseppina Monti, Vittorianna Tasco, Marco Dal Maschio, Giacomo Pruzzo, Benedetto Bozzini, Luciano Tarricone, Massimo De Vittorio, “Wireless system for biological signal recording with Gallium Arsenide High Electron Mobility Transistors as sensing elements Microelectronic Engineering,” Microelectronic Engineering published by Elsevier B. V. (Amsterdarm, Netherlands), Vol. 111, pp. 354-359, DOI:10.1016/j.mee.2013.02.089, ISSN: 0167-9317, 2013.
- G. Monti, L. Corchia, L. Tarricone, “UHF Wearable Rectenna on Textile Materials,” IEEE Transactions on Antennas and Propagation published by IEEE (Piscataway, NJ, USA), Vol. 61, Issue 7, pp. 3869–3873, DOI: 10.1109/TAP.2013.2254693, ISSN: 0018-926X, 2013.
- Meyer, D.A., J.R. Smith, A.P. Sample. “Analysis, Experimental Results, and Range Adaptation of Magnetically Coupled Resonators for Wireless Power Transfer.” Transactions on Industrial Electronics (2011): 544–554.

Textile rectenna: effect of the slits

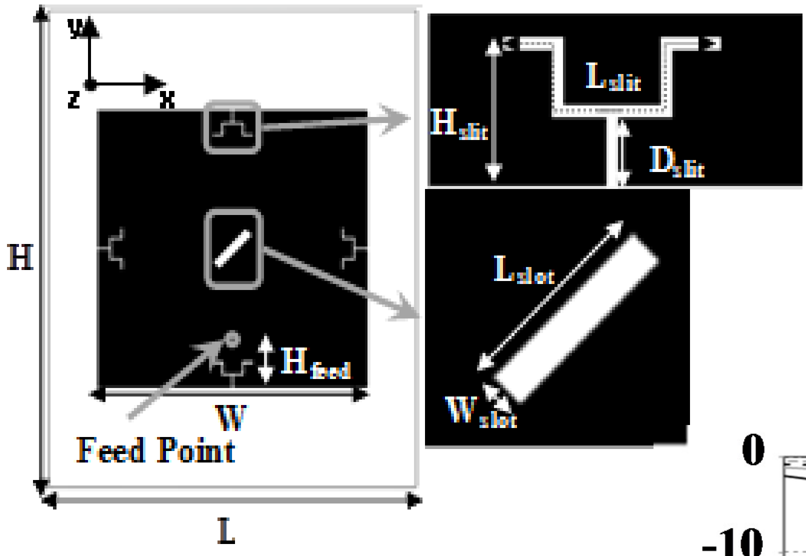

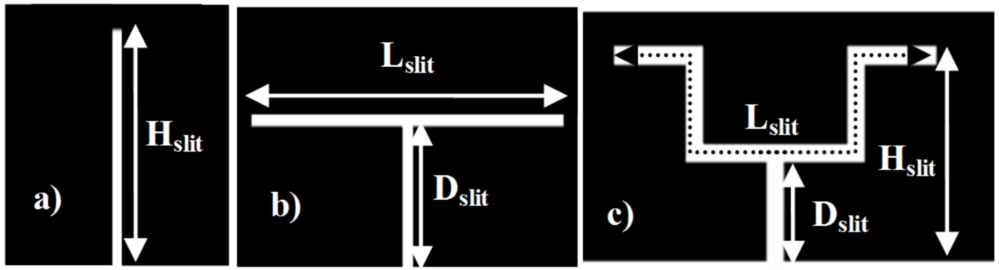

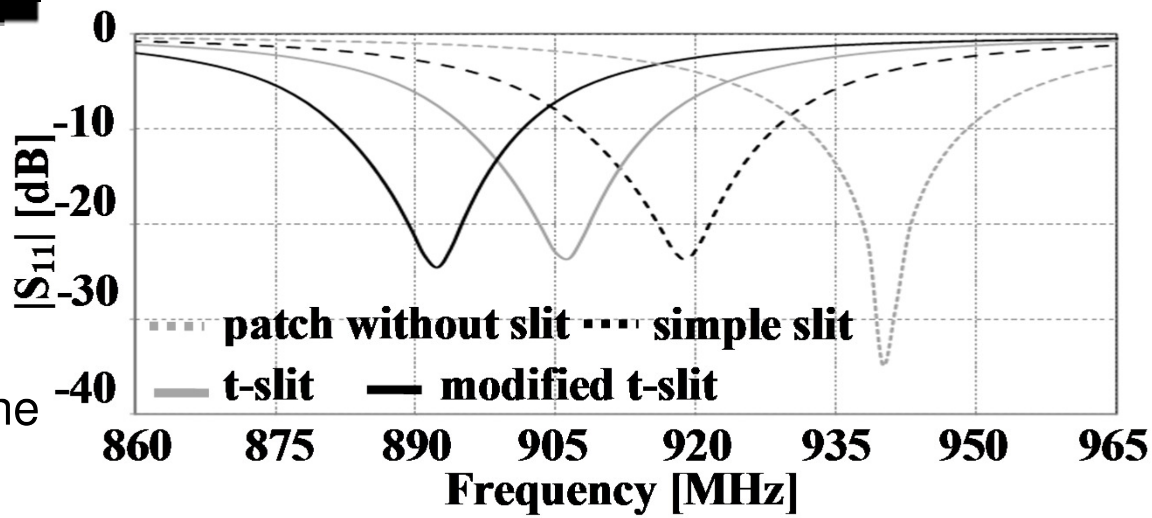

Numerical data calculated for different shapes of the slits on the edges of the patch antenna

Textile rectenna: effect of textile superstrate

Comparison between data calculated for the antenna without coverage and in the case of a superstrate of jeans (0.5 mm) or pile (1 mm): a) gain calculated by means of full-wave simulations at 892 MHz in the xz- and yz-plane; b) measured reflection coefficient.

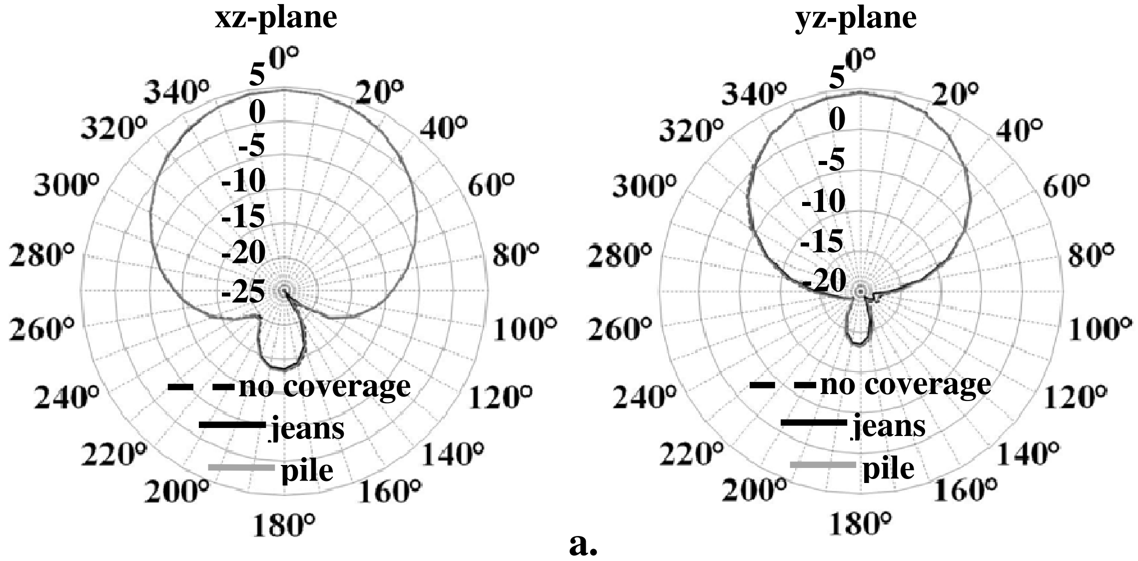

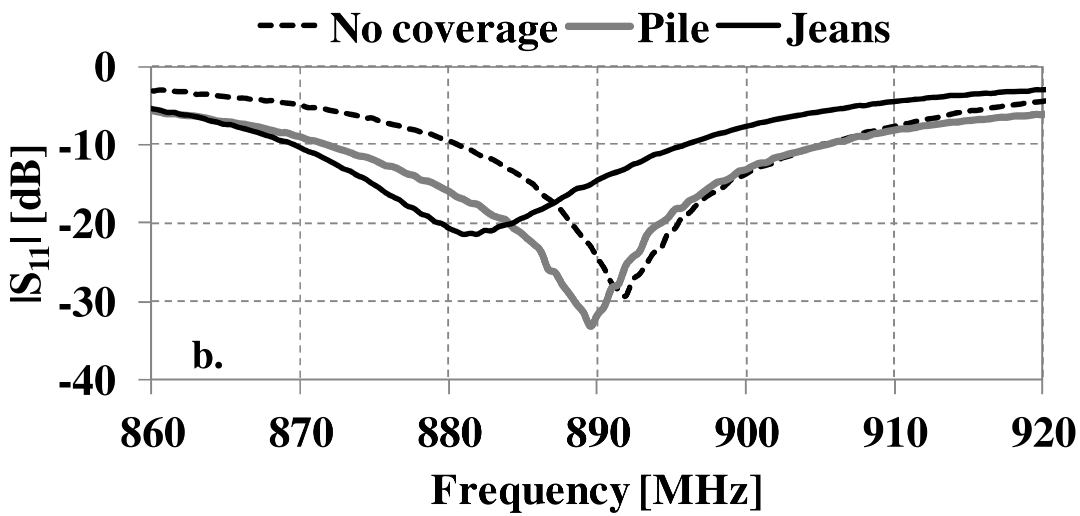

Textile rectenna

The connection between the antenna and the rectifier was realized by means of a shielded wire of copper with a radius of 0.25 mm applied in the same point used for the coaxial excitation of the antenna (the point referred as Feed Point in Fig. 2). Experimental tests were performed by using a Software-Defined Radio (SDR) platform [17]-[19].

Textile rectenna

The Software-Defined Radio (SDR) platform was used for experimental tests of the RF-to-DC conversion efficiency. The signal incident on the rectenna was generated by means of the GNUradio toolkit and the Universal Software Radio Peripheral (USRP) equipped with the RFX-900 daughterboar.

In order to avoid spurious reflections, experiments were performed in a large outdoor area and with a distance between the transmitting antenna (a 3 dBi monopole) and the rectenna of 1 m. Furthermore, loss due to polarization mismatches was minimized by adjusting the relative position of the transmitting and receiving antenna.

Textile rectenna

The PMM 8053A broadband field meter with the EP-183 isotropic probe was used to measure the power density incident on the antenna

$$\eta = \frac{P_{OUT,DC}}{\left(S_{RF} A_{eff}\right)} = \frac{\left(V_{DC}^2 / R_L\right)}{\left(S_{RF} A_{eff}\right)}$$

. It is worth underlining that (1) does not take into account the polarization mismatch between the transmitting monopole of the SDR platform and the proposed antenna. However, measurements were performed by adjusting the relative position of the transmitting and receiving antenna in order to minimize loss due to polarization mismatches. More in detail, the SDR monopole was oriented along the patch diagonal.

Prototype Non-woven Fabric

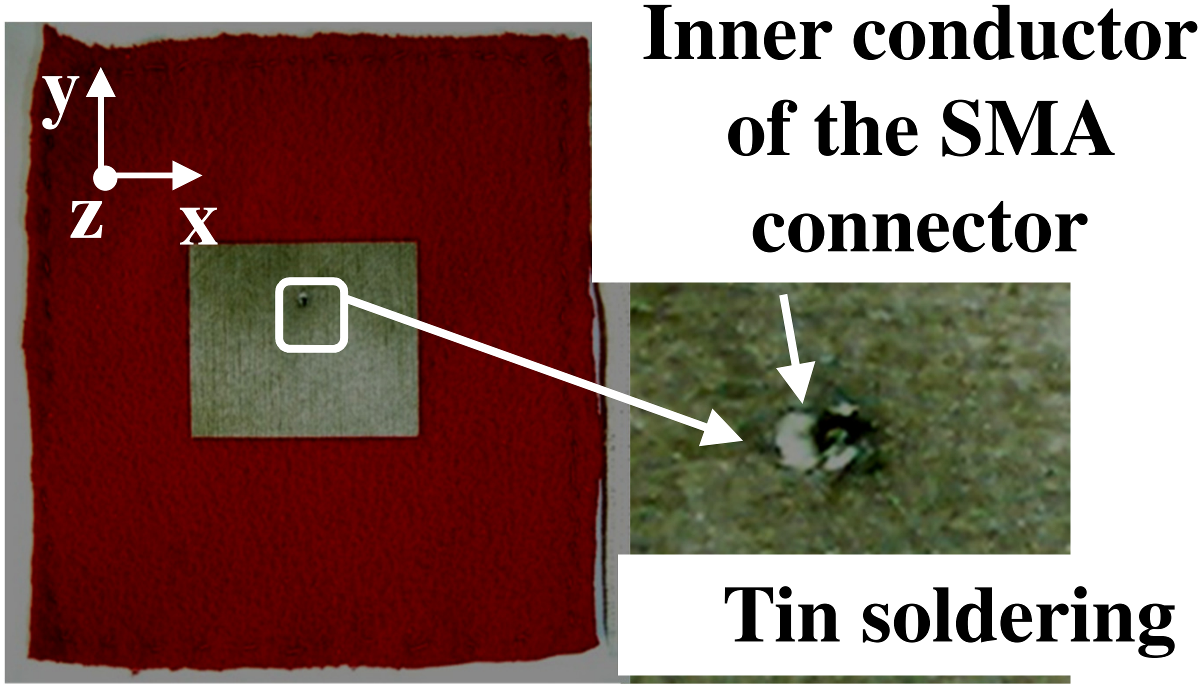

Conductive Material: Conductive fabric

- $\sigma = 2.27\ e^{5}$ S/m
- thickness = 0.11 mm

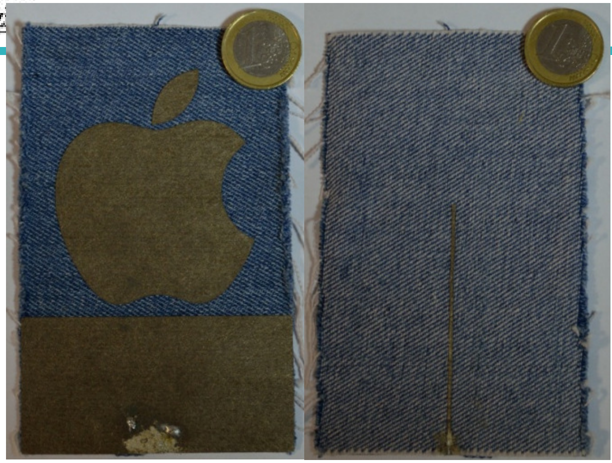

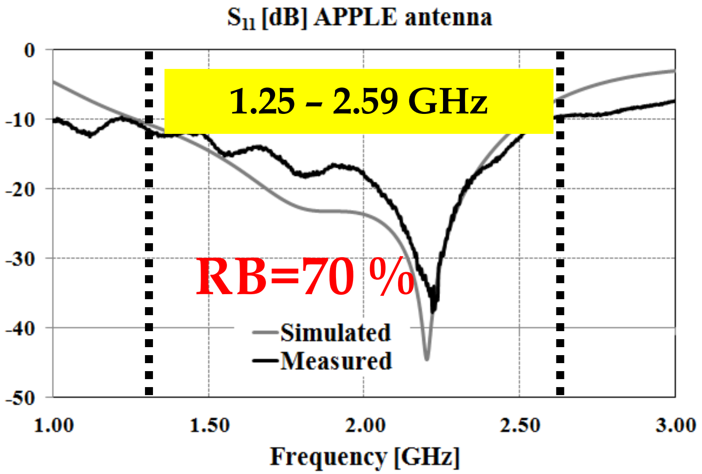

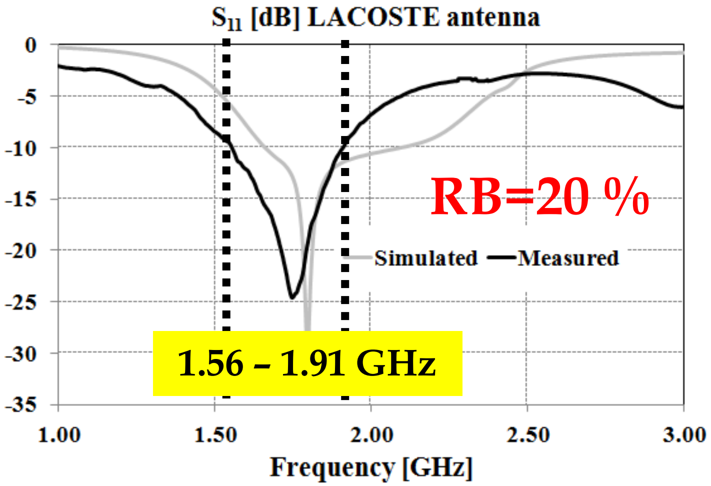

Conductive fabric: ADFORS Saint-Gobain

WPT link for medical implants: sensitivity analysis

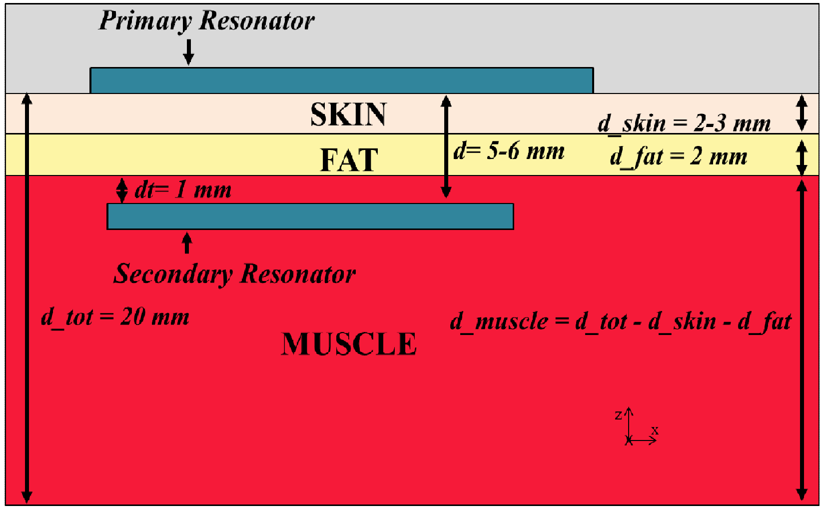

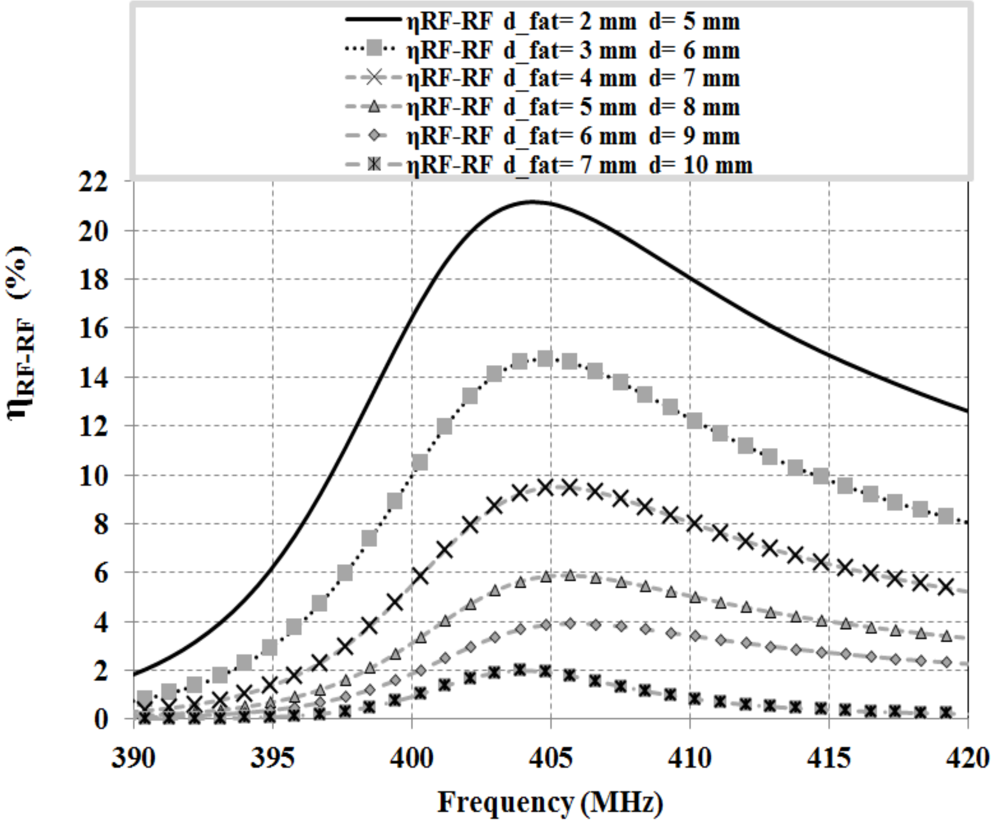

effect of the variation of skin thickness (d_fat) on the RF-RF conversion efficiency of the proposed WPT link. The solid black line denotes the $\eta_{RF\text{-}RF}$ obtained for the initial configuration

WPT link for medical implants: sensitivity analysis

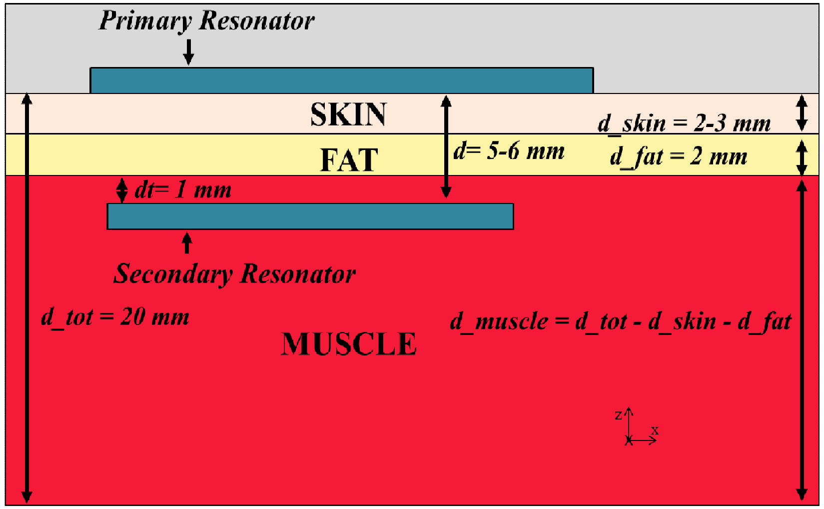

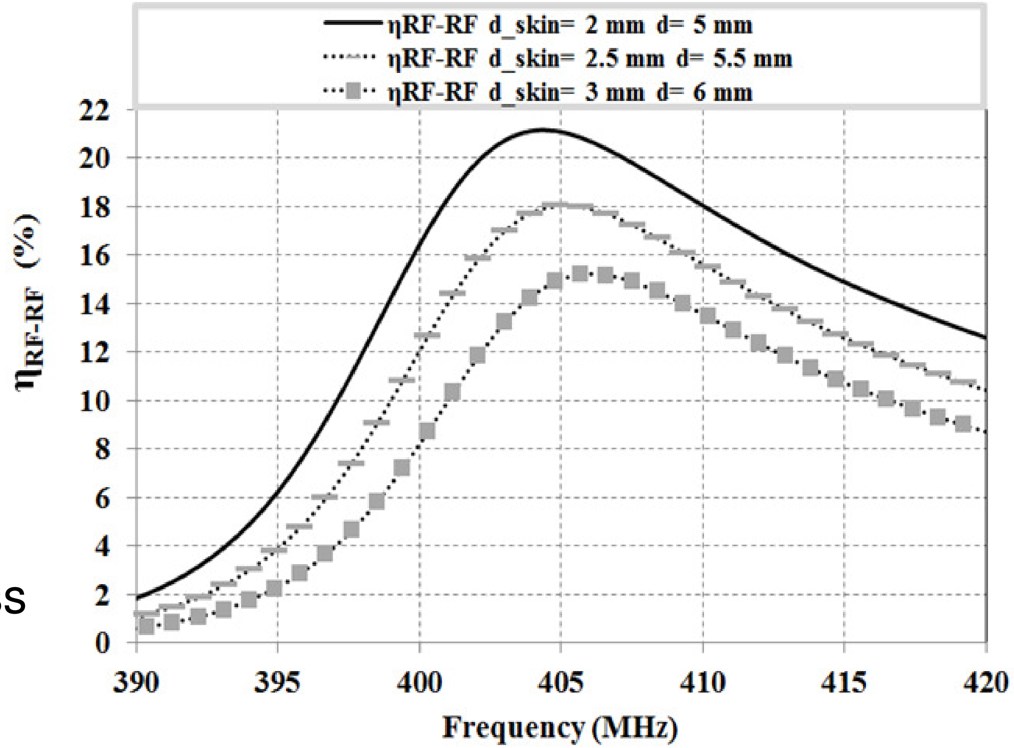

effect of the variation of skin thickness (d_skin) on the RF-RF conversion efficiency of the proposed WPT link. The solid black line denotes the $\eta_{RF\text{-}RF}$ obtained for the initial configuration

WPT link for medical implants: sensitivity analysis

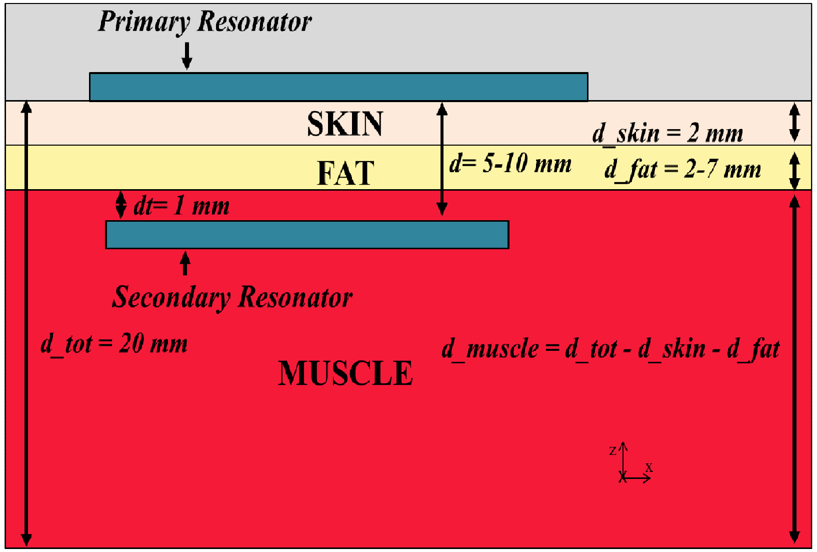

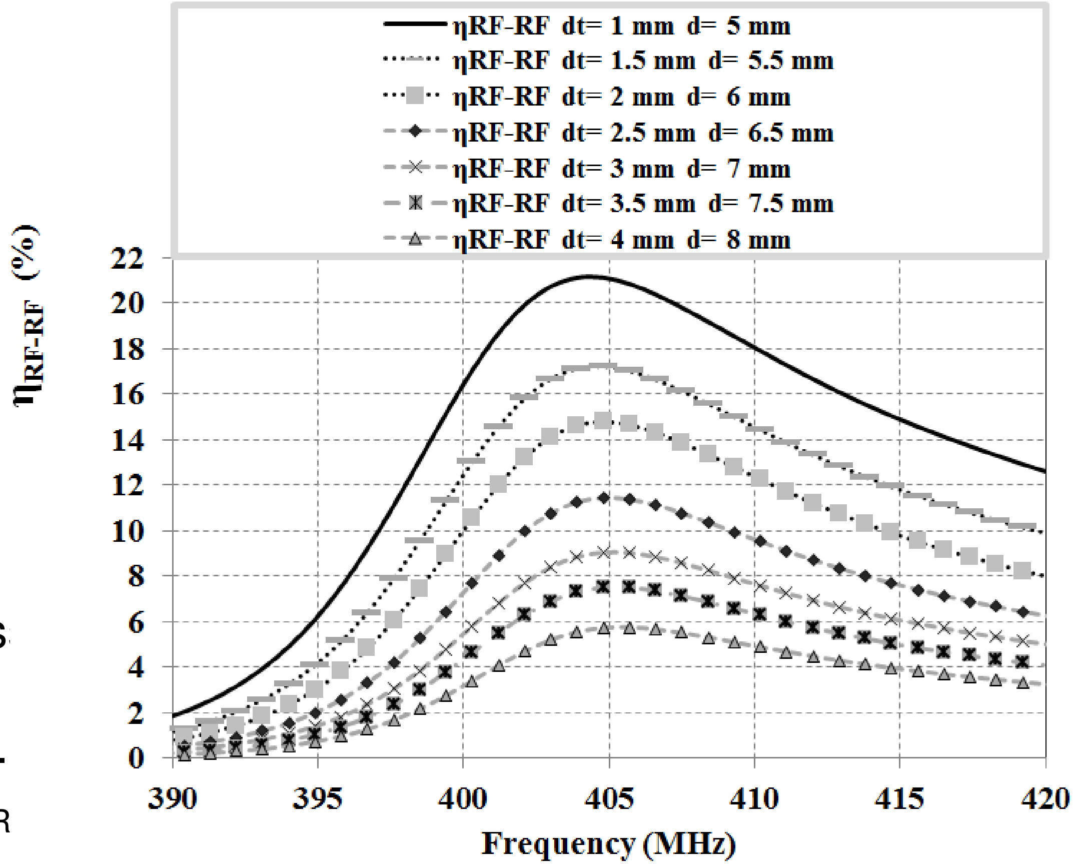

effect of the variation of skin thicknes (dt) on the RF-RF conversion efficiency of the proposed WPT link. The solid black line denotes the η_{RF-R} obtained for the initial configuration

WPT link for medical implants

TABLE I

Performance Comparison of the WPT Systems Proposed in [6-13]

Ref. paper	Operating frequency	Dimensions of the receiver (mm2)	Transfer Efficiency @ distance
[6]	100 kHz	(6x6)	16% @ 8 mm
[7]	13.56 MHz	(10x10)	31% @ 10 mm
[8]	13.56 MHz	(25x10)	58% @ 10 mm
[9]	6.78 MHz	(12x12)	38% @ 20 mm in air
[11]	1.6 GHz	(3x3)	0.06% @ 10 mm
[12]	1.86 GHz	(2x2)	0.025% @ distance ranging from 2 to 5 cm
[13]	434 MHz	(32.3x34.1)	4.6% @ 15 mm
Present work	403 MHz	(15x15)	21 % @ 5 mm

WPT link for medical implants

6. K. Jung, Y.H. Kim, E. Jung Choi, H. Jun Kim, and Y.J. Kim, “Wireless Power Transmission for Implantable Devices Using Inductive Component of Closed-Magnetic Circuit Structure”, *IEEE International Conference on Multisensor Fusion and Integration for Intelligent Systems*, Seoul, Korea, 2008.
7. U.M. Jow, and M. Ghovanloo, “Modeling and optimization of printed spiral coils in air, saline, and muscle tissue environments”, *IEEE Trans. on Biomedical circuit and Systems*, Vol. 45, No. 1, 21-22, 2009.
8. R.F. Xue, K.W. Cheng, and M. Je, “High-Efficiency Wireless Power Transfer for Biomedical Implants by Optimal Resonant Load Transformation”, *IEEE Trans. on Circuits and Systems*, Vol. 60, No. 4, 867-874, 2013.
9. A. Khripkov, W. Hong, and K. Pavlov, “Integrated Resonant Structure for Simultaneous Wireless Power Transfer and Data Telemetry”, *IEEE Antennas and Wireless Propagation Letters*, Vol. 11, 1659-1662, 2012.
10. A.S.Y. Poon, S. O’Driscoll, T.H. Meng, “Optimal Frequency for Wireless Power Transmission Into Dispersive Tissue”, *IEEE Trans. on Ant. and Propag.*, Vol. 58, No. 5, 2010.
11. A.J. Yeh, J.S. Ho, Y. Tanabe, E. Neofytou, R.E. Beygui, and A.S.Y. Poon, “Wirelessly powering miniature implants for optogenetic stimulation”, *Applied Phisycs Letters* 103, 163701, 2013.
12. A.J. Yeh1, J.S. Ho, Y. Tanabe, E. Neofytou, R. E. Beygui and A.S.Y. Poon, “A mm-Sized Wirelessly Powered and Remotely Controlled Locomotive Implant”, *Appl. Phys. Lett.*, Vol. 103, 2013.
13. G. Monti, L. Tarricone, C. Trane, “Experimental Characterization of a 434 MHz Wireless Energy Link For medical Applications”, *Progress In Electromagnetics Research C*, Vol. 30, 53-64, may 2012.

WPT link for medical implants

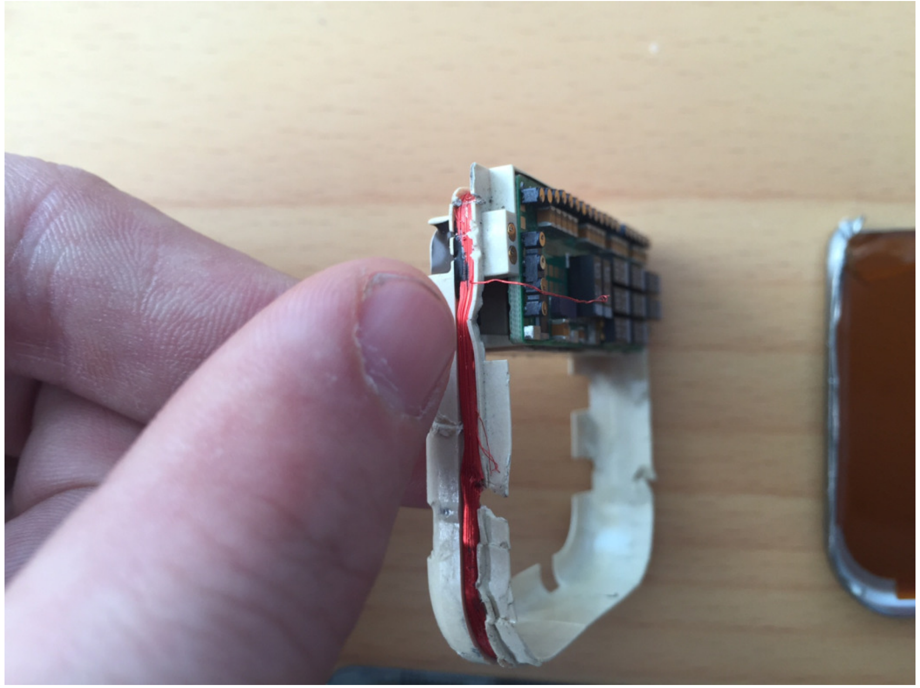

LAMPHAR: the resonator

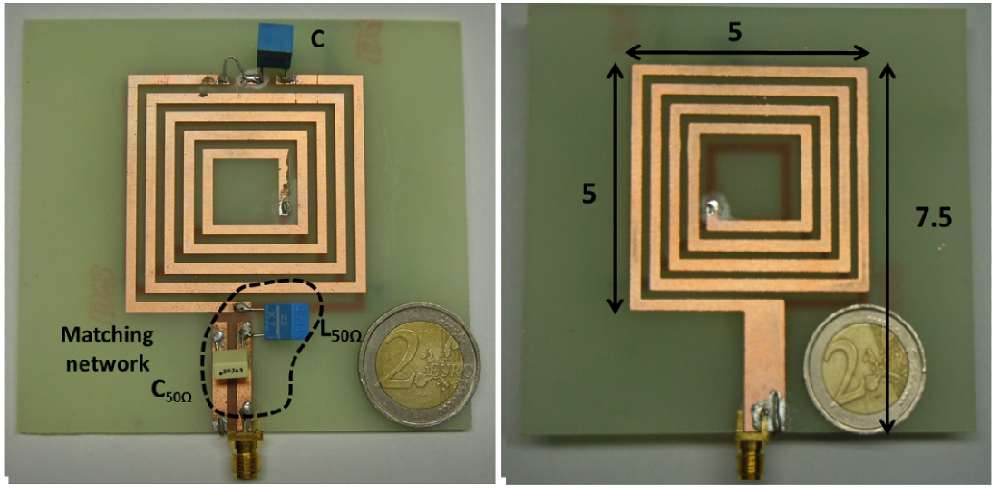

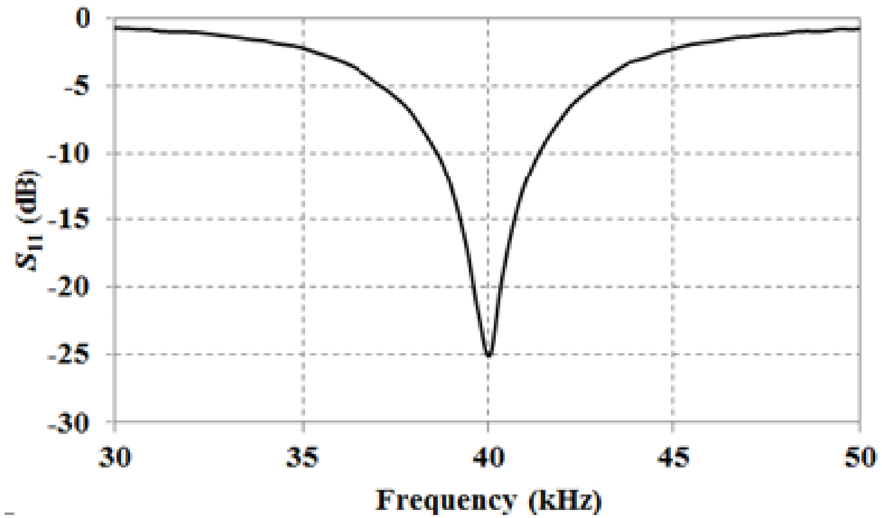

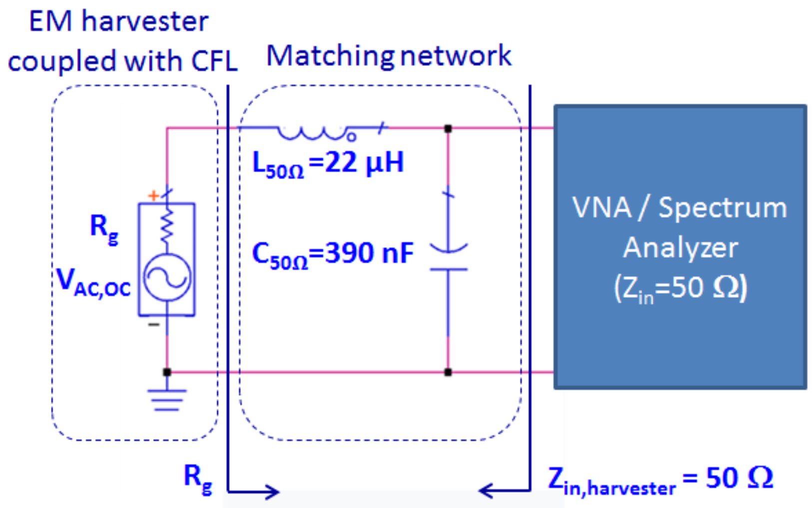

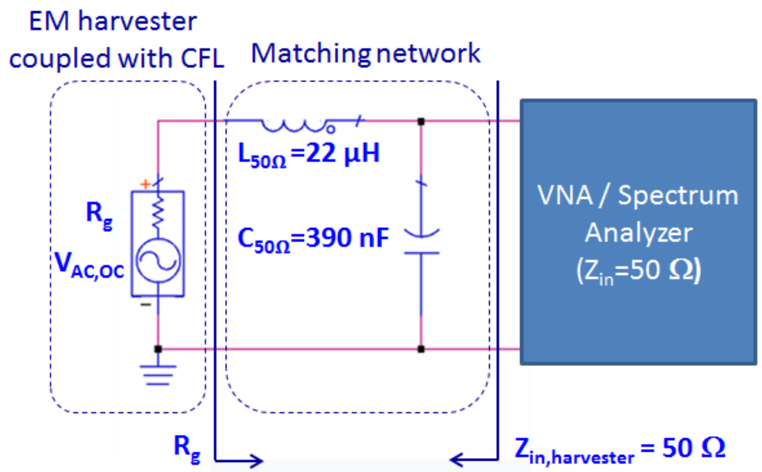

LAMPHAR: setup adopted for measuring the harvested RF spectrum

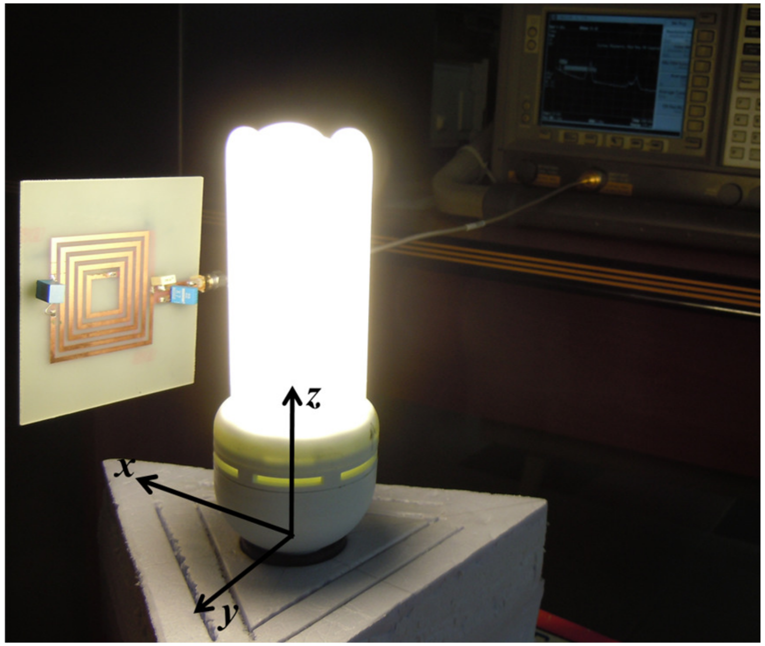

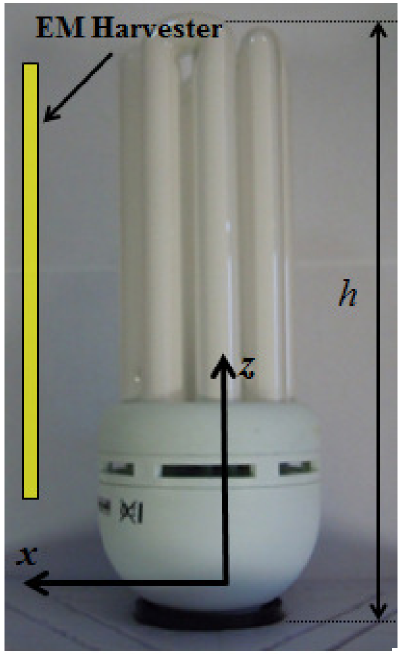

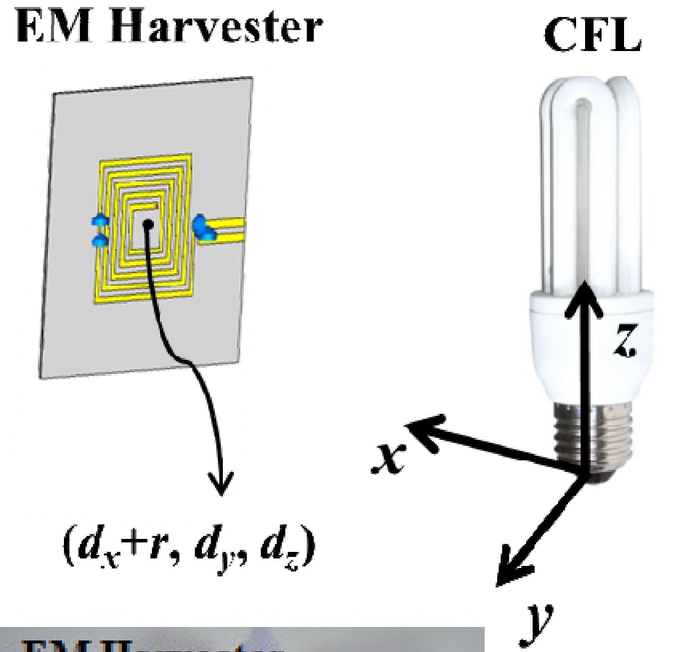

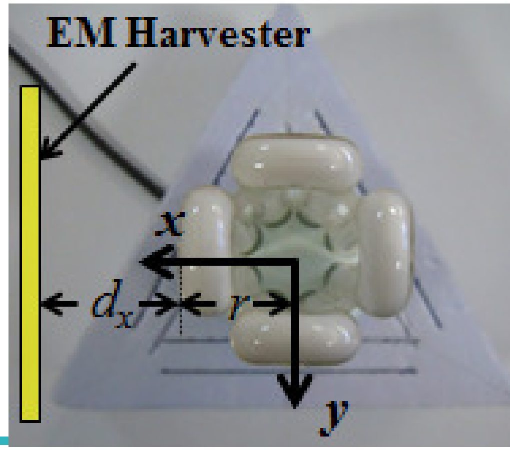

LAMPHAR: harvested RF spectrum

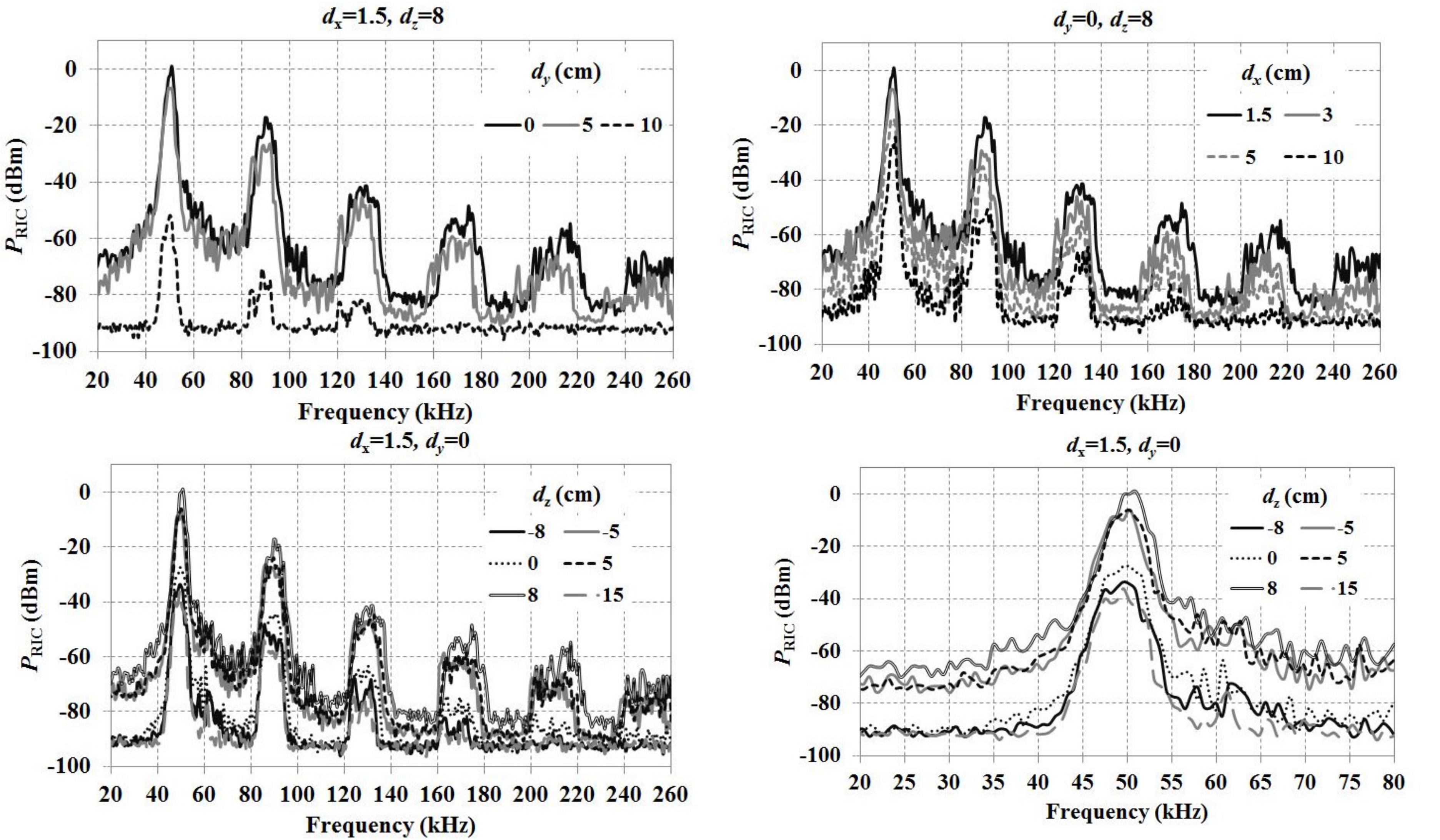

LAMPHAR

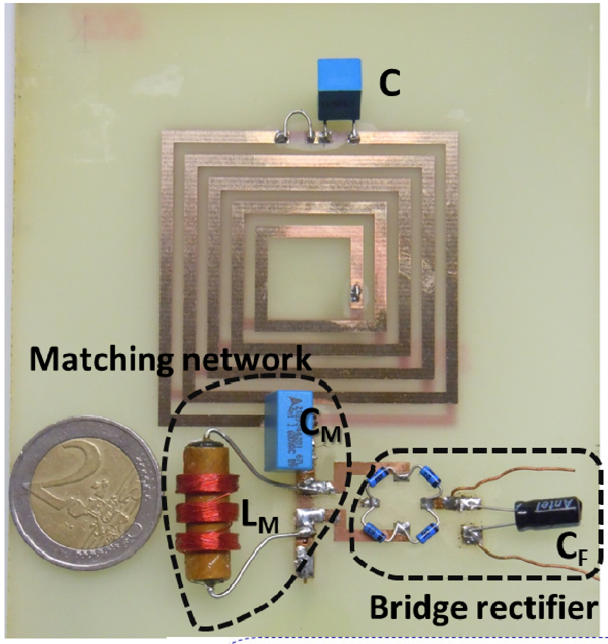

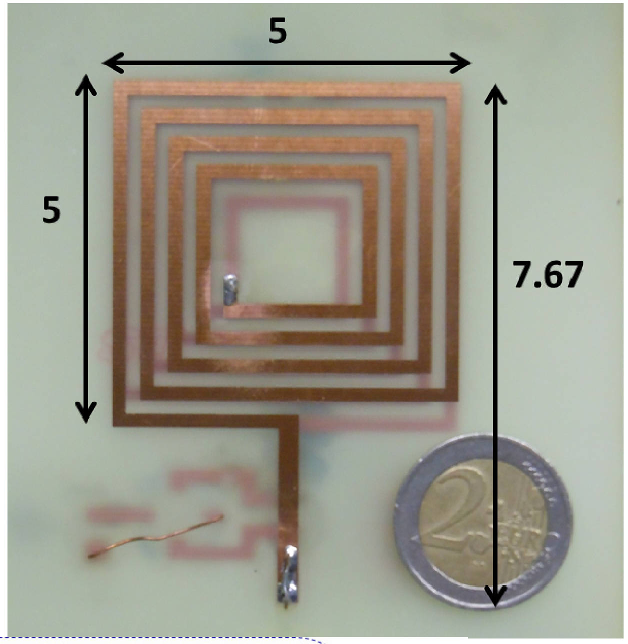

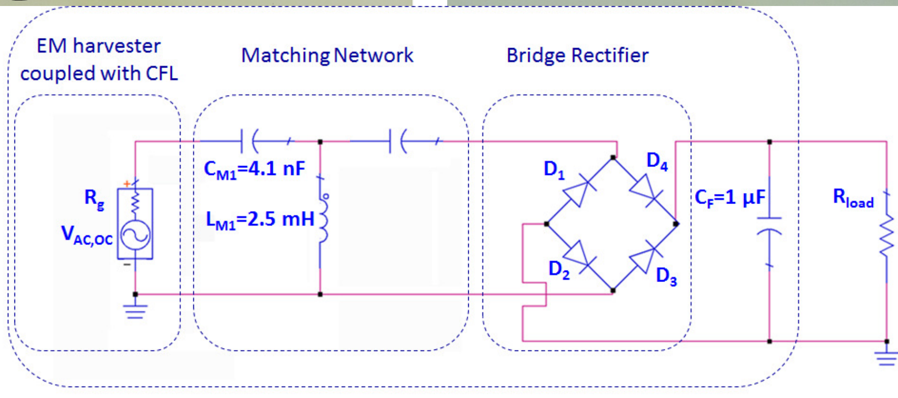

EM Resonant Energy Scavenger (RES)

LAMPHAR

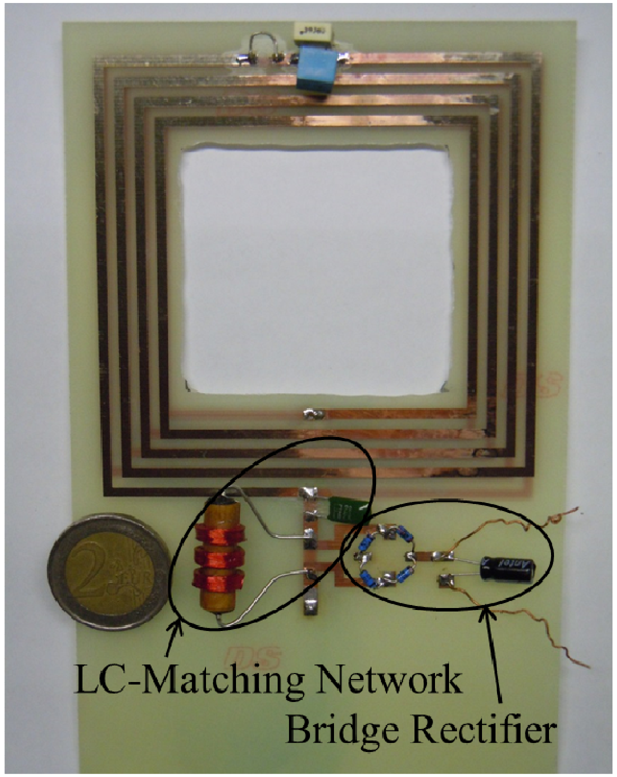

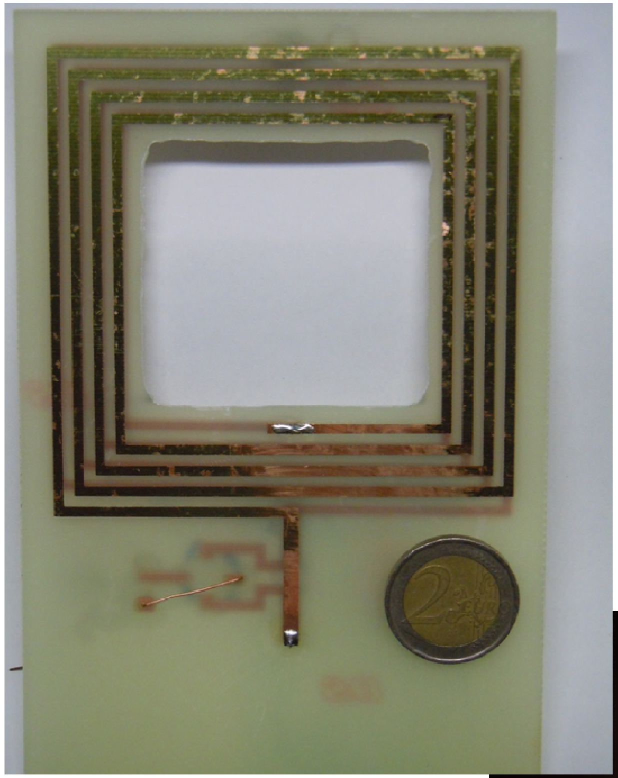

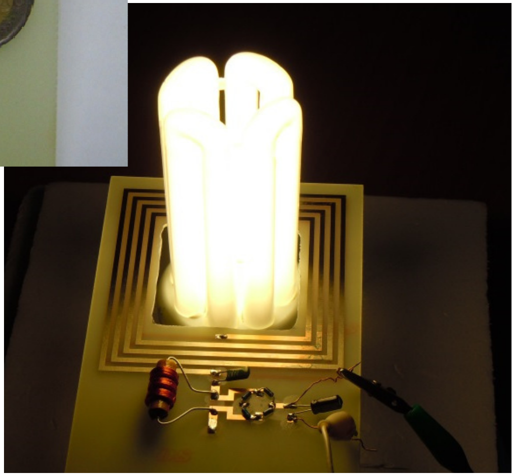

LAMPHAR

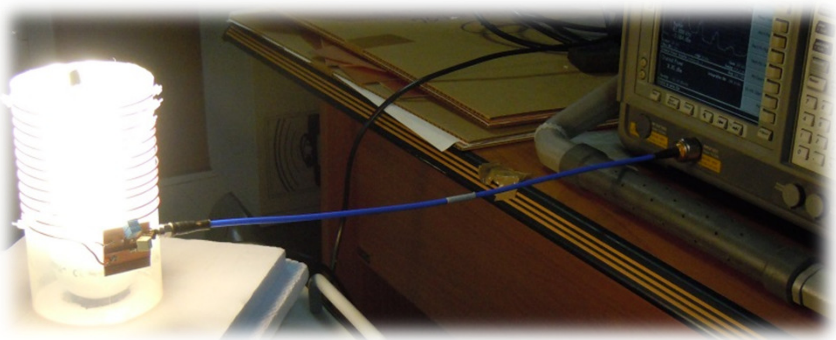

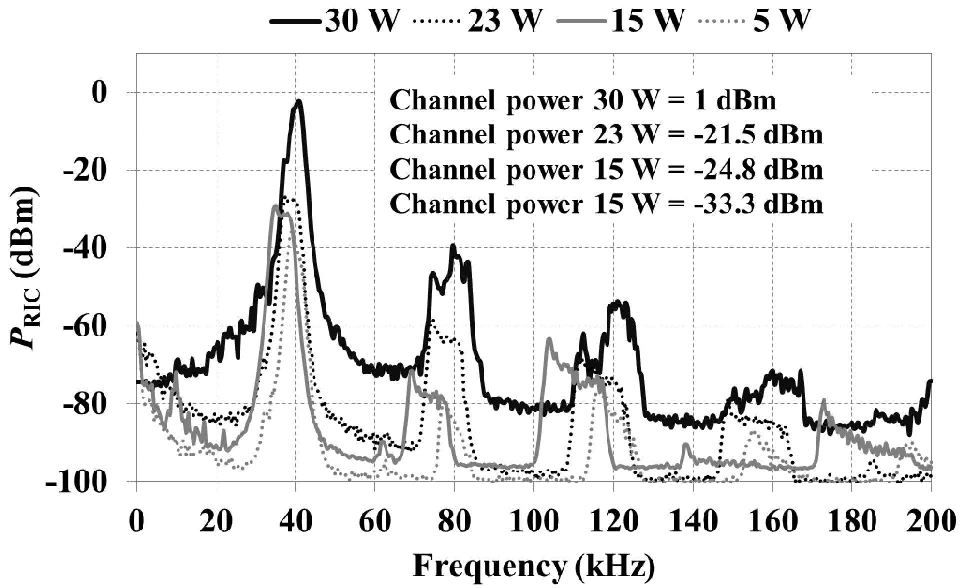
30 W
23 W
15 W
5 W
Channel power 30 W = 1 dBm
Channel power 23 W = -21.5 dBm
Channel power 15 W = -24.8 dBm
Channel power 15 W = -33.3 dBm
0
-20
-40
-60
-80
-100
P_{RIC} (dBm)
0 20 40 60 80 100 120 140 160 180 200
Frequency (kHz)

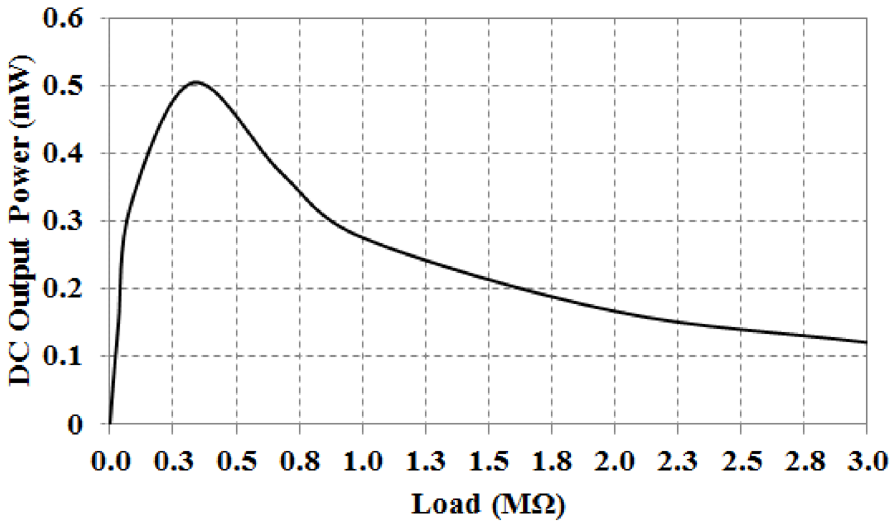
0.6
0.5
0.4
0.3
0.2
0.1
0
DC Output Power (mW)
0.0 0.3 0.5 0.8 1.0 1.3 1.5 1.8 2.0 2.3 2.5 2.8 3.0
Load (MΩ)

Admittance matrix representation of a two-port WPT link

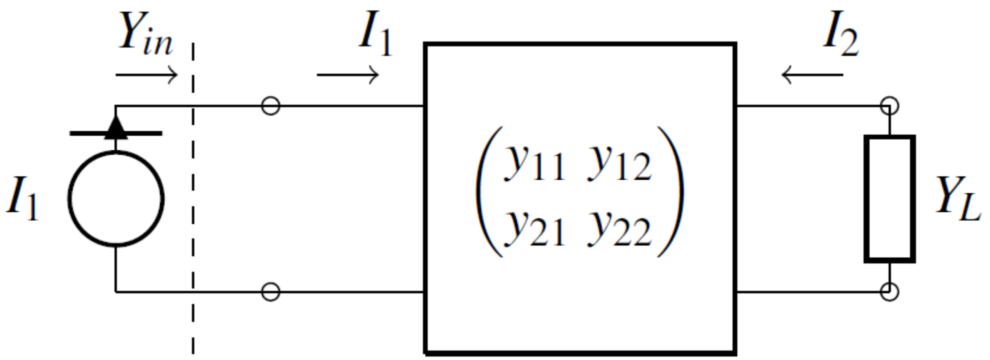

$$\mathbf{I} = \mathbf{Y}\mathbf{V}$$

$$\mathbf{Y} = \begin{pmatrix} y_{11} & y_{12} \\ y_{21} & y_{22} \end{pmatrix}$$

Input impedance of the network	$Y_{in} = G_{in} + jB_{in} = y_{11} - \frac{y_{12}^2}{y_{22} + Y_L}$
active power delivered by the voltage generator to the network	$\bar{P}_{in} = \frac{G_{in}}{2\|Y_{in}\|^2}\|I_1\|^2$
Available active power assuming that the internal admittance of the generator at port 1 is g_{11}	$P_0 = \frac{\|I_1\|^2}{8g_{11}}$

Admittance matrix representation of a two-port WPT link

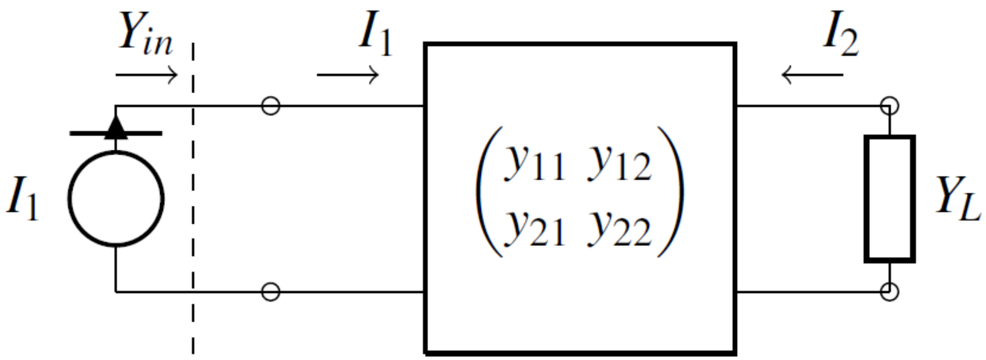

$$\mathbf{V} = \mathbf{Z}\mathbf{I}$$

$$\mathbf{Z} = \begin{pmatrix} z_{11} & z_{12} \\ z_{21} & z_{22} \end{pmatrix}$$

Goal:

Determine the expression of the load $Y_L = G_L + j B_L$ that maximizes either the efficiency or the power on the load

$$\bar{P}_L = \frac{G_L}{2\,|Y_L|^2}|I_2|^2 \qquad \eta = \frac{\bar{P}_L}{\bar{P}_{in}} = \frac{G_L}{G_{in}}\left|\frac{y_{12}}{y_{22}+Y_L}\right|^2$$

Admittance matrix representation of a two-port WPT link

It is convenient to define the parameters

$$\chi_y^2 = \frac{b_{12}^2}{g_{11}g_{22}} \qquad \xi_y^2 = \frac{g_{12}^2}{g_{11}g_{22}}$$

$$\mu_y = b_{11}/g_{11} \qquad \nu_y = b_{22}/g_{22}$$

$$\theta_{r,y} = \sqrt{1+\chi_y^2}\sqrt{1-\xi_y^2}, \qquad \theta_{x,y} = \chi_y \xi_y .$$

By using these parameters the Y-matrix can be expressed as

$$\mathbf{Y} = \begin{pmatrix} g_{11}\,(j\,\mu_y + 1) & \sqrt{g_{11}\,g_{22}}\,(\xi_y + j\,\chi_y) \\ \sqrt{g_{11}\,g_{22}}\,(\xi_y + j\,\chi_y) & g_{22}\,(j\,\nu_y + 1) \end{pmatrix}$$

By using the above reported parameters, the problem becomes fully equivalent to the one solved in the case of an impedance matrix representation of the network

Admittance matrix representation of a two-port WPT link

Table 2 Admittance matrix representation of a two-port WPT link: a summary of the parameters' values for the approaches that maximize efficiency and power. The parameters have the following meanings: $\chi_y = b_{12}/\sqrt{g_{11}g_{22}}$, $\xi_y = b_{12}/\sqrt{g_{11}g_{22}}$, $\theta_{r,y} = \sqrt{1+\chi_y{}^2}\sqrt{1-\xi_y{}^2}$, $\theta_{x,y} = \chi_y\xi_y$. The power has been normalized w.r.t. $P_0 = |I_1|^2/(8g_{11})$.

Parameter	maximum efficiency	maximum power
G_L	$g_{22}\theta_r$	$g_{22}\theta_{r,y}^2/(\theta_{x,y}^2+1)$
B_L	$g_{22}\theta_{x,y} - b_{22}$	$-b_{22} + g_{22}\theta_{x,y} + g_{22}\theta_{x,y}\theta_{r,y}^2/(\theta_{x,y}^2+1)$
G_{c1}	0	0
B_{c1}	$b_{12}g_{12}/g_{22} - b_{11}$	$b_{12}g_{12}/g_{22} - b_{11}$
G_{in}	$g_{11}\theta_{r,y}$	$2g_{11}\theta_{r,y}^2/(1+\theta_{r,y}^2+\theta_{x,y}^2)$
B_{in}	0	0
P_{in}	$4/\theta_{r,y}$	$2(1+\theta_{r,y}^2+\theta_{x,y}^2)/(\theta_{r,y}^2)$
P_L	$4\eta^e/\theta_{r,y}$	$(\xi_y^2+\chi_y^2)/\theta_{r,y}^2$
η	$\eta^e = (\xi_y^2+\chi_y^2)/((1+\theta_{r,y})^2+\theta_{x,y}^2)$	$(\xi_y^2+\chi_y^2)/(2(1+\theta_{r,y}^2+\theta_{x,y}^2))$

However, considering the facilities in our availability, we decided to use the iterative procedure described in the paper. This method is based on comparisons between full-wave simulations and measurements, as a consequence, the method, besides providing the electromagnetic parameters of the dielectric layer to be used in full-wave simulations, allows determining the best simulation setup (i.e., how to set the simulation parameters). In our experience, this method allows obtaining a good match between simulated and measured data for microwave devices fabricated by using non-conventional materials.

WPT for medical implants: geometry

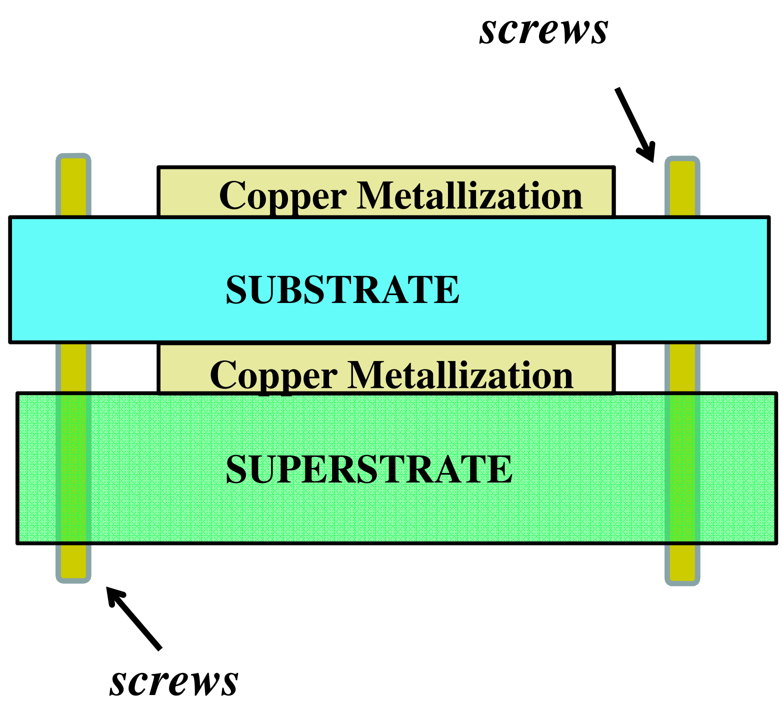

Substrate→ Arlon DiClad 880 (ε_r= 2.17, tanδ= 0.0009, and h= 0.508 mm)
Superstrate →Arlon AR1000 (ε_r=9.7, and tanδ= 0.003, and h= 0.610 mm)

The theorem was originally misunderstood (notably by Joule) to imply that a system consisting of an electric motor driven by a battery could not be more than 50% efficient since, when the impedances were matched, the power lost as heat in the battery would always be equal to the power delivered to the motor. In 1880 this assumption was shown to be false by either Edison or his colleague Francis Robbins Upton, who realized that maximum efficiency was not the same as maximum power transfer. To achieve maximum efficiency, the resistance of the source (whether a battery or a dynamo) could be made close to zero. Using this new understanding, they obtained an efficiency of about 90%, and proved that the electric motor was a practical alternative to the heat engine.

The condition of maximum power transfer does not result in maximum efficiency. he efficiency is only 50% when maximum power transfer is achieved, but approaches 100% as the load resistance approaches infinity, though the total power level tends towards zero. Efficiency also approaches 100% if the source resistance approaches zero, and 0% if the load resistance approaches zero. In the latter case, all the power is consumed inside the source (unless the source also has no resistance), so the power dissipated in a short circuit is zero

The theorem also applies where the source and/or load are not totally resistive. This invokes a refinement of the maximum power theorem, which says that any reactive components of source and load should be of equal magnitude but opposite phase. (*See below for a derivation.*) This means that the source and load impedances should be *complex conjugates* of each other. In the case of purely resistive circuits, the two concepts are identical. However, physically realizable sources and loads are not usually totally resistive, having some inductive or capacitive components, and so practical applications of this theorem, under the name of complex conjugate impedance matching, do, in fact, exist.
If the source is totally inductive (capacitive), then a totally capacitive (inductive) load, in the absence of resistive losses, would receive 100% of the energy from the source but send it back after a quarter cycle. The resultant circuit is nothing other than a resonant LC circuit in which the energy continues to oscillate to and fro. This is called reactive power. Power factor correction (where an inductive reactance is used to "balance out" a capacitive one), is essentially the same idea as complex conjugate impedance matching although it is done for entirely different reasons.